A Thesis for the Degree of Doctor of Philosophy

Preparation and characterization of titanium silicalite-1, RHO zeolite and CHA zeolite membranes

LIU BO

Graduate School of Science and Engineering

Yamaguchi University, Japan

March 2016

博士後期課程学位論文

チタニウムシリカライト-1, RHO ゼオライト, CHA ゼオライト膜の作製と特性評価

柳　波

山口大学大学院理工学研究科

環境共生系専攻

2016 年 3 月

Contents

Abstract

Preparation and characterization of titanium silicalite-1, RHO zeolite and CHA zeolite membranes

Zeolite membranes have attracted increasing attention in separation and/or membrane reactor fields, because of their thermal and chemical stability, and high separation performance. The MFI zeolites partially replaced framework Si^{4+} with some heteroatoms, such as titanium silicalite-1 (TS-1), exhibit catalytic activity for some reactions. Recently we have developed the membrane reactor through TS-1 membrane on porous tubular supports, which could combine the catalysis reaction of selective oxidation of IPA with H_2O_2, with the membrane separation through TS-1 membrane. The selective separation of CO_2 from natural gas and flu gas is of great potential importance, both in increasing the energy efficiency and in carbon capture. RHO and CHA zeolite can separate CO_2 from CH_4 with the remarkable selectivity on the basis of pore diameter and selective adsorption. Zeolite RHO and CHA membrane, therefore, have greatly potential for application on CO_2 separation.

In this thesis, we devoted our attention to investigate the preparation and application of three types of zeolite membranes such as TS-1, RHO and CHA membrane. This thesis was divided into 7 chapters. Introduction section was arranged in Chapter 1. Chapter 2 offered a detailed elucidation on the optimization of the preparation process of TS-1 membrane and on the catalytic performance of the resulting membranes. Chapter 3 and Chapter 4 were concerned with the preparation and characterization of RHO membrane in the presence of organic structural directing agent (OSDA) and in the absence of OSDA, respectively. Chapter 5 offered a new fluoride route that was adopted for the preparation of CHA zeolite (Si/Al = 2.5–3.5) in the absence of OSDAs. Chapter 6 displayed a novel post-modification method using imidazolium-based room temperature ionic liquids (RTILs) precursors to patch CHA membrane defects for improving CO_2/CH_4 selectivity. Chapter 7 summarized the main results and conclusions obtained in this thesis.

In chapter 2, the TS-1 membrane with high catalytic activity was prepared on porous mullite tubular support by *in-situ* hydrothermal synthesis with the synthesis recipe of SiO_2: 0.031Titanium n-butoxide: 0.35Tetrapropylammonium hydroxide: 28 H_2O. Optimized preparation process displayed well reproducibility. Supplementary addition of H_2O_2 to the synthesis solution after removals of bubbles in preparation process had great effect on the catalytic performance of as-synthesized TS-1 membrane. Furthermore, the pretreatment of support may have effect on the morphology of surface zeolitic layer of TS-1 membrane.

In chapter 3, pure RHO membrane with high density and well intergrowth have been prepared on the surface of porous α-Al_2O_3 tube support using 18 Crown 6 as OSDA. Fluoride salts such as NaF have great effect on the morphologies of RHO crystals and lead to well intergrowth of RHO zeolite crystals. Fluoride may favor the crystallization of RHO zeolite as a mineralizing agent. Higher content of organic template (18C6/Al_2O_3=5) may lead to form a dense intergrowth RHO zeolite crystal layer.

In chapter 4, an organic template-free route for synthesizing RHO membranes by the secondary growth method is provided. RHO zeolite membrane showed CO_2/N_2 and CO_2/CH_4 ideal selectivities higher than the Knudsen selectivities. On the other hand, the ideal CO_2/N_2 selectivities were smaller than the reported adsorption selectivities. Contribution of non-zeolitic permeation is one reason for the smaller selectivity. Diffusivity of CO_2 is suspected to be small in RHO zeolitic pores due to the strong affinity lowering the CO_2-selectivity of RHO membranes. RHO membranes showed dehydration performance in water/ethanol and water/isopropanol separations. The highest separation factor obtained for water/isopropanol was 1390 at an isopropanol feed concentration of 95 wt% with a total flux of 0.77 kg m^{-2} h^{-1}. The membrane showed similar separation properties after 30 hours of total testing time, suggesting robustness of the membrane.

In chapter 5, CHA membranes were prepared in the absence of OSDAs. The crystallization kinetics of the fluoride-derived CHA and the effects of gel SiO_2/Al_2O_3 ratio, gel F^-/SiO_2 ratio, fluoride source and synthesis temperature on the morphology

and composition of crystals were investigated. A certain amount of the specific fluoride source (NH_4F) dominated the crystallization of CHA phase in the competitive growth of MER/CHA phases. The fluoride-derived CHA by in-situ synthesis had a particle size of 15-20 μm. Seeded-in-gel synthesis increased the crystallization rate and resulted in the smaller crystals with higher BET surface area and micropore volume. The location of fluorine anion in zeolite framework and the role of fluoride salts on CHA crystallization were also demonstrated.

In chapter 6, the novel precursors were used for membrane surface modification for CHA membranes. Imidazolium-based room temperature ion liquids (RTIL) were effectively grafted on membrane surface by silylation reaction in order to reduce the numbers and sizes of the defects, and thus CO_2/CH_4 selectivies of the membranes were greatly improved. The influences of the type of the cation of RTILs, the type of the balanced anions and treatment conditions on membrane performance were studied. CO_2/CH_4 selectivity of modified membranes was mostly depended on the type of the balanced anion of RTILs, which indicates that the adsorption properties of RTILs over CO_2 are important for CO_2/CH_4 separation by membranes.

要　　旨

チタニウムシリカライト-1, RHO ゼオライト, CHA ゼオライト膜の作製と特性評価

ゼオライト膜は熱化学的安定性を有し、高い分離性能を示すことから、分離や膜反応において注目されている。チタノシリケート（TS-1）などの部分的にヘテロ原子がフレームワーク中の Si^{4+}を置換した MFI 型ゼオライトは触媒活性を示す。近年、我々は H_2O_2 を伴った、IPA の選択的酸化反応へ適用する TS-1 膜の開発を行い、膜分離に触媒反応を組み合わせることが可能となった。煙道ガスや天然ガスからの CO_2 選択分離は、燃料の発熱量の増加や炭素回収の両方において、とても重要である。RHO と CHA ゼオライトの孔径と極性に基づく優れた CO_2/CH_4 選択性から、RHO と CHA ゼオライト膜は CO_2 分離への適用に大きな可能性を秘めている。本論文では TS-1 膜、RHO 膜、CHA 膜の 3 種類のゼオライト膜の製膜とその適用を検討した。本論文は 7 章から構成されている。第 1 章に緒言、第 2 章に TS-1 膜の製膜過程の最適化と触媒性能の解明を示した。 第 3 章では、有機構造規定剤を用いた RHO 膜の製膜と特性評価を行い、第 4 章では、有機構造規定剤を用いない RHO 膜の製膜と特性評価を行った。第 5 章では、有機構造規定剤を用いずにフッ素を用いて合成した CHA ゼオライト膜の製膜と特性評価を行った。第 6 章では、CHA 膜の欠陥を塞ぎ、CO_2/CH_4 選択性を向上させるために、イミダゾリウムを基にした室温イオン液体（RTILs）を用いた新しい後修飾法の開発を行った。第 7 章では、本論文の結論を述べた。

第 2 章では、出発原料モル比が、SiO_2：チタニウム - n - ブトキシド：テトラ - n - プロピルアンモンウムヒドロキシド：H_2O＝1.0：0.031：0.35：28 の合成レシピで、*in-situ* で水熱合成して多孔質ムライト支持体上に製膜した TS-1 膜が高い触媒活性を示すことを明らかにした。最適化された製膜過程は良い再現性を示した。製膜過程で気泡を取り除いた後、合成液に H_2O_2 を補充することが、TS-1 膜の触媒活性に大きな影響を与えることも見出した。さら

に、支持体の前処理方法が TS-1 膜表面の形態に影響を与えることを明らかにした。合成液のエージング温度も TS-1 膜の結晶径に影響を与えた。

第 3 章では 18 クラウン 6 を有機構造規定剤として用いることで、緻密でよく相互成長した RHO 膜を□-Al_2O_3 多孔質支持体上に初めて製膜出来ることを明らかにした。フッ化ナトリウムは RHO 結晶の形態に大きな影響を及ぼし、RHO 結晶の相互成長を導く。さらに、有機構造規定剤の濃度を高くすることで、緻密な RHO ゼオライト膜を形成出来ることが判った。

第 4 章では、有機構造規定剤を使わずに二次成長法によって RHO 膜が製膜出来ることを明らかにした。有機構造規定剤を用いない方法では、適切な前駆体懸濁液のモル組成、水熱合成条件、種層の形成が RHO 膜の形成に大きな影響を与えた。構造規定剤を用いない方法では、膜を合成する際に、高価な有機構造規定剤の消費や焼成時の欠陥の形成、規定剤焼成時の排ガスによる環境への汚染を避けられ、実用化に有利な方法である。

第 5 章では、CHA ゼオライト（Si/Al=2.5~∞）の有機構造規定剤を用いた、種を用いた製膜と種を用いない製膜方法について述べた。CHA の結晶化速度、溶液の SiO_2/Al_2O_3 組成比の影響、溶液の F^-/SiO_2 組成比の影響、フッ素源の種類、合成温度について検討した。特にフッ化アンモニウムを添加した場合、MER 相の成長に比べて、CHA 相の結晶化が支配的となることを明らかにした。フッ素源を加えて種を用いずに合成した CHA の粒径は 15~20 μm であったが、種を用いた合成により、結晶化速度が増加し、高い BET 表面積とミクロ孔体積を有する小さな結晶を得ることができた。ゼオライトフレームワーク中へのフッ素イオンの取り込みと CHA 結晶化におけるフッ化塩の影響を実証出来た。

第 6 章では、新しい前駆体を用いた CHA 膜の表面修飾法を報告した。イミダゾリウムを基にした室温イオン液体（RTIL）を用いて、欠陥の数や大きさを減らすためのシリル化反応により CHA 膜表面をグラフト化した結果、CO_2/CH_4 選択性が大きく向上することを明らかにした。RTILs のカチオン種、対アニオン種、処理条件の影響について検討し、修飾した CHA 膜の CO_2/CH_4 選択性は RTILs の対アニオン種に大きく依存し、RTILs の CO_2 吸着特性が

CO_2/CH_4 の膜分離において重要であることを示した。

List of publications

1. Preparation of chabazite membranes by secondary growth using zeolite-T-directed chabazite seeds.

   Rongfei Zhou, Yuqin Li, Bo Liu, Na Hu, Xiangshu Chen, Hidetoshi Kita

   Microporous and Mesoporous Materials, 175 (2013)128-135

2. Synthesis of low silica-CHA zeolite chabazite in fluoride media without organic structural directing agents and zeolites.

   Bo Liu, Yihong Zheng, Na Hu, Tian Gui, Yuqin Li, Fei Zhang, Rongfei Zhou, Xiangshu Chen, Hidetoshi Kita

   Microporous and Mesoporous Materials, 196 (2014)270-276

3. Preparation of Rho zeolite membranes on tubular supports

   Bo Liu, Izumi Kumakiri, Kazuhiro Tanaka, Xiangshu Chen, Hidetoshi Kita

   Membrane,2016 (Accepted)

Tables

Figures

Chapter 1 General Introduction

1.1 Zeolite

Zeolites are porous aluminosilicalite which have uniform, molecular-sized pores (0.2-2 nm). The framework is composed of four-connected SiO_4 or AlO_4 tetrahedral as TO_4 units, where the tetrahedral framework T atom could also be substituted by B, Ge, Fe, P, Ti etc. Zeolite can be classifed as small pore, medium pore and large pore microporous materials. Small pore structures have six, eight or nine membered rings, medium pore structures have ten membered rings, and large pore zeolites have twelve membered rings.[1] Zeolites could application on adsorption, catalytic and ion-exchange due to their unique selective adsorption, high surface area, excellent chemical and thermal stability. MFI-, LTA- and FAU- type zeolites are common structures that attract tremendous interest both in academic and industry. NaA zeolite (LTA-type) with an equal framework Si/Al ratio that has extremely hydrophilic property, which has been brought into the market for application in dehydration of alchol solution by prepared as a supported membrane material. Titanium silicalite-1 (TS-1) with MFI structure is an excellent catalyst for some oxidation reactions with hydrogen peroxide as oxidant under mild conditions.

Zeolites are usually synthesis from the gel mixture of silica source, aluminum source, alkali and/or an organic structure directing agents (OSDA), and the mineralizing agents (hydroxyl or fluoride anions) by hydrothermal treated at the temperature from 373 to 473 K.[2,3]

1.1.1 Zeolite Titanium Silicalite-1

Titanium Silicalite-1(TS-1) is a crystalline zeotype material in which substitution of Si by Ti and formed tetrahedral [TiO_4] into silicalite-1 framework with a MFI structure.[4] TS-1 was the most noticeable due to its high activity and chemical

stability in a wide range of oxidation reactions, such as selective oxidation of small molecules of alcohols, alkanes, epoxidation alkenes, hydroxylation of aromatics and ammoximation of cyclohexanone to cyclohexanone oxime with H_2O_2 under mild conditions. [5-15] The catalytic activity displays strong size dependence because of the catalytic reaction mainly take place inside the zeolite pores. The smaller particles (less than 300 nm) lead to higher activity due to its larger specific outer surface area and less pore diffusion limitation.[16] TS-1 could be prepared by hydrothermal synthesis using tetraethylorthotitanates (TEOT) as titanium source, tetraethyl orthosilicalite (TEOS) as silicon source, tetrapropylammonium hydroxide (TPAOH) as organic template.[6]

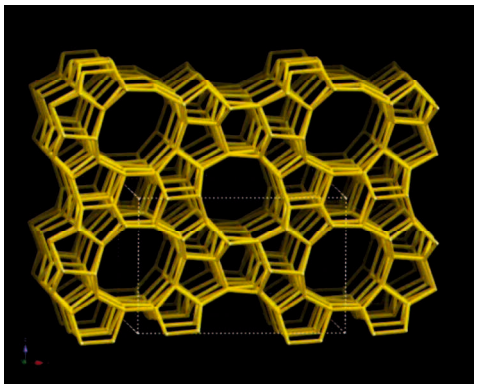

Figure 1-1. Framework type MFI viewed along [010].[17]

1.1.2 Zeolite RHO

Zeolite RHO has a small pores (0.36 nm ×3.6 nm), a relative low Si/Al ratio (2.5-5) and very high pore volume (0.26 cm^3 g^{-1}, the pore volumes of 0.36 cm^3 g^{-1} if no pore space is taken up by extra-framework cations).[17] A remarkably high CO_2/CH_4 adsorption selectivity of RHO zeolite is reported, which is originated from the smaller zeolitic pore size than the size of CH_4 molecule (0.38 nm), strong affinity to CO_2 and the high pore volume.[18]

Zeolite RHO displayed good catalytic property for selective synthesis of

dimethylamine from ammonia and methanol.[19-24] Zeolite RHO has great potential for application as a CO_2 selective adsorbent or as a hydrogen storage material due to its flexibility framework.[25-28] RHO zeolite could be synthesized through the hydrothermal technique both in the presence of organic structural directing agents (OSDAs) and in the absence of OSDAs.[28-31] But it is difficult to obtain the pure single phase unless under the conditions of free of impurities without using 18-crown-6 as OSDA. Pure zeolite RHO crystals could be much easily obtained using 18-Crown-6 ether (1,4,7,10,13,16-hexaoxacyclooctadecane) as OSDA. [28, 31] However, OSDAs should be removed beforehand the applications of RHO zeolites. High cost and the calcination may leads to the formation of defects in/among crystals. Pure RHO zeolite has been synthesized successfully in the absence of cesium cations using polydiallyldimethylammonium chloride (PDADMAC) as the template agent. However, the crystallization time need as long as 8–60 days.[32]

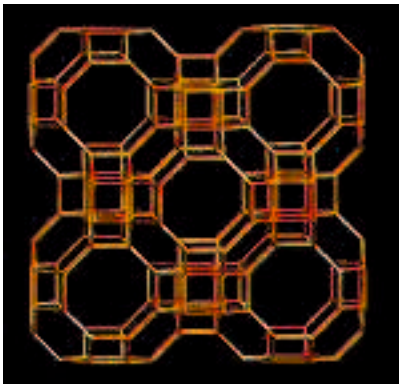

Figure 1-2. Framework type RHO viewed along [001].[17]

1.1.3 Zeolite CHA

CHA-type molecular sieve framework owns a 3-dimensional interconnected pore system with 8-membered ring windows (3.8 Å×3.8 Å) and a relatively low framework density (15.1 T/1000 $Å^3$). Low-silica (chabazite), high-silica (SSZ-13) CHA zeolites and silicoaluminophosphate-34 (SAPO-34) that belongs to CHA-type molecular sieves have attracted many attentions for applications of the separation and catalysis,

in the form of powder and membrane. SAPO-34 molecular sieve was an important catalyst for methanol-to-olefins process. Chabazite and SSZ-13 zeolite were utilized to absorb CO_2 [33] and to catalysis NO_x to NH_3.[34] Chabazite, and (K, Na, Li, Mg, Ca, Ba) ion-exchanged versions of chabazite, have been used in adsorption based processes for air purification and CO_2 capture from combustion flue gases by Webley and co-workers.[35, 36] Also, in patents assigned to Air Products and Chemicals.[37, 38]

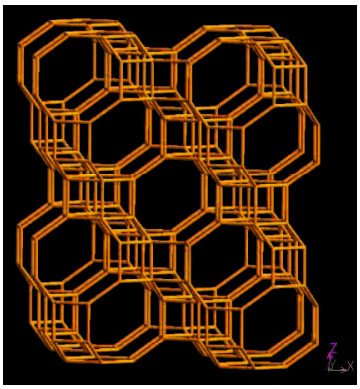

Figure 1-3. Framework type CHA viewed along [010].[17]

1.2 Zeolite membrane

Zeolite membranes have been investigated in various applications, including gas separations, such as carbon dioxide and hydrogen recovery, liquid separations such as dehydration, catalysis as membrane reactor due to their uniform, molecular-size pores, excellent thermal, high mechanical and chemical stability. MFI type zeolite is the most studied type of zeolite membranes for gas separations, [39-48] while various other types, such as LTA[49-51], MOR[52-57], FAU[58-62], CHA[63-67], MEL[68], AFI[69], FER[70], BEA[71], GIS[72], ANA[73], DON[74], OFF[75] and ATN[75] have aslo been employed as separation membranes.

1.2.1 Synthesis of zeolite membranes

Zeolite membranes are usually prepared by *in-situ* hydrothermal synthesis and secondary (or seeded) hydrothermal synthesis method. Hydrothermal synthesis

involves crystallization of a zeolite layer onto a porous support from a gel that is usually composed of water (deionized or distilled water), silica source (colloidal silica, tetraethyl orthosilicalite or fumed silica powders), aluminum source (aluminium hydroxide, sodium aluminate, aluminium nitrate or aluminum sulfate), organic structural directing agents, and sometimes a mineralizing agent (sodium hydroxide, potassium hydroxide or fluoride salts). It consists of placing a suitable support in contact with a precursor gel or clear solution in an autoclave. The hydrothermal reaction time, temperature, and gel composition for crystallization depend on the different type of zeolites. Generally, porous mullite, alumina or stainless steel tubes or discs are often used as supports.

In-situ hydrothermal synthesis is the most common method used to prepare supported zeolite membranes. Zeolite crystals nucleate on the surface of support and then grow to form a continuous zeolite film under hydrothermal conditions. The hydrothermal synthesis conditions such as gel compositions, hydrothermal reaction temperature and time, and template wipe-off have great effect on the synthesis of high quality zeolite membranes. Crystals could also nucleate in the bulk solution, which is not preferred as competitive growth and the crystals grow on the surface of support may be very difficult.

The secondary (or seeded) growth method is an effective technique for the preparation of high quality supported zeolite membranes. Zeolite nucleation is largely decoupled from zeolite growth by depositing or coating or vacuumed seeding a layer of zeolite seed crystals for the promotion of nucleation of crystals on the support surface. The coating methods include rub-coating zeolite powders by hands or dip-coating or vacuumed seeding zeolite particles in suspension with a relative low pH environment. Generally, the secondary growth method requires much more dilute synthesis solution (a diluted precursor gel or solution may avoided or weaken homogeneous nucleation in bulk solution), lower synthesis temperature and shorter synthesis time as compared with *in-situ* hydrothermal synthesis. It is much easy to preparation of much dense, well intergrowth and continuous zeolite film on the

surface of support using secondary hydrothermal growth technique since it decouples nucleation from growth.

1.2.2 Separation mechanism of zeolite membrane

Zeolite membranes separate mixtures by molecular sieving, selective-adsorption and differences in diffusion rates. For the molecular sieving, larger molecules are excluded from the pores due to their size, while smaller molecules can diffuse through the pores. As for the selective adsorption, the adsorbed molecules are effectively transported through the membrane. The separation mechanism for water/organic separations is mainly by selective-adsorption due to the hydrophilic/hydrophobic nature of zeolites. The third separation mechanism rely on differences in diffusion rates, molecules with high diffusivity may be separated from the slower diffusing molecules.

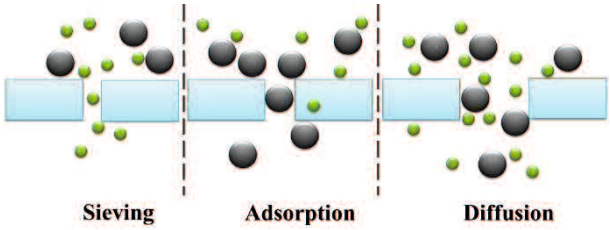

Figure 1-4. Three mechanisms for separation in a zeolite membrane

In addition to zeolite pores, zeolite membranes with reasonable separation performance have non-zeolitic defects such as inter-crystalline boundaries. The adsorption diffusion mechanism also applies to these defects. In addition, Knudsen diffusion contributes to transport through pores larger than 2 nm.

1.3 Applications of zeolite membranes

1.3.1 Application on gas separation

High volume discharge of CO_2 into the atmosphere due to consumption of large amounts of fossil fuels has become one of the most serious global environmental problems. Separation and recovery of CO_2 from natural gas and flue gas are, therefore, of great interest. Due to the membrane separation is energy-efficient, selective removal of CO_2 from flue gas and natural gas by means of membrane separation has been studied very actively. Zeolite membranes grew on porous substrates become good candidates for CO_2 separation from natural gas due to its unique molecular sieve, selective absorption and high thermal and mechanical stabilities.

CO_2 separation has been reported for membranes of different type of zeolite frameworks with different pore size and adsorption properties. Many kinds of zeolite membranes such as FAU-type (12-ring large pore), MFI-type (10-ring medium pore) and ERI-type, DDR-type and CHA-type (8-ring small pore) were reported to application in CO_2 separation. Hasegawa *et al.* [76] reported an FAU-type zeolite membrane with a CO_2/CH_4 selectivity of 28 and CO_2/N_2 selectivity of 78 at 308K. Bernal *et al.*[77] using stainless steel tubular supported MFI-type (ZSM-5) membranes for the separation of CO_2/N_2 mixtures and obtained a CO_2/N_2 separation factor of 13.7 with a permeance of 2.6×10^{-6} mol $(m^2\ s\ Pa)^{-1}$. Cui *et al.* [78] reported a porous tubular supported T-type zeolite membrane displayed extremely CO_2/CH_4 separation selectivity of 400 and had a CO_2 permeance of 4.6×10^{-8} mol $(m^2\ s\ Pa)^{-1}$ at a pressure drop of 0.1 MPa. Tomita *et al.*[79] prepared a DDR membrane had a CO_2/CH_4 selectivity of 280 and a CO_2 permeance of 7×10^{-8} mol $(m^2\ s\ Pa)^{-1}$ for the CO_2/CH_4 mixture. Zhou *et al.*[67] prepared a SSZ-13 (high silica CHA) zeolite membrane displayed a very high CO_2/CH_4 selectivity of 300 and had a high CO_2 permeance of 2.9 at 0.2 MPa feed pressure.

Zeolite membrane also received great attract for H_2 separation. MFI-type zeolite is

the most studied type of zeolite membranes for H_2 separations due to its pore size and ease of preparation. Tang *el al.*[80] modified a MFI-type zeolite membrane by catalytic cracking of methyl diethoxysilane and the modified zeolite membrane displayed a H_2/CO_2 perm-selectivity of 68 and had a H_2 permeance of 2.94×10^{-7} mol $(m^2\ s\ Pa)^{-1}$. Wang *el al.* [81,82] prepared a highly stable bilayer MFI-type zeolite membrane exhibited H_2 permeance of 1.2×10^{-7} mol $(m^2\ s\ Pa)^{-1}$ and H_2/CO_2, H_2/CO and H_2/H_2O vapor selectivity of 23, 28 and 180, respectively.

1.3.2 Application on organic liquid separation

Separation of water from organic component

General, hydrophilic zeolite membranes are used for dehydration from organics due to their strongly water adsorption property, while the hydrophobic zeolite membranes are often used to separate organics from water. The LTA-type zeolite membranes are highly selective in the separation of water from organic solutions because of their extremely hydrophilic and their suitable pore size (smaller than water but larger than most organic molecules). The hydrophilic NaA (LTA-type) zeolite membranes with excellent pervaporation performance have been applied in industry for dehydration from alchol solution by Mitsui Engineering and Shipbuilding Co. Ltd.[83] However, NaA zeolite membranes have low acid resistance because of its low framework Si/Al ratio. Some kinds of zeolite membranes with much higher Si/Al ratios with fine hydrophilicity and relative acid-stability, such as T-, X- , Y-type and ZSM-5 are also used for removed water from alchol solutions. However, the fluxes and separation factors are generally low because of their medium or larger pore size for these membranes. Zeolite membranes with small pores and medium framework Si/Al ratios, such as MOR-type (have large channels of 0.67 × 0.7 nm but with hydrophilic small channels of 0.26 × 0.56 nm, with a framework Si/Al ratios of 5-6) and CHA-type (0.38 nm pore size, with a framework Si/Al ratios of 2-∞) zeolite membranes would be much preferred for the separation of water in water-rich and acidic surroundings mixtures because of their suitable pore size, good hydrophilic property and high

chemical stability.

Separation of organic compounds from water

Highly hydrophobic zeolite membranes, such as MFI-type (silicalite-1[84], ZSM-5[85]), and β-type[86] have been used to separate organic compounds from water. Hydrophobic silicalite-1 membrane is possible to concentrate bioethanol due to its high pervaporation performance in the separation of an ethanol/water mixture, which has an important potential to replace the extremely energy consuming distillation process.

Lin *et al.* [47] reported a tubular supported Silicalite-1 membrane with a 14 mol/m^2 h flux and an ethanol/H_2O separation factor of 106 for a 5 wt. % ethanol/water feed at 333 K. Matsuda *et al.*[87] reported a silicone-coated silicalite-1 membrane with a higher separation factor (125), but a significantly lower flux (3.7 mol/m^2 h) for a 4 wt.% ethanol/H_2O feed at 303 K.

Organic/organic mixtures

Zeolite membranes have been employed to separate organic mixtures due to its selective adsorption and/or suitable molecular size pores. Methyl tert-Butyl Ether (MTBE) is an important organic that often used as a gasolines additive. It usually made from isobutylene and methanol.[88] MTBE is more organophilic than methanol. High hydrophobic silicalite-1(0.55 nm pore size) membrane could be used to separate methanol (0.39 nm) from MTBE (0.62 nm) due to molecular sieving and selective sorption. Sano *et al.*[89] prepared a silicalite-1 zeolite membrane that displayed high methanol perm-selectivity from methanol/MTBE mixtures. High hydrophilic FAU (0.73 nm pore size) zeolite membrane could also be used to separate methanol from MTBE due to an adsorption/diffusion mechanism. Kita *et al.*[90] showed that NaY (FAU) zeolite membrane could separate methanol from methanol/MTBE mixture with a high separation factor (10,000) for a 5 wt.% methanol/MTBE feed at 323 K.

1.3.3 Application on chemical catalytic reaction

Zeolite membranes are also promising for catalytic membrane reactor processes

where the separation process integrated with catalytic reaction can improve reaction selectivity by selectively removing one of the products from the reaction mixture or by the controlled addition of a reactant through the membrane. The reaction conversion also can be improved by removing one of the products in equilibrium limited reaction.

Jeong *et al.*[91] reported a porous α-Al_2O_3 tube supported FAU-type zeolite membrane used in the selective separation of benzene and hydrogen from cyclohexane. The conversion of cyclohexane in the FAU-zeolite membrane reactor improved from 32.2% (calculated equilibrium value) to 72.1% at 473K due to the simultaneous removal of hydrogen and benzene from the reaction site. Ying *et al.* [92] reported a novel Fe-ZSM-5 zeolite membrane for catalytic wet peroxide oxidation of phenol in a membrane reactor. The phenol conversion reached as high as 95% with Fe loading around 25% at the temperature of 353 K. Lu *et al.*[93] reported a titanium silicalite-1 membrane for the hydroxylation of phenol to hydroquinone and catechol and displayed a high selectivity for phenol (> 95%). Salomón *et al.*[94] used mordenite and NaA zeolite membranes to selective-removal of water produced in the esterification of methyl-*tert*-butyl ether (MTBE) from *tert*-butanol and methanol. The conversions obtained in the zeolite membrane reactor were higher than the equilibrium predictions.

1.4 Scope and objective of this work

In this thesis, we will study the preparation and application of titanium silicalite-1 (TS-1) membrane, RHO membrane and CHA membrane. The research emphasis will be of the preparation of TS-1 membrane and the application it in some oxidation. To study the PV-aided catalytic performance of titanium silicalite-1 (TS-1) membrane, optimization the preparation process of TS-1 membrane, especially to improve the reproducibility. These research results and discussions will be listed in chapter 2. Zeolite RHO is able to successfully separate CO_2 from CH_4 with the highest

selectivity ever observed on the basis of pore diameter and surface polarity as many researchers reported, but as we know from literatures that it has yet no open report about the preparation of RHO membrane. We will try to prepare RHO membrane on porous mullite and α-Al_2O_3 tubular support by hydrothermal method in the presence of organic structure directing agent (18 Crown 6 ether) or in the absence of any organic template, and its single gas and PV performance will be test. The related results will be written in chapter 3 and 4. CHA zeolite (Si/Al=2.5-3.5) will be prepared in the absence of organic structural directing agents (OSDAs) by *in-situ* and seeded synthesis. The crystallization kinetics of the fluoride-derived chabazite and the effects of gel SiO_2/Al_2O_3 ratio, gel F^-/SiO_2 ratio, fluoride source and synthesis temperature on the morphology and composition of crystals will be investigated. The related results will be written in chapter 5. A novel post-modification using imidazolium-based room temperature ionic liquids (RTILs) precursors was designed to patch CHA membrane defects for improving CO_2/CH_4 selectivity. The influences of the type of the cation of RTILs, the type of the balanced anions and treatment conditions on membrane performance will be study. The related results and discussions will be written in chapter 6. In chapter 7 the main results and conclusions obtained in this thesis will be reviewed.

References

[1] M. Den Exter, J. Jansen, J. van de Graaf, F. Kapteijn, J. Moulijn, H. Van Bekkum, Zeolite-based membranes preparation, performance and prospects, Studies in Surface Science and Catalysis, 102 (1996) 413-454.

[2] C.S. Cundy, P.A. Cox, The hydrothermal synthesis of zeolites: Precursors, intermediates and reaction mechanism, Microporous and Mesoporous Materials, 82 (2005) 1-78.

[3] A. Corma, M.E. Davis, Issues in the Synthesis of Crystalline Molecular Sieves:

Towards the Crystallization of Low Framework-Density Structures, ChemPhysChem, 5 (2004) 304-313.

[4] J. To, P. Sherwood, A.A. Sokol, I.J. Bush, C.R.A. Catlow, H.J. van Dam, S.A. French, M.F. Guest, QM/MM modelling of the TS-1 catalyst using HPCx, Journal of Materials Chemistry, 16 (2006) 1919-1926.

[5] M. Taramasso, G. Perego, B. Notari, Preparation of porous crystalline synthetic material comprised of silicon and titanium oxides, in, Google Patents, 1983.

[6] C. Neri, B. Anfossi, A. Esposito, F. Buonomo, Process for the epoxidation of olefinic compounds, in, Google Patents, 1989.

[7] S. Bordiga, S. Coluccia, C. Lamberti, L. Marchese, A. Zecchina, F. Boscherini, F. Buffa, F. Genoni, G. Leofanti, XAFS Study of Ti-Silicalite: structure of framework Ti (IV) in the presence and absence of reactive molecules (H_2O, NH_3) and comparison with Ultraviolet-Visible and IR results, The Journal of Physical Chemistry, 98 (1994) 4125-4132.

[8] G. Peregot, G. Bellussi, C. Corno, M. Taramasso, F. Buonomot, A. Esposito, Titanium-silicalite: a novel derivative in the pentasil family, Studies in Surface Science and Catalysis, 28 (1986) 129-136..

[9] T. Blasco, M.A. Camblor, A. Corma, P. Esteve, A. Martínez, C. Prieto, S. Valencia, Unseeded synthesis of Al-free Ti-β zeolite in fluoride medium: a hydrophobic selective oxidation catalyst, Chemical Communications, (1996) 2367-2368.

[10] M. Moliner, P. Serna, A. Cantín, G. Sastre, M.J. Díaz-Cabañas, A. Corma, Synthesis of the Ti− silicate form of BEC polymorph of β-zeolite assisted by molecular modeling, The Journal of Physical Chemistry C, 112 (2008) 19547-19554.

[11] P. Wu, T. Tatsumi, T. Komatsu, T. Yashima, Hydrothermal Synthesis of a Novel Titanosilicate with MWW Topology, Chemistry Letters, (2000) 774-775.

[12] C. Perego, A. Carati, P. Ingallina, M.A. Mantegazza, G. Bellussi, Production of titanium containing molecular sieves and their application in catalysis, Applied Catalysis A: General, 221 (2001) 63-72.

[13] V. Hulea, F. Fajula, J. Bousquet, Mild oxidation with H_2O_2 over Ti-containing

molecular sieves—a very efficient method for removing aromatic sulfur compounds from fuels, Journal of Catalysis, 198 (2001) 179-186.

[14] B. Notari, Titanium silicalites, Catalysis Today, 18 (1993) 163-172.

[15] R. Landau, G. Sullivan, D. Brown, Propylene-oxide by the co-product process, Chemtech, 9 (1979) 602-607.

[16] International Zeolite Association: http://www.iza-structure.org/

[17] M. Palomino, A. Corma, J.L. Jordá, F. Rey, S. Valencia, Zeolite RHO: a highly selective adsorbent for CO_2/CH_4 separation induced by a structural phase modification, Chemical Communications, 48 (2012) 215-217.

[18] M.M. Lozinska, J.P. Mowat, P.A. Wright, S.P. Thompson, J.L. Jorda, M. Palomino, S. Valencia, F. Rey, Cation Gating and Relocation during the Highly Selective “Trapdoor” Adsorption of CO_2 on Univalent Cation Forms of Zeolite RHO, Chemistry of Materials, 26 (2014) 2052-2061.

[19] L. Abrams, D.R. Corbin, M. Keane, Synthesis of dimethylamine by zeolite RHO: A rational basis for selectivity, Journal of Catalysis, 126 (1990) 610-618.

[20] D.R. Corbin, S. Schwarz, G.C. Sonnichsen, Methylamines synthesis: A review, Catalysis Today, 37 (1997) 71-102.

[21] L.H. Callanan, C.T. O'Connor, E. van Steen, The effect of the adsorption properties of steamed zeolite RHO on its methanol amination activity, Microporous and Mesoporous Materials, 35 (2000) 163-172.

[22] L.H. Callanan, E. van Steen, C.T. O'Connor, Improved selectivity to lower substituted methylamines using hydrothermally treated zeolite RHO, Catalysis Today, 49 (1999) 229-235.

[23] H.-Y. Jeon, C.-H. Shin, H.J. Jung, S.B. Hong, Catalytic evaluation of small-pore molecular sieves with different framework topologies for the synthesis of methylamines, Applied Catalysis A: General, 305 (2006) 70-78.

[24] S. Altwasser, R. Gläser, J. Weitkamp, Ruthenium-containing small-pore zeolites for shape-selective catalysis, Microporous and Mesoporous Materials, 104 (2007) 281-288.

[25] V.V. Krishnan, S.L. Suib, D.R. Corbin, S. Schwarz, G.E. Jones, Encapsulation studies of hydrogen on cadmium exchanged zeolite RHO at atmospheric pressure, Catalysis Today, 31 (1996) 199-205.

[26] H. Langmi, A. Walton, M. Al-Mamouri, S. Johnson, D. Book, J. Speight, P. Edwards, I. Gameson, P. Anderson, I. Harris, Hydrogen adsorption in zeolites A, X, Y and RHO, Journal of Alloys and Compounds, 356 (2003) 710-715.

[27] H. Langmi, D. Book, A. Walton, S. Johnson, M. Al-Mamouri, J. Speight, P. Edwards, I. Harris, P. Anderson, Hydrogen storage in ion-exchanged zeolites, Journal of Alloys and Compounds, 404 (2005) 637-642.

[28] S. Araki, Y. Kiyohara, S. Tanaka, Y. Miyake, Crystallization process of zeolite RHO prepared by hydrothermal synthesis using 18-crown-6 ether as organic template, Journal of Colloid and Interface Science, 376 (2012) 28-33.

[29] H.E. Robson, D.P. Shoemaker, R.A. Ogilvie, P.C. Manor, Synthesis and crystal structure of zeolite RHO—a new zeolite related to Linde type A, in, 1973.

[30] L. Garces, V. Makwana, B. Hincapie, A. Sacco, S. Suib, Selective N, N-methylation of aniline over cocrystallized zeolites RHO and zeolite X (FAU) and over Linde type L (Sr, K-LTL), Journal of Catalysis, 217 (2003) 107-116.

[31] T. Chatelain, J. Patarin, E. Fousson, M. Soulard, J. Guth, P. Schulz, Synthesis and characterization of high-silica zeolite RHO prepared in the presence of 18-crown-6 ether as organic template, Microporous Materials, 4 (1995) 231-238.

[32] S. Liu, P. Zhang, X. Meng, D. Liang, N. Xiao, F.-S. Xiao, Cesium-free synthesis of aluminosilicate RHO zeolite in the presence of cationic polymer, Microporous and Mesoporous Materials, 132 (2010) 352-356.

[33] M.R. Hudson, W.L. Queen, J.A. Mason, D.W. Fickel, R.F. Lobo, C.M. Brown, Unconventional, highly selective CO_2 adsorption in zeolite SSZ-13, Journal of the American Chemical Society, 134 (2012) 1970-1973.

[34] L. Ren, L. Zhu, C. Yang, Y. Chen, Q. Sun, H. Zhang, C. Li, F. Nawaz, X. Meng, F.-S. Xiao, Designed copper-amine complex as an efficient template for one-pot synthesis of Cu-SSZ-13 zeolite with excellent activity for selective catalytic reduction

of NOx by NH_3, Chemical Communications, 47 (2011) 9789-9791.

[35] R.K. Singh, P. Webley, Adsorption of N_2, O_2, and Ar in potassium chabazite, Adsorption, 11 (2005) 173-177.

[36] J. Zhang, R. Singh, P.A. Webley, Alkali and alkaline-earth cation exchanged chabazite zeolites for adsorption based CO_2 capture, Microporous and Mesoporous Materials, 111 (2008) 478-487.

[37] F.N. Ridha, P.A. Webley, Anomalous Henry's law behavior of nitrogen and carbon dioxide adsorption on alkali-exchanged chabazite zeolites, Separation and Purification Technology, 67 (2009) 336-343.

[38] C.G. Coe, D.A. Roberts, Process for the purification of permanent gases using chabazite adsorbents, in, Google Patents, 1988.

[39] T.C. Bowen, H. Kalipcilar, J.L. Falconer, R.D. Noble, Pervaporation of organic/water mixtures through B-ZSM-5 zeolite membranes on monolith supports, Journal of Membrane Science, 215 (2003) 235-247.

[40] W.J. Bakker, L.J. Van Den Broeke, F. Kapteijn, J.A. Moulijn, Temperature dependence of one-component permeation through a silicalite-1 membrane, AIChE Journal, 43 (1997) 2203-2214.

[41] J. Hedlund, J. Sterte, M. Anthonis, A.-J. Bons, B. Carstensen, N. Corcoran, D. Cox, H. Deckman, W. De Gijnst, P.-P. de Moor, High-flux MFI membranes, Microporous and Mesoporous Materials, 52 (2002) 179-189.

[42] T. Sano, H. Yanagishita, Y. Kiyozumi, F. Mizukami, K. Haraya, Separation of ethanol/water mixture by silicalite membrane on pervaporation, Journal of Membrane Science, 95 (1994) 221-228.

[43] M.C. Lovallo, A. Gouzinis, M. Tsapatsis, Synthesis and characterization of oriented MFI membranes prepared by secondary growth, American Institute of Chemical Engineers. AIChE Journal, 44 (1998) 1903.

[44] A. Burggraaf, Z. Vroon, K. Keizer, H. Verweij, Permeation of single gases in thin zeolite MFI membranes, Journal of Membrane Science, 144 (1998) 77-86.

[45] M. Noack, P. Kölsch, J. Caro, M. Schneider, P. Toussaint, I. Sieber, MFI

membranes of different Si/Al ratios for pervaporation and steam permeation, Microporous and Mesoporous Materials, 35 (2000) 253-265.

[46] K. Wegner, J. Dong, Y. Lin, Polycrystalline MFI zeolite membranes: xylene pervaporation and its implication on membrane microstructure, Journal of Membrane Science, 158 (1999) 17-27.

[47] X. Lin, H. Kita, K.-i. Okamoto, A novel method for the synthesis of high performance silicalite membranes, Chemical Communications, (2000) 1889-1890.

[48] T.Q. Gardner, A.I. Flores, R.D. Noble, J.L. Falconer, Transient measurements of adsorption and diffusion in H-ZSM-5 membranes, AIChE Journal, 48 (2002) 1155-1167.

[49] K. Aoki, K. Kusakabe, S. Morooka, Gas permeation properties of A-type zeolite membrane formed on porous substrate by hydrothermal synthesis, Journal of Membrane Science, 141 (1998) 197-205.

[50] H. Kita, K. Horii, Y. Ohtoshi, K. Tanaka, K.-I. Okamoto, Synthesis of a zeolite NaA membrane for pervaporation of water/organic liquid mixtures, Journal of Materials Science Letters, 14 (1995) 206-208.

[51] J. Hedlund, B. Schoeman, J. Sterte, Ultrathin oriented zeolite LTA films, Chemical Communications, (1997) 1193-1194.

[52] A. Navajas, R. Mallada, C. Téllez, J. Coronas, M. Menéndez, J. Santamaría, Preparation of mordenite membranes for pervaporation of water-ethanol mixtures, Desalination, 148 (2002) 25-29.

[53] N. Nishiyama, K. Ueyama, M. Matsukata, A defect-free mordenite membrane synthesized by vapour-phase transport method, J. Chem. Soc., Chem. Commun., (1995) 1967-1968.

[54] S. Yamazaki, K. Tsutsumi, Adsorption characteristics of synthesized mordenite membranes, Adsorption, 3 (1997) 165-171.

[55] X. Lin, E. Kikuchi, M. Matsukata, Preparation of mordenite membranes on α-alumina tubular supports for pervaporation of water–isopropyl alcohol mixtures, Chemical Communications, (2000) 957-958.

[56] R. Zhou, Z. Hu, N. Hu, L. Duan, X. Chen, H. Kita, Preparation and microstructural analysis of high-performance mordenite membranes in fluoride media, Microporous and Mesoporous Materials, 156 (2012) 166-170.

[57] M.-H. Zhu, S.-L. Xia, X.-M. Hua, Z.-J. Feng, N. Hu, F. Zhang, I. Kumakiri, Z.-H. Lu, X.-S. Chen, H. Kita, Rapid Preparation of Acid-Stable and High Dehydration Performance Mordenite Membranes, Industrial & Engineering Chemistry Research, 53 (2014) 19168-19174.

[58] Z. Wang, I. Kumakiri, K. Tanaka, X. Chen, H. Kita, NaY zeolite membranes with high performance prepared by a variable-temperature synthesis, Microporous and Mesoporous Materials, 182 (2013) 250-258.

[59] I. Kumakiri, K. Hashimoto, Y. Nakagawa, Y. Inoue, Y. Kanehiro, K. Tanaka, H. Kita, Application of FAU zeolite membranes to alcohol/acrylate mixture systems, Catalysis Today, 236 (2014) 86-91.

[60] H. Kita, K. Fuchida, T. Horita, H. Asamura, K. Okamoto, Preparation of faujasite membranes and their permeation properties, Separation and Purification Technology, 25 (2001) 261-268.

[61] K. Kusakabe, T. Kuroda, K. Uchino, Y. Hasegawa, S. Morooka, Gas permeation properties of ion-exchanged faujasite-type zeolite membranes, American Institute of Chemical Engineers. AIChE Journal, 45 (1999) 1220.

[62] S. Li, V.A. Tuan, J.L. Falconer, R.D. Noble, X-type zeolite membranes: preparation, characterization, and pervaporation performance, Microporous and Mesoporous Materials, 53 (2002) 59-70.

[63] H. Kalipcilar, T.C. Bowen, R.D. Noble, J.L. Falconer, Synthesis and separation performance of SSZ-13 zeolite membranes on tubular supports, Chemistry of Materials, 14 (2002) 3458-3464.

[64] J.C. Poshusta, V.A. Tuan, J.L. Falconer, R.D. Noble, Synthesis and permeation properties of SAPO-34 tubular membranes, Industrial & Engineering Chemistry Research, 37 (1998) 3924-3929.

[65] R. Zhou, Y. Li, B. Liu, N. Hu, X. Chen, H. Kita, Preparation of chabazite

membranes by secondary growth using zeolite-T-directed chabazite seeds, Microporous and Mesoporous Materials, 179 (2013) 128-135.

[66] Y. Hasegawa, H. Hotta, K. Sato, T. Nagase, F. Mizukami, Preparation of novel chabazite (CHA)-type zeolite layer on porous α-Al_2O_3 tube using template-free solution, Journal of Membrane Science, 347 (2010) 193-196.

[67] Y. Zheng, N. Hu, H. Wang, N. Bu, F. Zhang, R. Zhou, Preparation of steam-stable high-silica CHA (SSZ-13) membranes for CO_2/CH_4 and C_2H_4/C_2H_6 separation, Journal of Membrane Science, 475 (2015) 303-310.

[68] V.A. Tuan, S. Li, R.D. Noble, J.L. Falconer, Preparation and pervaporation properties of a MEL-type zeolite membrane, Chemical Communications, (2001) 583-584.

[69] Y. Chiou, T. Tsai, S. Sung, H. Shih, C. Wu, K. Chao, Synthesis and characterization of zeolite (MFI) membrane on anodic alumina, J. Chem. Soc., Faraday Trans., 92 (1996) 1061-1066.

[70] N. Nishiyama, K. Ueyama, M. Matsukata, Synthesis of FER membrane on an alumina support and its separation properties, Studies in Surface Science and Catalysis, 105 (1997) 2195-2202.

[71] V.A. Tuan, S. Li, J.L. Falconer, R.D. Noble, In situ crystallization of beta zeolite membranes and their permeation and separation properties, Chemistry of Materials, 14 (2002) 489-492.

[72] J. Dong, Y. Lin, In situ synthesis of P-type zeolite membranes on porous α-alumina supports, Industrial & Engineering Chemistry Research, 37 (1998) 2404-2409.

[73] N. Nishiyama, K. Ueyama, M. Matsukata, Synthesis of defect-free zeolite-alumina composite membranes by a vapor-phase transport method, Microporous Materials, 7 (1996) 299-308.

[74] T. Muñoz, K.J. Balkus, Preparation of oriented zeolite UTD-1 membranes via pulsed laser ablation, Journal of the American Chemical Society, 121 (1999) 139-146.

[75] K. Tanaka, R. Yoshikawa, C. Ying, H. Kita, K.-i. Okamoto, Application of zeolite

membranes to esterification reactions, Catalysis Today, 67 (2001) 121-125.

[76] Y. Hasegawa, T. Tanaka, K. Watanabe, Separation of CO_2/CH_4 and CO_2/N_2 systems using ion-exchanged FAU-type zeolite membranes with different Si/Al ratios, Korean Journal of Chemical Engineering, 19(2002) 309-313.

[77] M.P. Bernal, J. Coronas M. Menéndez, J. Santamaría, Separation of CO_2/N_2 mixtures using MFI - type zeolite membranes, AIChE Journal, 50 (2004) 127-135.

[78] Y. Cui, H. Kita, K.-i. Okamoto, Preparation and gas separation performance of zeolite T membrane, Journal of Materials Chemistry, 14 (2004) 924-932.

[79] T. Tomita, K. Nakayama, H. Sakai, Gas separation characteristics of DDR type zeolite membrane, Microporous and Mesoporous Materials, 68 (2004) 71-75.

[80] Z. Tang, S.-J. Kim, G.K. Reddy, J. Dong, P. Smirniotis, Modified zeolite membrane reactor for high temperature water gas shift reaction, Journal of Membrane Science, 354 (2010) 114-122.

[81] H. Wang, Y. Lin, Synthesis and modification of ZSM-5/silicalite bilayer membrane with improved hydrogen separation performance, Journal of Membrane Science, 396 (2012) 128-137.

[82] H. Wang, X. Dong, Y. Lin, Highly stable bilayer MFI zeolite membranes for high temperature hydrogen separation, Journal of Membrane Science, 450 (2014) 425-432.

[83] S.L. Wee, C.T. Tye, S. Bhatia, Membrane separation process—pervaporation through zeolite membrane, Separation and Purification Technology, 63 (2008) 500-516.

[84] T. Sano, M. Hasegawa, Y. Kawakami, Y. Kiyozumi, H. Yanagishita, D. Kitamoto, F. Mizukami, Potentials of silicalite membranes for the separation of alcohol/water mixtures, Studies in Surface Science and Catalysis, 84 (1994) 1175-1182.

[85] S. Li, V.A. Tuan, R.D. Noble, J.L. Falconer, A Ge-substituted ZSM-5 zeolite membrane for the separation of acetic acid from water, Industrial & Engineering Chemistry Research, 40 (2001) 6165-6171.

[86] V.A. Tuan, L.L. Weber, J.L. Falconer, R.D. Noble, Synthesis of B-substituted β-zeolite membranes, Industrial & Engineering Chemistry Research, 42 (2003) 3019-3021.

[87] H. Matsuda, H. Yanagishita, H. Negishi, D. Kitamoto, T. Ikegami, K. Haraya, T. Nakane, Y. Idemoto, N. Koura, T. Sano, Improvement of ethanol selectivity of silicalite membrane in pervaporation by silicone rubber coating, Journal of Membrane Science, 210 (2002) 433-437.

[88] T.C. Bowen, R.D. Noble, J.L. Falconer. Fundamentals and applications of pervaporation through zeolite membranes, Journal of Membrane Science, 245 (2004) 1-33.

[89] T. Sano, M. Hasegawa, Y. Kawakami, H. Yanagishita, Separation of methanolrmmethyl-tert-butyl ether mixture by pervaporation using silicalite membrane, Journal of Membrane Science, 107 (1995) 193.

[90] H. Kita, T. Inoue, H. Asamura, K. Tanaka, K. Okamoto, NaY zeolite membrane for the pervaporation separation of methanol–methyl tert-butyl ether mixtures, Chemical Communications, (1997) 45-46.

[91] B.H. Jeong, K.I. Sotowa, K. Kusakabe, Catalytic dehydrogenation of cyclohexane in an FAU-type zeolite membrane reactor, Journal of Membrane Science, 224 (2003) 151-158.

[92] Y. Yan, S. Jiang, H. Zhang, X. Zhang, Preparation of novel Fe-ZSM-5 zeolite membrane catalysts for catalytic wet peroxide oxidation of phenol in a membrane reactor, Chemical Engineering Journal, 259 (2015) 243-251.

[93] C. Lu, R. Chen, W. Xing, W. Jin, N. Xu, A submerged membrane reactor for continuous phenol hydroxylation over TS‐1, AIChE Journal, 54 (2008) 1842-1849.

[94] M.A. Salomón, J. Coronas, M. Menéndez, J. Santamaría, Synthesis of MTBE in zeolite membrane reactors, Applied Catalysis A: General, 200 (2000) 201-210.

Chapter 2 Catalytic Activity of Titanium Silicalite-1 Crystals and Tubular Supported TS-1Membrane

2.1 Introduction

TS-1 zeolite has MFI structure containing Ti^{4+} in the framework with a media pore system (0.55 nm).[1] TS-1 is known as an efficient catalyst for selective oxidation of small molecules of alcohols, alkanes, epoxidation alkenes, hydroxylation of aromatics and ammoximation of cyclohexanone to cyclohexanone oxime with H_2O_2 under mild conditions.[2-8]

However, one disadvantage limit TS-1 zeolite powder application as catalyst, which is the difficulty in recovering the nano-size powders from the catalytic reaction mixture.[9-12] The supported TS-1 membrane as a catalytic membrane reactor can successfully resolve this problem and what's more important is that it can make the reaction process continuous. When TS-1 membrane is used for the catalysis reaction under pervaporation condition, the substrate molecules are transported to the outer surface of a zeolite layer and diffuse into the channels of TS-1 crystal and be adsorbed on the active sites, and thus undergo reactions over active sites of the zeolite.[13]

There are few reports on the supported TS-1 membrane due to the difficulty in preparation.[14] TS-1 films and membranes have been prepared on monoliths [15, 16] and other supports[17-20] by different synthesis methods. Our group have devoted to many efforts on the preparation of porous tubular supported TS-1 membrane for years. Nowadays, some results have been sketchily reported, including the separation ability of TS-1 membrane prepared by hydrothermal and microwave method and the catalytic activity of TS-1 membrane prepared by hydrothermal method.[21, 22] A thorough investigation is necessary for further understanding the property of TS-1 membrane and optimizing the preparation process of TS-1 membrane to improve the reproducibility. In this work, the effect of reaction condition of the oxidation of IPA on the catalytic activity of TS-1 membrane and the reproducibility of TS-1 membrane

was studied.

2.2 Experiment

2.2.1 Materials and Instrumental

Preparation of zeolite membranes was carried out in titanium autoclaves at a certain temperature under autogeneous pressure. Silicon and titanium sources were tetraethyl orthosilicalite (TEOS, Aldrich, 98wt%), titanium n-butoxide (TBOT, Aldrich, 97wt%), respectively. Tetrapropylammonium hydroxide (TPAOH, Kanto Chem. Ltd., 20.3 wt % in H_2O) was used as template. Deionized water was obtained from a Milipore Mill-Q purification system.

Mullite tubes with an average pore size of 1.3μm and with 10 cm in length were used as supports. The powders collected from the bottom of the autoclave were characterized by X-ray diffraction (XRD, SHIMADZU XRD-6100) with CuKα radiation, Fourier transformed infrared (FT-IR, JASCO FT/IR-610) spectroscopy using KBr pellets technique and UV − vis spectroscopy (JASCO, V-500).

The compositions of the feed and permeate were analyzed by a gas chromatograph (Shimadzu GC-8A) for the IPA oxidation reaction.

2.2.2 Support tubes pretreatment methods

Method 1:

1) Mullite support tubes washed by boiling water for 1h;

2) Ultrasonic cleaning 10 min for 3 times;

3) Drying at 353 K for overnight;

4) Vacuum drying at 473 K for 2h before vertically placed into autoclave for hydrothermal synthesis;

Method 2:

1) Polish out surface of the mullite tube supports by NO.600 mesh sand paper;

2) Ultrasonic cleaning 10 min for 3 times;

3) Drying at 353 K for overnight;

2.2.3 TS-1 membrane preparation

TS-1 membranes were prepared by *in-situ* method on the surface of porous mullite tubes with the synthesis recipe of TEOS: 0.031TBOT: 0.35TPAOH: $28H_2O$. The mixture solution of 3.39g TBOT and 35g water was stirred and cooled to 273 K in an ice bath. The TBOT immediately formed a white gelatinous precipitate. After a few minutes 20g of 30% H_2O_2 was slowly added drop-wise into this suspension under stirring in ice bath. The white precipitate gradually dissolved under continuous stirring in ice bath and the colour of the suspension changed from white via yellow to orange. There are amount of bubbles need to remove, which were mainly formed during the stirring process for the first 1 hour. About 10g of H_2O_2 solution was needed to supplementary to the clear red orange solution (titanium source) before mixed with TEOS and TPAOH solution. A clear deep red orange solution was obtained after another 1 hour of stirring under ice bath. Then the above orange solution was added to the mixture of 66.9g TEOS, 110.5g TPAOH and 20.3g deionized water which had been stirred rapidly for 1 hour at room temperature. The pre-synthesis clear solution need stirring at relative low ambient temperature for about 30 minutes (***Stirring method 1***). When the ambient temperature increased relative high as in summer season, the pre-synthesis clear solution need stirring in ice bath for 20 minutes and then stirred for another 30 minutes at room temperature (***Stirring method 2***). The resultant mixture was clear pale yellow solution.

The obtained precursor solutions were poured into the titanium autoclave in which supports were mounted and crystallized statically at the pre-set temperature for a given time in a convection oven. After crystallization, the autoclave was taken out and quenched with water. The membranes obtained from autoclave were washed with hot

distilled water and dried at 353 K for overnight, and then were calcined in air to remove the template at 773 K for 30 h by using a computer-controlled muffle furnace with heating and cooling rates of 0.3 and 0.4 °C/min, respectively.

2.2.4 PV-aided catalysis reaction over TS-1 membranes

The catalytic performance of the as-synthesized TS-1 membranes was tested by pervaporation-aided method (Figure 2-1). The feed aqueous solution mixed with IPA and H_2O_2 with a concentration of 1.67 mol L^{-1}(IPA/H_2O_2 molar ratio of 1:1), and it need heated to 323 K under stirring. Under the PV condition, the catalysis reaction would take place when the substrates permeated through the membrane from the feed side to the permeation side. Samples of feed and permeation were periodically collected and analyzed by gas chromatography. During PV, a proper amount of substrates were added into the feed solution at intervals to keep the constant feed concentration. The total flux (J) and the conversions of IPA (Conv. IPA) were given by using the following criteria:

$$J\,[kg \cdot m^{-2} \cdot h^{-1}] = \frac{m}{A \times t} \quad (1)$$

$$C_{onv.\ IPA} = (M_{actone})_{Permeate}/(M_{actone}+M_{IPA})_{\ Permeate} \times 100 \quad (2)$$

Where m is the mass of the permeate (kg); A is the effective area of the membrane in contact with the feed (m^2); t is the permeation time (h); $M_{acetone}$ and M_{IPA} represented the molar fraction of acetone and IPA in the permeate side;

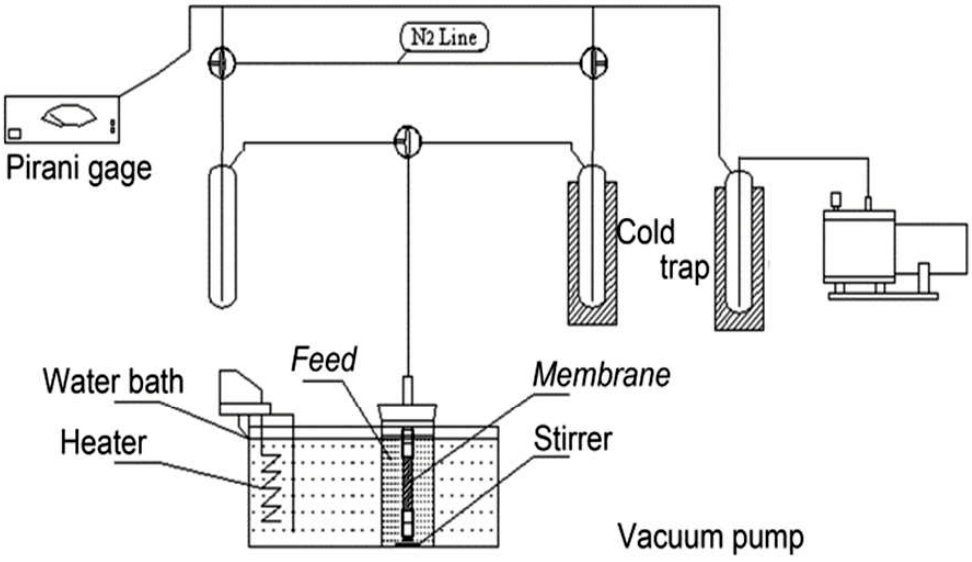

Figure 2-1. PV-aided catalysis reaction experiment apparatus

2.3 Results and discussion

2.3.1 Catalysis reaction over TS-1 powders

TS-1 powders were collected from the bottom of the autoclave, which were used to hydrothermal synthesis of TS-1 membranes.

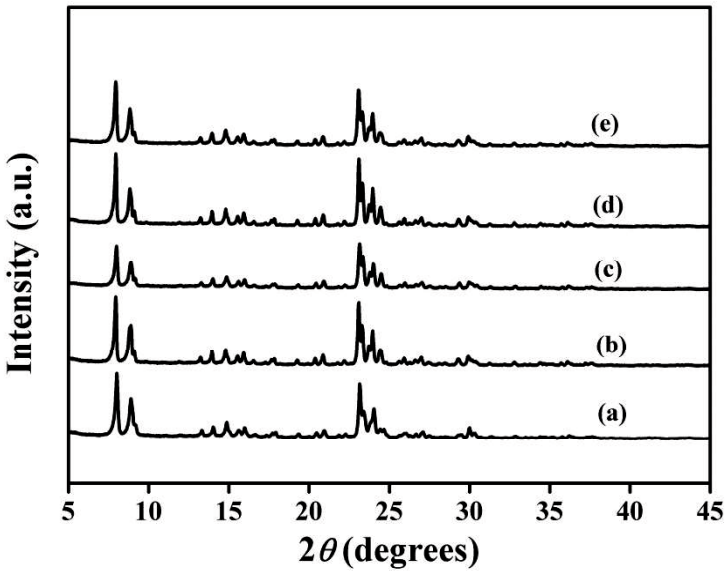

Figure 2-2. XRD patterns of (a) MFI seed and TS-1 powders of (b) TS-I, (c) TS-II, (d) TS-III and (e) TS-IV.

Crystal structures of the powder products were identified by x-ray diffraction (XRD) using a SHIMADZU XRD-6100 diffractometer with CuKα radiation. The spectra were recorded over the range of Bragg angles 5° $\leqslant 2\theta \leqslant$ 45° at a scanning rate of 0.02° per 10 seconds and the XRD patterns of some representative samples are presented in Figure 2-2. In all cases, the patterns showed excellent evidence of MFI structure as well as high crystallinity under the synthesis conditions examined. In comparison with silicalite-1, the patterns of Ti containing samples show a single diffraction peak at 2θ of 24.45°, indicating a change from a monoclinic symmetry (silicalite-1) to an orthoRHOmbic symmetry (titanium silicalite, TS-1). No other phases were detected by XRD.

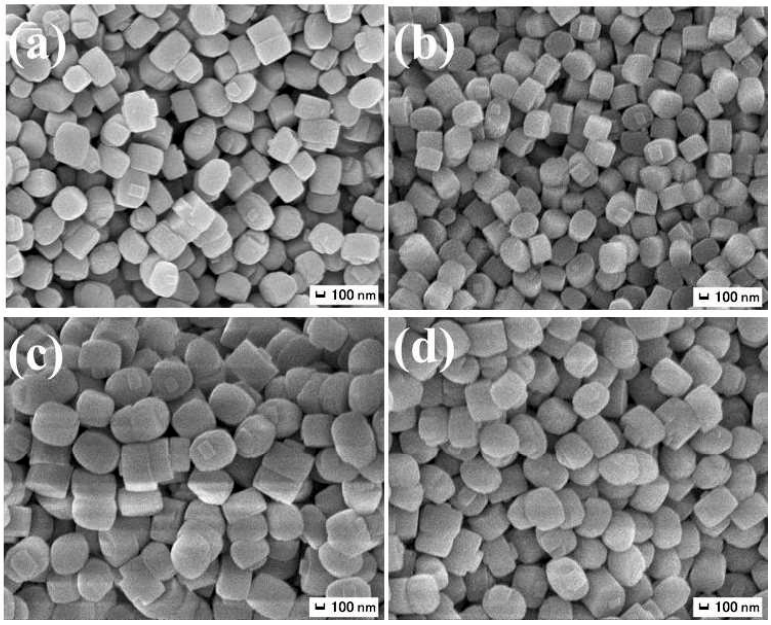

Figure 2-3. SEM images of TS-1 powders (a) TS-I powder, (b) TS-II powder, (c) TS-III powder and (d) TS-IV powder

Table 2-1 IPA catalytic by TS-1 powder

	Acid pretreatment	Reaction temperature(K)	Perm.IPA$_0$ (wt.%)	Perm.IPA (wt.%)	Conv.IPA (%)
TS-I Powder$_1$	Without	323	9.17	6.86	25.19
TS-I Powder$_2$	5M H_2SO_4	323	8.74	3.16	63.84
TS-1I powder	5M HNO_3	323	8.27	1.53	81.50
TS-III powder	5M HNO_3	323	8.27	1.91	76.90
TS-1V powder	5M HNO_3	333	10.0	1.73	82.70
TS-II powder	5M HNO_3	333	10.0	1.81	81.90
recation media	IPA:10wt.%, IPA/H_2O_2(mole ratio=1), IPA=1.67mol/L				
mixture solution	50ml				
TS-1 powder	0.5g		recation time	2h	

Catalytic activity in liquid-phase IPA by H_2O_2 has been investigated in a 100 ml batch reactor at reflux conditions (approx. 323 K) in deionized water 50 ml, with 0.5 g catalyst, 10 g IPA, and 10 ml H_2O_2 30 % in H_2O. Product analysis was performed with a gas chromatograph equipped (Shimadzu GC-8A). All of the as-synthesized TS-1 powders with the size around 200 - 300 nm displayed high IPA conversions after acid pretreatment.

The high activity of TS-1 for different catalytic oxidations of hydrocarbons is attributed to the selective activation of H_2O_2 by isolated tetrahedral Ti species in the crystalline walls.[23] IR spectrum (Figure 2-4a) shows a characteristic absorption peak of the transition metal substituted zeolites at 960 cm^{-1}, indicating the incorporation of titanium into the lattice framework. The absence of any other hetero-phase of titanium oxide is proved by the UV – vis spectrum (Figure 2-4b). An

absorption band at 190-220 nm was assigned to the charge transfer of tetrahedral Ti species was observed, which indicates four-coordinated tetrahedral Ti species in the zeolite framework of TS-1.[24] A well defined absorption band around 310-330 nm that is attributed to extra-framework octahedral TiO_2 [25] was not observed. No other peaks are observed, which demonstrates that there is no octahedral Ti or anatase TiO_2.

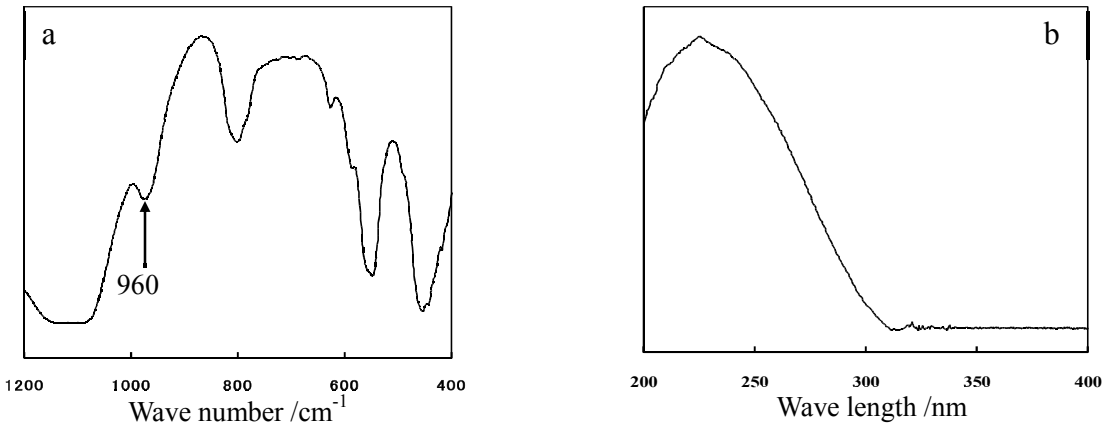

Figure 2-4. FTIR pattern (a) and diffuse-reflectance UV – vis spectrum (b) of TS-1 powder.

2.3.2 Catalysis reaction over TS-1 membranes

The process of preparation of gel solution is very important for the titanium to enter effectively into the silicalite framework and form isolated tetrahedral Ti species in the crystalline walls, while not TiO_2 out of the framework, which has been proved that only the titanium in the framework is effective for the oxidation reaction with H_2O_2. [21, 23] If there are differences in the relative rates of hydrolysis of the two alkoxides, then the precipitation of solid TiO_2 or SiO_2 can occur. Monomeric SiO_4^{4-} species could formed from $Si(OC_2H_5)_4$ and keep stable in the presence of high concentration of TPA^+ ions, while avoid SiO_2 formed in the mixture solution.[26] But titanium ions are not stable in the presence of high concentration of TPAOH with high pH, Ti-alkoxides may hydrolyze to Ti-hydroxides, which would lead to form solid TiO_2 after calcination.[26]

Table 2-2 PV catalytic performance of TS-1 membranes for the oxidation of iso-propanol with H_2O_2

No.	Support pretreatment Method	H_2O_2 (g)	Supplementary H_2O_2 (g)	Stirring method	Mass present in permeate		Total flux (kg/m^2h)	Acetone product flux (kg/m^2h)	Conversion of IPA %
					Acetone	IPA			
TS-1	1	15	0	1	4.39	43.25	0.8	0.035	9.2
TS-2	1	15	0	1	4.95	49.38	0.72	0.036	9.1
TS-3	1	18	0	1	7.59	9.2	1.22	0.093	45.2
TS-4	1	18	0	1	7.35	6.65	1.12	0.082	52.5
TS-5	2	20	7.5	1	5.95	1.41	1.00	0.060	80.84
TS-6	2	20	7.5	1	6.32	1.83	0.92	0.058	79.5
TS-7	1	20	10	1	8.04	2.01	1.25	0.101	80.00
TS-8	1	20	10	1	8.96	1.88	1.3	0.116	82.64
TS-9	without	20	12.7	2	7.43	13.56	0.92	0.068	35.40
TS-10	without	20	12.7	2	7.88	16.35	0.94	0.074	32.52
TS-11	2	20	1.0	2	8.42	2.01	1.01	0.085	80.73
TS-12	2	20	1.0	2	8.60	1.96	1.08	0.093	81.44
TS-13	2	20	7.9	1	6.52	2.38	1.02	0.067	73.26
TS-14	2	20	7.9	1	6.81	2.42	1.10	0.075	73.78
TS-15	2	20	9.6	2	8.47	1.47	1.13	0.096	85.21
TS-16	2	20	9.6	2	9.32	1.68	1.04	0.097	84.72
TS-17	2	20	8.3	2	7.27	2.82	1.03	0.076	72.52
TS-18	2	20	8.3	2	7.46	2.47	1.09	0.081	75.12
TS-19	2	20	7.2	2	8.02	1.91	1.11	0.089	80.77
TS-20	2	20	7.2	2	7.70	1.96	1.04	0.080	79.71

Note: synthesis recipe: TEOS: 0.031TBOT: 0.35TPAOH: $28H_2O$

Synthesis condition: 423 K, 72 h. 10 cm mullite tube as support.

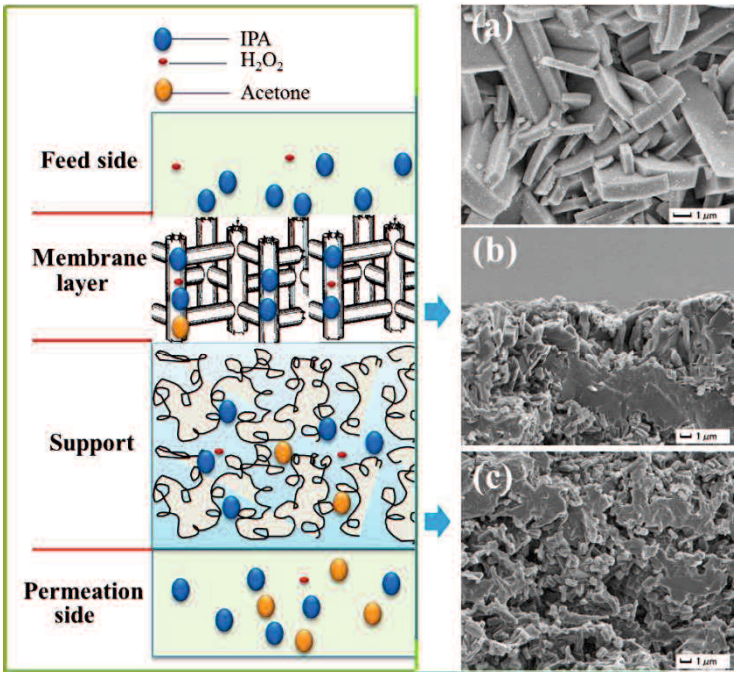

Figure 2-5. Mass transfer model of reactant molecules through TS-1 membrane reactor [13], and SEM images of the membrane of run No. TS-7 (a) surface, (b) cross section and (c) inter-section inside.

The membrane of run No.TS-7 (as seen in Figure 2-5) has large size (larger than 10 μm) and well intergrowth crystals and dense zeolitic layer, which should be unfavorable to the catalysis reaction due to the high diffusion resistance and less catalytic activity surface area. TS-1 is a silicalite-1 structure that has strong hydrophobic property. Larger size of TS-1 crystals or dense zeolitic layer would preferential adsorb IPA molecules in TS-1 channel and make some catalytic active sites be deactivated due to its dense and thick zeolite membrane layer with IPA selective permeantion. This deactivation could be effectively avoided if the size of TS-1 crystals were quite small (less than 300 nm), because smaller crystals should have higher hydrophilic property resulted from the silanol groups on their larger specific surface. As seen in Figure 2-6, the membrane of run No.TS-6 has smaller crystals (about 1.5 μm) in the surface of mullite support, no zeolitic layer formed and the nano-size crystals dispersed well in all vacant spaces, which nearly had an equivalent IPA and H_2O_2 permeation.

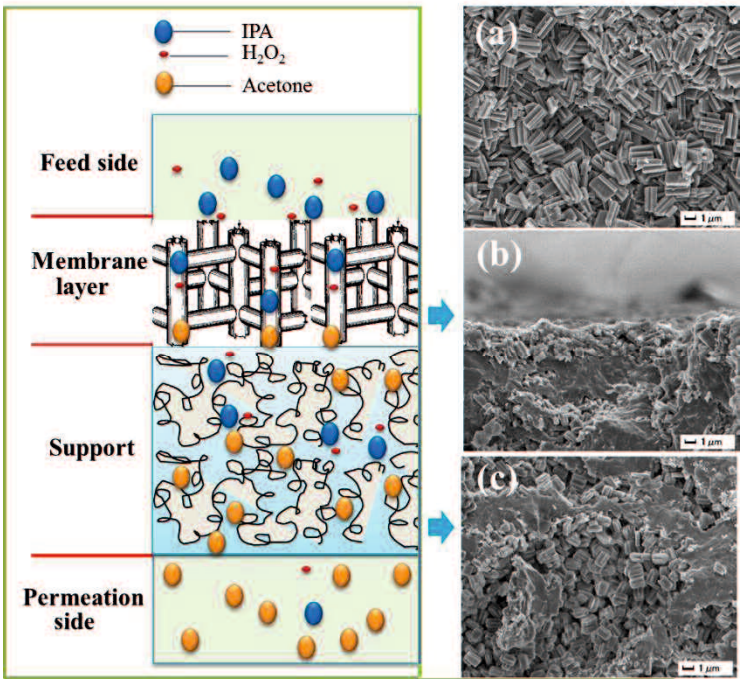

Figure 2-6. Mass transfer model of reactant molecules through TS-1 membrane reactor [13], and SEM images of the membrane of run No. TS-6 (a) surface, (b) cross section and (c) inter-section inside.

2.3.3 Influence of H_2O_2 concentration

It is well known that MFI-type zeolites can be crystallized using a wide range of H_2O/SiO_2 ratios. Since TS-1crystals are formed from the solution phase with high TPAOH content and low water concentration, the concentration of the active nuclei may change on dilution with water.

The addition of 30 wt. % H_2O_2 solution not only as a role lead titanium n-butoxide hydrolysis as stable Ti^{4+} in the mixture solution, but also as part role of water concentration since very low water concentration in the synthesis composition. During the process of preparation of titanium source, large amount of bubbles need to be removed, which were mainly formed during the stirring of titanium source for the first 1 hour. In order to keep constant of water concentration, amount of H_2O_2 solution was needed to supplementary to the clear red orange solution (titanium source) before mixed with TEOS and TPAOH solution.

Table 2-3 PV catalytic performance of TS-1 membranes for the oxidation of iso-propanol with H_2O_2

No.	H_2O_2 (g)	Supplementary H_2O_2	Mass present in permeate		Total flux	Acetone product flux	Conversion of IPA
		(g)	Acetone	IPA	(kg/m^{2}h)	(kg/ m^{2}h)	%
TS-1	**15**	**0**	**4.39**	**43.25**	**0.8**	**0.035**	**9.2**
TS-2	**15**	**0**	**4.95**	**49.38**	**0.72**	**0.036**	**9.1**
TS-3	**18**	**0**	**7.59**	**9.2**	**1.22**	**0.093**	**45.2**
TS-4	**18**	**0**	**7.35**	**6.65**	**1.12**	**0.082**	**52.5**
TS-5	**20**	**7.5**	**5.95**	**1.41**	**1.00**	**0.060**	**80.84**
TS-6	**20**	**7.5**	**6.32**	**1.83**	**0.92**	**0.058**	**79.5**

Note: synthesis recipe: TEOS: 0.031TBOT: 0.35TPAOH: 28H_2O

Synthesis condition: 423 K, 72 h. 10 cm mullite tube as support.

To analysis the PV catalytic performance of as-synthesized TS-1 membranes for the IPA conversion from table 2-3, we found that membrane of run No.TS-1 prepared by addition few amount of 30 wt. % H_2O_2 solution (15g) displayed low IPA conversion (9.2 %). The membrane of run No.TS-4 was prepared by addition much more amount of H_2O_2 (18g) in the solution of titanium source, which displayed much higher IPA conversion (52.5 %). The membrane of run No.TS-5 was prepared by further increased the amount of H_2O_2 from 18g to 20g and supplementary relevant amount of H_2O_2 after remove the bubbles, which displayed relative higher catalytic activity with the IPA conversion of 80.84 %.

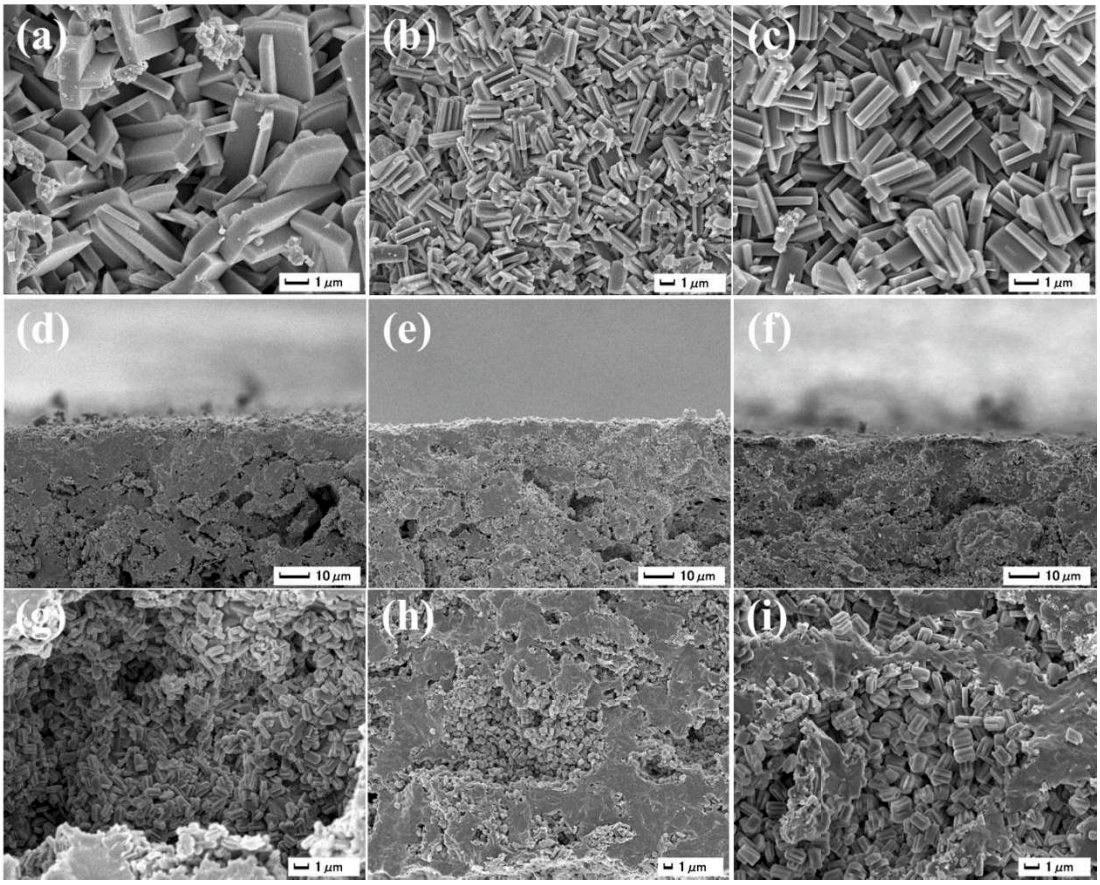

Figure 2-7. SEM images of as-synthesized TS-1 membranes. Surface of (a) TS-1, (b) TS-4 and (c) TS-6; Cross section of (d) TS-1, (e) TS-4 and (f) TS-6; Inter section of (g) TS-1, (h) TS-4 and (i) TS-6.

Figure 2-7 shows the SEM images of the as-synthesized TS-1 membranes prepared by different H_2O_2 concentrations. For the membrane of run No.TS-1 (as seen in Figure 2-7a), large crystals with size more than 10 μm was found on the support surface which should be unfavorable to the catalysis reaction due to the high diffusion resistance and less catalytic activity surface area. It is not clear why large crystals formed on the surface of support with low concentration of H_2O_2 as the membrane of run No. TS-1. The concentration of the active nuclei may increased since an amount of water removed through removals of bubbles. The crystallization rate of the crystals may increased and the crystals growth on the surface of support may significantly influenced. By comparison with the membrane of run No.6, the membrane of run No.TS-4 displayed lower IPA conversion. As seen in Figure 2-7b, e and h, it is strange that the membrane of run No.TS-4 existed smaller crystals in surface, no

zeolitic layer formed in the surface of mullite support and the nano-size crystals also dispersed well in vacant spaces inside the porous mullite support, which should has high catalytic activity. For the preparation of the membrane of run No.TS-6, much more amount of H_2O_2 was added and still supplementary H_2O_2 during the process of preparation of pre-synthesis reaction solution, which may lead titanium to enter effectively into the silicalite framework and form isolated titanium with four valences and also keep constant of water concentration.

2.3.4 Influence of support pretreatment method

Table 2-4 shows the IPA oxidation over as-synthesized TS-1 membranes with H_2O_2. The as-synthesized TS-1 membranes prepared by using the un-pretreatment mullite support always displayed relative lower IPA conversion. TS-1 membranes with high catalytic activity by using the pretreated mullite supports displayed well reproducibility. The surface of the mullite tubular support was relative rough so it had better to pretreat the out surface of the mullite support. What one seeks to pursue in zeolite membrane synthesis, well intergrowth and high density zeolitic layer are aim to high quality zeolite membrane with good separation performance. But TS-1 membrane are used to application as catalysis for selective activation of H_2O_2 under mild conditions. It plays a direct role in the catalytic reaction not as membrane-assisted reactors with separation function.

Well intergrowth and thick zeolitic layer should be unfavorable to the catalysis reaction due to the high diffusion resistance and less catalytic activity surface area. Pretreatment the support may have effluence on the surface morphology of TS-1 membrane on the out surface of tubular support, especially for the surface crystal size (as seen in Figure 2-8a, 2-8b and 2-8c).

Table 2-4 PV catalytic performance of TS-1 membranes for the oxidation of iso-propanol with H_2O_2

No.	Support pretreatment Method	H_2O_2 (g)	Supplementary H_2O_2 (g)	Mass present in permeate		Total flux	Acetone product flux	Conversion of IPA
				Acetone	IPA	(kg/m^{2}h)	(kg/ m^{2}h)	%
TS-7	**1**	**20**	**10**	**8.04**	**2.01**	**1.25**	**0.101**	**80.00**
TS-8	**1**	**20**	**10**	**8.96**	**1.88**	**1.3**	**0.116**	**82.64**
TS-5	**2**	**20**	**7.5**	**5.95**	**1.41**	**1.00**	**0.060**	**80.84**
TS-6	**2**	**20**	**7.5**	**6.32**	**1.83**	**0.92**	**0.058**	**79.5**
TS-9	**without**	**20**	**12.7**	**7.43**	**13.56**	**0.92**	**0.068**	**35.40**
TS-10	**without**	**20**	**12.7**	**7.88**	**16.35**	**0.94**	**0.074**	**32.52**

Note: synthesis recipe: TEOS: 0.031TBOT: 0.35TPAOH: 28H_2O
Synthesis condition: 423 K, 72 h. 10 cm mullite tube as support.

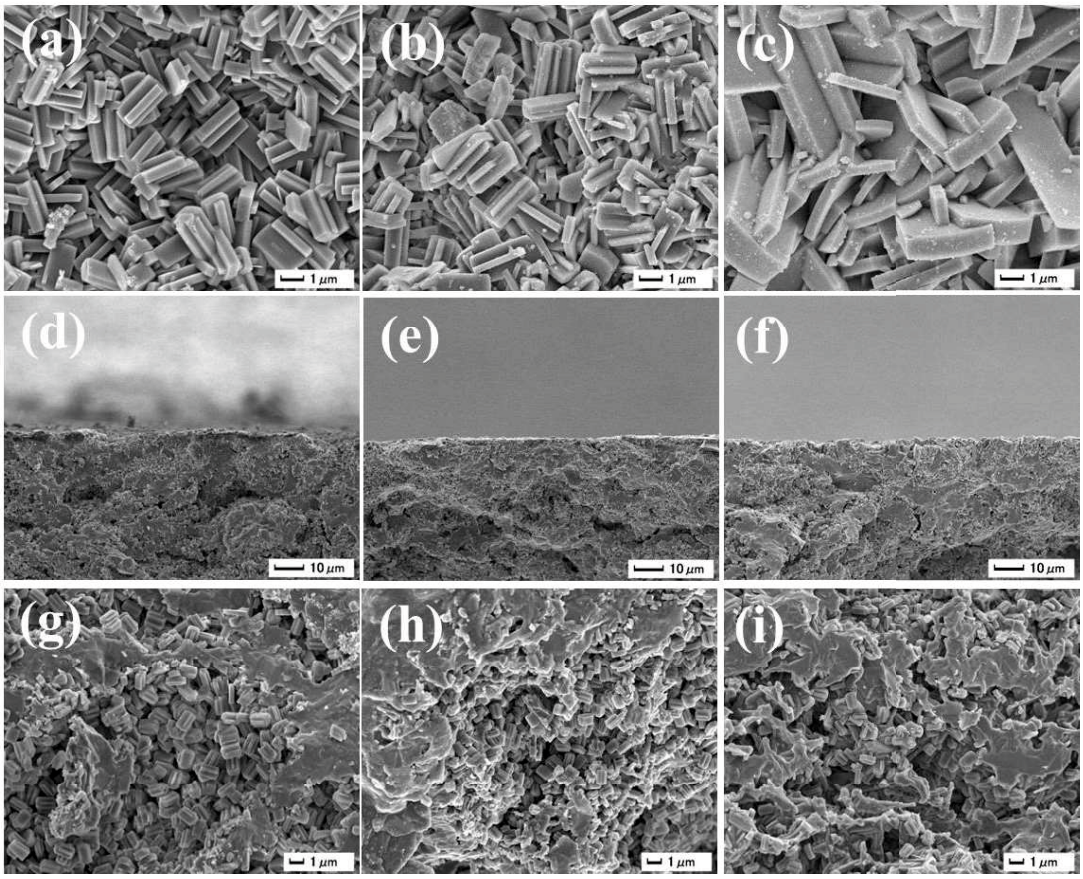

Figure 2-8. SEM images of as-synthesized TS-1 membranes. Surface of (a) TS-6, (b) TS-7 and (c) TS-9; Cross section of (d) TS-6, (e) TS-7 and (f) TS-9; Inter section of (g) TS-6, (h) TS-7 and (i) TS-9.

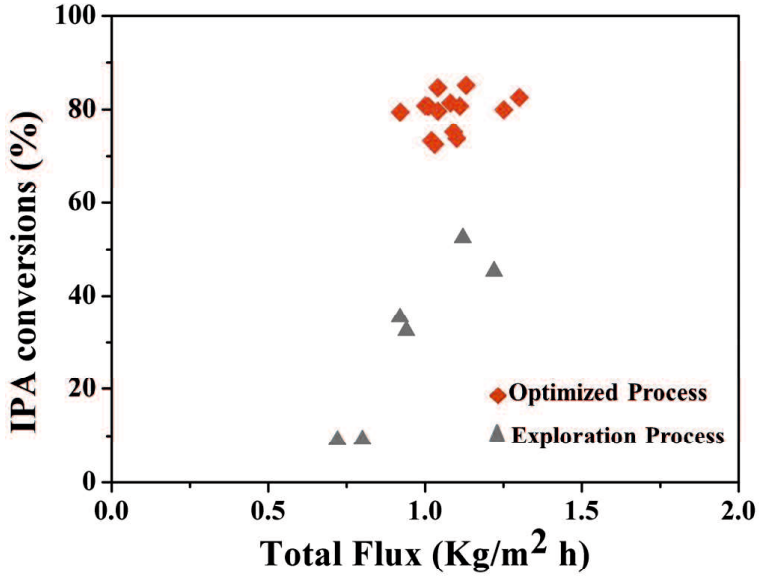

Figure 2-9. The IPA conversions of as-synthesized TS-1 membranes

The IPA conversions of as-synthesized TS-1 membranes are shown in figure 2-9. The porous tubular supported TS-1 membranes with high catalytic activity were prepared by *in-situ* hydrothermal synthesis through the optimized preparation process and displayed good reproducibility.

2.4 Conclusions

The porous tubular mullite support titanium silicalite-1 membrane with high catalytic activity was prepared by in-situ hydrothermal synthesis with the synthesis recipe of SiO_2: 0.031 TBOT: 0.35 TPAOH: 28 H_2O. Optimized preparation process displayed well reproducibility. Supplementary addition of H_2O_2 to the synthesis solution after removals of bubbles in preparation process had great effect on the catalytic performance of as-synthesized TS-1 membrane. Furthermore, the pretreatment of support may have effect on the morphology of surface zeolitic layer of TS-1 membrane.

2.5 References

[1] M. Taramasso, G. Perego, B. Notari, Preparation of porous crystalline synthetic material comprised of silicon and titanium oxides, in, Google Patents, 1983.

[2] B. Notari, Titanium silicalites, Catalysis Today, 18 (1993) 163-172.

[3] W.O. Parker, R. Millini, Ti coordination in titanium silicalite-1, Journal of the American Chemical Society, 128 (2006) 1450.

[4] D. Chandra, A. Bhaumik, Highly active 2D hexagonal mesoporous titanium silicate synthesized using a cationic-anionic mixed-surfactant assembly, Ind. Eng. Chem. Res., 45 (2006) 4879.

[5] Z. Zhong, X. Liu, R. Chen, W. Xing, N. Xu, Adding Microsized Silica Particles to the Catalysis/Ultrafiltration System: Catalyst Dissolution Inhibition and Flux Enhancement, Ind. Eng. Chem. Res., 48 (2009) 4933.

[6] F. Bonino, A. Damin, G. Ricchiardi, M. Ricci, G. Span, R. D'Aloisio, A. Zecchina, C. Lamberti, C. Prestipino, S. Bordiga, Ti-peroxo species in the TS-1/H_2O_2/H_2O system, J. Phys. Chem. B., 108 (2004) 3573

[7] F. Bonino, A. Damin, S. Bordiga, C. Lamberti, A. Zecchina, Interaction of CD3CN and pyridine with the Ti(IV) centers of TS-1 catalysts: A spectroscopic and computational study, Langmuir, 19 (2003) 2155.

[8] J.E. Gallot, D. Trong M.P. Kapoor, S. Kaliaguine, Kinetic modeling of n-hexane oxyfunctionalization over titanium silicalites: Effects of titanium content, Ind. Eng. Chem. Res., 36 (1997) 3458.

[9] R. Landau, G. Sullivan, D. Brown, Propylene-oxide by the co-product processes, Chemtech, 9 (1979) 602-607.

[10] A. Tuel, Y.B. Taarit, Comparison between TS-1 and TS-2 in the hydroxylation of phenol with hydrogen peroxide, Applied Catalysis A: General, 102 (1993) 69-77.

[11] G. Zhang, J. Sterte, B.J. Schoeman, Preparation of colloidal suspensions of discrete TS-1 crystals, Chemistry of materials, 9 (1997) 210-217.

[12] J.-i. Ozaki, K. Takahashi, M. Sato, A. Oya, Preparation of ZSM-5 nanoparticles

supported on carbon substrate, Carbon, 44 (2006) 1243-1249.

[13] P. Chen, Ph.D. Thesis, Yamaguchi University, Yamaguchi, 2007.

[10] E. McLeary, J. Jansen, F. Kapteijn, Zeolite based films, membranes and membrane reactors: Progress and prospects, Microporous and Mesoporous Materials, 90 (2006) 198-220.

[14] L.T.Y. Au, J.L.H. Chau, C.T. Ariso, K.L. Yeung, Preparation of supported Sil-1, TS-1 and VS-1 membranes: Effects of Ti and V metal ions on the membrane synthesis and permeation properties, Journal of Membrane Science, 183 (2001) 269-291.

[15] W. Kim, T. Kim, W. Ahn, Y. Lee, K. Yoon, Synthesis, characterization and catalytic properties of TS-1 monoliths, Catalysis letters, 91 (2003) 123-127.

[16] K. Jung, Y. Shul, A new method for the synthesis of TS-1 monolithic zeolite, Microporous and mesoporous materials, 21 (1998) 281-288.

[17] A. Esposito, C. Neri, F. Buonomo, Process for oxidizing alcohols to aldehydes and/or ketones, in, Google Patents, 1984.

[18] K.T. Jung, Y.G. Shul, Preparation of transparent TS-1 zeolite film by using nanosized TS-1 particles, Chemistry of materials, 9 (1997) 420-422.

[19] K. Jung, J. Hyun, Y. Shul, K.K. Koo, Nanoparticle synthesis of titanium silicalite for fiber, film, and monolith formation, AIChE journal, 43 (1997) 2802-2808.

[20] Y. Lee, W. Ryu, S.S. Kim, Y. Shul, J.H. Je, G. Cho, Oriented growth of TS-1 zeolite ultrathin films on poly (ethylene oxide) monolayer templates, Langmuir, 21 (2005) 5651-5654.

[21] P. Chen, X. Chen, X. Chen, H. Kita, Preparation and catalytic activity of titanium silicalite-1 zeolite membrane with TPABr as template, Journal of Membrane Science, 330 (2009) 369-378.

[22] X. Chen, P. Chen, H. Kita, Pervaporation through TS-1 membrane, Microporous and Mesoporous Materials, 115 (2008) 164-169.

[23] G. Peregot, G. Bellussi, C. Corno, M. Taramasso, F. Buonomot, A. Esposito, Titanium-silicalite: a novel derivative in the pentasil family, Studies in Surface

Science and Catalysis, 28 (1986) 129-136.

[24] S.B. Shin, D. Chadwick, Kinetics of heterogeneous catalytic epoxidation of propene with hydrogen peroxide over titanium silicalite (TS-1), Industrial & Engineering Chemistry Research, 49 (2010) 8125-8134.

[25] F. Boccuzzi, S. Coluccia, G. Ghiotti, C. Morterra, A. Zecchina, Infrared study of surface modes on silica, The Journal of Physical Chemistry, 82 (1978) 1298-1303.

[26] A. Van der Pol, A. Verduyn, J. Van Hooff, Why are some titanium silicalite-1 samples active and others not?, Applied Catalysis A: General, 92 (1992) 113-130.

Chapte 3 Preparation of RHO Membrane in the Presence of 18 Crown 6

3.1 Introduction

Zeolite membranes have been investigated in various applications, including gas separations, such as CO_2/CH_4 and hydrogen recovery, and liquid separations such as dehydration. MFI type zeolite is the most studied type of zeolite membranes for gas separations, while various other types, such as A(LTA)[1], Y(FAU)[2,3], T[4], DDR[5] and CHA[6,7] membranes have also been reported for their unique CO_2-selective permeations.

RHO zeolite is an aluminosilicate zeolite firstly reported by H.E Robson et al.[8], which is consisted by a connection of α-cages via double eight-rings (D8Rs).[9] Zeolite RHO has a small pores (3.6 Å ×3.6 Å), a relative low Si/Al ratio (2.5-5) and very high pore volume (0.26 cm^3 g^{-1}, the pore volumes of 0.36 cm^3 g^{-1} if no pore space is taken up by extra-framework cations).[10-12]

A remarkably high CO_2/CH_4 adsorption selectivity of RHO zeolite is reported,[13] which is originated from the smaller zeolitic pore size than the size of CH_4 molecule (3.8 Å), strong affinity to CO_2 and the high pore volume. The size of RHO zeolitic pore is larger than the size of water but smaller than the size of alcohols and other organics. Accordingly, RHO membrane is expected to show high separation properties in e.g. CO_2/CH_4 and water/organics mixture separations. However, RHO membranes have not been reported in our knowledge.

With the use of 18-crown-6 ether as organic template agent, the high crystallinity and pure RHO zeolite crystals were success to be prepared. RHO zeolite membranes were also prepared in the presence of 18Crown6 on the porous mullite, NS-1 and α-Al_2O_3 supports. Some key synthesis parameters such as hydrothermal temperature and time, different type of support tubes, gel compositions and template wipe-off were preliminary investigated. Fluorides (F^-) as sole mineralizing agent or the

combinative one were reported to accelerate the crystallization of high-silica and all-silica zeolites and decrease the crystal defects. The crystallization rate for both powdery and membranous zeolites together with crystal morphologies depended on the addition amount of fluoride salts. The RHO membrane were prepared by using different fluoride salts (NaF, NH_4F, HF and KF). The alkalinity has strong influence on film growth and crystallinity. The effects of alkalinity of zeolite growth were investigated using synthesis solutions containing a mixture of CsOH and NaOH. The Cs_2O/Al_2O_3 ratio of the initial gel was kept constant at 0.3, while the concentration of OH^- was systematically varied. Single gas (H_2, CO_2, N_2, CH_4) permeation test were utilized to evaluate the separation performance of as-synthesized membranes under 0.1 MPa at 308 K.

3.2 Experiment

3.2.1 Synthesis of RHO zeolite by using 18 Crown 6 as organic structure directing agent.

Zeolite RHO was prepared from a mixture of colloidal silica, sodium aluminate, sodium hydroxide, cesium hydroxide, and distilled water using hydrothermal synthesis. The starting mixture was prepared by dissolving the organic species (18 Crown 6, Wako Pure Chemical Industries, Ltd) in distilled water. Sodium hydroxide (Wako Pure Chemical Industries, Ltd), the cesium source (Sigma–Aldrich, 50 wt. % solution) and sodium aluminate (Wako Pure Chemical Industries, Ltd) were successively added. After complete dissolution, the colloidal silica (LUDOX HS-40, 40 wt. % suspension in water) was slowly poured in the thoroughly stirred solution. The gel formed was aged at room temperature for 24 h in a closed polypropylene bottle under continuous stirring. The composition of the final mixture was prepared with a molar ratio of 10 SiO_2:1Al_2O_3:1.8 Na_2O:0.3 Cs_2O:0.5 18C6:100 H_2O. The pH of the starting mixture was higher than 13. The crystallization was carried out under

static conditions in PTFE-lined stainless-steel autoclaves at 383 K for 48 to 96 hours. After hydrothermal treatment, the solids obtained were filtered, washed with distilled water until the pH of the filtrate was neutral and then dried at 353 K overnight.

3.2.2 Synthesis of RHO zeolite by organic template-free method

The organic template-free RHO crystals were prepared with a synthesis recipe of 10.8 SiO_2:1 Al_2O_3:3 Na_2O:0.4 Cs_2O:110 H_2O. At first, a certain amount of sodium hydroxide was added to deionized water and the mixture was stirred for about 10 min for complete dissolving. While stirring, a sufficient amount of cesium hydroxide according to the gel formula was added to the solution. Then sodium aluminate was added to the solution and was stirred for another 10 min. After that, a sufficient amount of colloidal silica was added to the solution, the gel was stirred for 24 hours at ambient temperature. Then, the prepared gels were poured into PTFE autoclaves for heating 4 days. The products were washed with distilled water until the pH of the filtrate was neutral and then dried at 353 K overnight, and then were calcined in air to remove the template at 723 K for 6 h by using a computer-controlled muffle furnace with a same heating and cooling rate of 1.2 °C/min.

3.2.3. Synthesis of RHO zeolite membrane.

The outer surface of porous 10-cm-long mullite and α-Al_2O_3 supports were rub-coated with RHO zeolite seeds. The gel was prepared by mixing 18 Crown 6 (Wako Pure Chemical Industries, Ltd), sodium hydroxide(Wako Pure Chemical Industries, Ltd), sodium aluminate(Wako Pure Chemical Industries, Ltd), aqueous cesium hydroxide solutions (Sigma–Aldrich, 50 wt.% solution), colloidal silica (LUDOX HS-40, 40 wt.% suspension in water) and deionized water. The resulted precursor gel had a molar ratio of 10 SiO_2:1Al_2O_3:1.8 Na_2O:0.3 Cs_2O:0.5 18C6:600 H_2O. After 6 h aging, 300 g gel was placed in an autoclave and two seeded supports were vertically immersed into the gel. The hydrothermal synthesis was carried out at 383 K for a given time. After synthesis, the autoclave was cooled down to room

temperature and the as-synthesized membranes were washed using deionized water for several batches until the solution become neutral, and dried at 353 K overnight, and then were calcined in air to remove the template at 723 K for 6 h by using a computer-controlled muffle furnace with heating and cooling rates of 0.2 and 0.3 °C/min, respectively.

3.2.4 Characterization

Crystal structures of the powder products and RHO membranes were identified by x-ray diffraction (XRD) using a SHIMADZU XRD-6100 diffractometer with CuKα radiation. The spectra were recorded over the range of Bragg angles $5° \leq 2\theta \leq 45°$ at a scanning rate of 0.02° per 10 seconds. The morphology of RHO zeolite powders and membranes were observed using the field emission scanning electron microscopy (FE-SEM, JEOL JSM 6335F).

3.3 Results and discussion

3.3.1 Characterization of RHO crystals and RHO membranes

Figure 3-1 shows the XRD patterns of as-synthesized solid powders, there is no impurity peaks appear in the XRD figure indicated that all of the powders are pure RHO crystals. RHO-1 and RHO-3 were prepared by using 18 Crown 6 as organic structure directing agent with the gel composition of 10 SiO_2:1Al_2O_3:1.8 Na_2O:0.3 Cs_2O:0.5 18C6:100 H_2O at 383 K for 2 days, which the difference is that RHO-3 was prepared by adding RHO-1 as seeds. It is well known that adding seed crystals of directed phases to starting synthesis gels increases the rate of crystallization, and shortens the time required for the crystallization to be completed. So, the addition of seed crystals to crystallization system can enhance the crystallization rate and improve the purity of crystal product. From the XRD and SEM characterization, RHO crystals (RHO-3) showed much higher crystallinity by seed-assisted method.

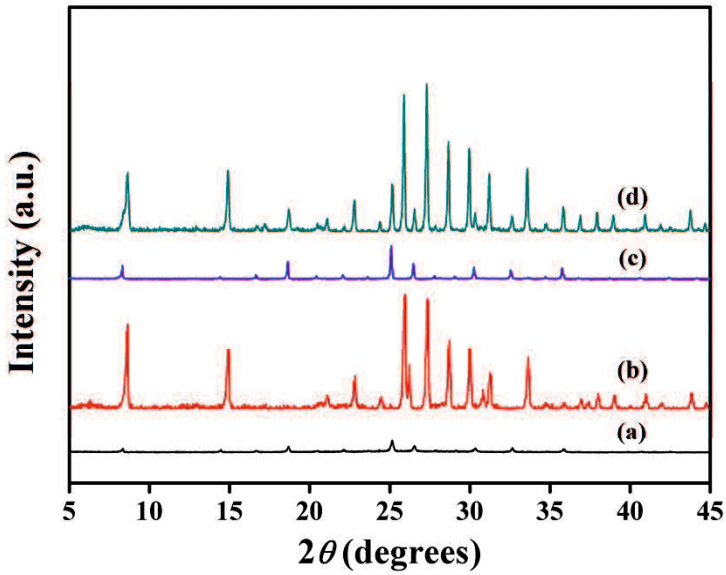

Figure 3-1. XRD patterns of as-synthesized powders (a) RHO-1, (b) RHO-2, (c) RHO-3 and (d) RHO-4.

RHO-2 and RHO-4 were obtained from organic free method with the synthesis recipe of 10.8 SiO_2:1 Al_2O_3:3 Na_2O:0.4 Cs_2O:110 H_2O at 363 K for 6 days and 373 K for 4 days, respectively. Pure RHO phase could be obtained at synthesis temperatures from 363 to 373 K. The synthesis time decreased with the increased of synthesis temperature for the samples. The size of crystals increased from 0.6 μm to 0.8 μm as the synthesis temperature increased from 363 to 373 K, as shown in Figure 3-2b and d. The kinetic of crystallization increased with increase of synthesis temperature, which could be the reason for that synthesis time decreased and particle sizes were increased.

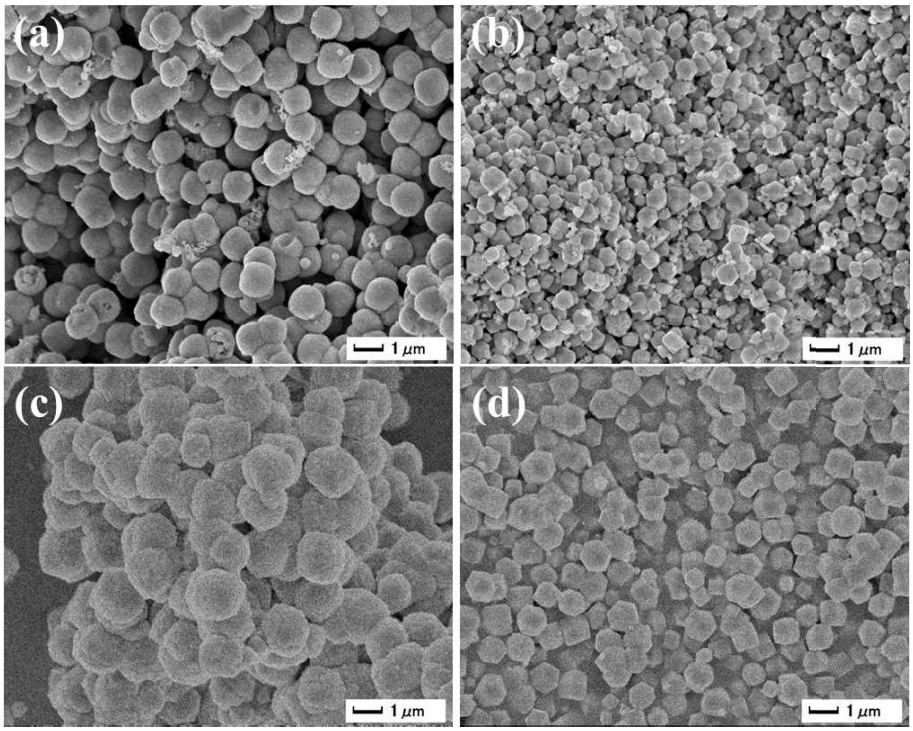

Figure 3-2. SEM images of RHO zeolite powder (a) RHO-1, (b) RHO-2, (c) RHO-3 and (d) RHO-4.

Figure 3-3 shows the XRD patterns of zeolite RHO and tubular RHO membrane. Pure and high crystallinity RHO membrane could be prepared with the synthesis recipe of $10SiO_2$:1.0 Al_2O_3:1.8 Na_2O:0.3 Cs_2O: 0.5 18C6: 500 H_2O: 0.5 NaF at 383 K for 6 days. The morphology of membrane was observed with SEM. As shown in Figure 3-4, after hydrothermal synthesis, a relative dense zeolite film with a thickness of 3 μm formed on the outer surface of α-Al_2O_3 tube. The zeolitic layer is composed of well intergrown crystals. But unfortunately, some pinholes are clearly to be found in the surface of RHO zeolite membrane, which has great influence on the light gas separation. As revealed in XRD patterns (Figure 3-3), the membrane only exhibited the typical peaks of the RHO structure and α-Al_2O_3, which indicated that the pure RHO membrane was prepared by using 18 Crown 6 as organic structure directing agent.

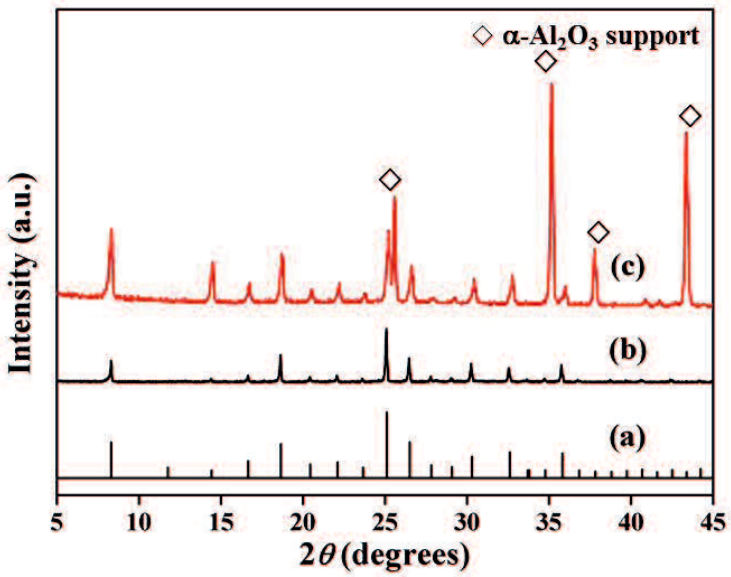

Figure 3-3. XRD patterns of (a) simulated RHO-type framework, (b) as-synthesized zeolite RHO-3 and (c) as-synthesized membrane of RHO-17.

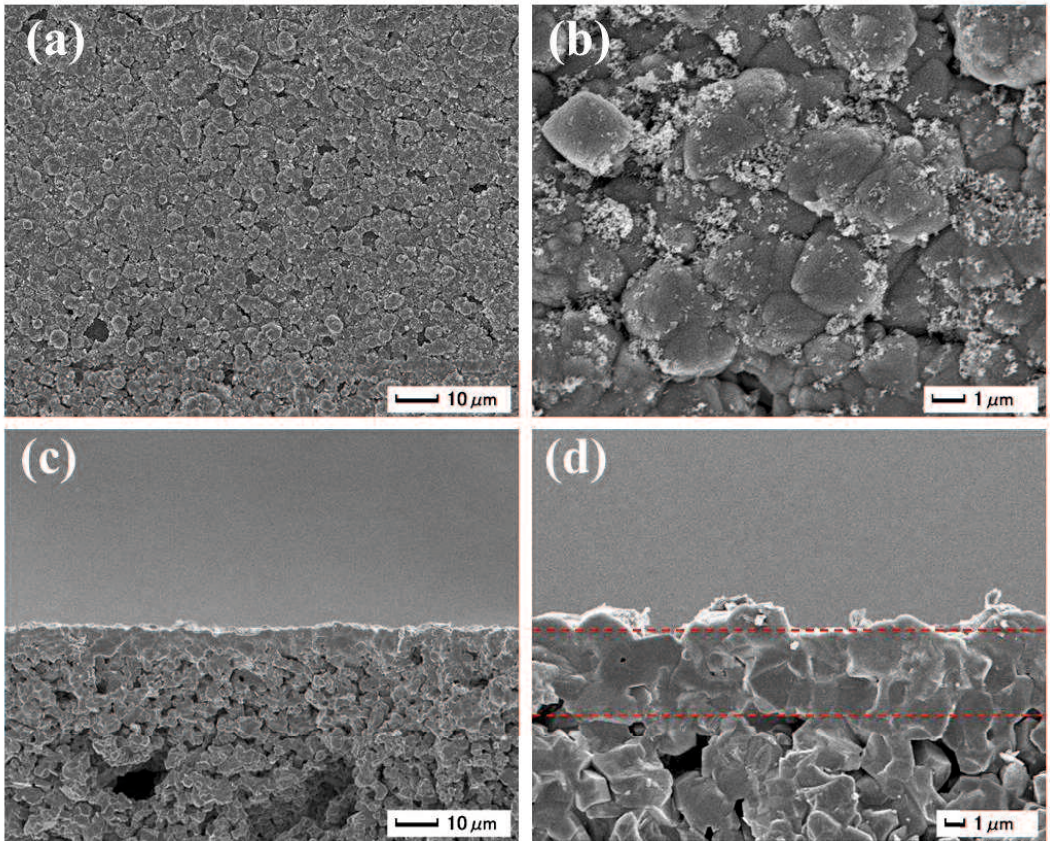

Figure 3-4. SEM images of the membrane of RHO-17 (a), (b) surface and (c), (d) cross section.

Table 3-1 Synthesis compositions and single-gas performance of as-synthesized RHO membranes.

No	Support	SiO_2	Al_2O_3	Na_2O	Cs_2O	18C6	H_2O	Synthesis conditions		F^- source	F^-	Seed	Phase (XRD)	Single gas Permeance (10^{-7}mol m^{-2} s^{-1} Pa^{-1})					Ideal selectivity	
								T (K)	Time(d)					He	H_2	CO_2	N_2	CH_4	CO_2/N_2	CO_2/CH_4
RHO-1	Mullite	10	1	1.8	0.3	1	600	373	7	--	0	RHO-1	RHO	Leaked						
RHO-2	Mullite	10.8	1	1.8	0	0.5	500	383	6	--	0	RHO-4	RHO	6.88	12.39	4.01	5.08	5.57	0.79	0.72
RHO-3	Mullite	10	1	1.8	0.3	0.5	600	393	3	--	0	RHO-1	RHO	Leaked						
RHO-4	Mullite	10	1	1.8	0.3	0.5	600	423	3	--	0	RHO-1	CHA							
RHO-5	Mullite	10	1	1.8	0.3	0.5	600	383	4	NaF	0.5	RHO-1	RHO		27.74	10.64	15.53	14.92	0.69	0.71
RHO-6	Mullite	10	1	3	0.4	0.5	600	383	3	--	0	RHO-2	RHO	11.87	23.14	12.31	17.9	20.05	0.69	0.61
RHO-7	Mullite	10	1	1.8	0.3	0.5	600	383	3	NaF	0.5	RHO-3	RHO	Leaked						
RHO-8	Mullite	10	1	1.8	0.3	1	600	383	3	--	0	RHO-2	RHO		25.05	1.87	3.17	4.69	0.59	0.4
RHO-9	Mullite	10	1	1.8	0.3	0.5	600	383	4	NaF	1	RHO-2	RHO		28.94	10.2	14.91	15.82	0.68	0.64
RHO-10	Mullite	10	1	1.8	0.3	0.5	600	383	4	NaF	2	RHO-2	RHO		28.83	8.96	13.44	15.59	0.67	0.57
RHO-11	Mullite	10	1	1.8	0.3	0.5	600	383	4	NH_4F	0.5	RHO-2	RHO		18.1	6.03	9.29	12.11	0.65	0.50
RHO-12	Mullite	10	1	1.8	0.3	0.5	600	383	4	HF	0.5	RHO-2	RHO		20.88	5.21	9.72	11.98	0.54	0.43
RHO-13	Mullite	10	1	1.8	0.3	0.5	600	383	4	KF	0.5	RHO-2	RHO		12.7	1.82	4.14	4.8	0.44	0.38
RHO-14	Mullite	10	1	3	0.3	0.5	600	383	3	NaF	0.5	RHO-2	RHO		9.32	2.8	3.18	3.5	0.88	0.8
RHO-15	Mullite	10	1	4	0.3	0.5	600	383	4	NaF	0.5	RHO-2	RHO+CHA							
RHO-16	Mullite	10	1	5	0.3	0.5	600	383	4	NaF	0.5	RHO-2	RHO+CHA							
RHO-17	a-Al_2O_3	10.8	1	1.8	0.3	0.5	500	383	6	--	0	RHO-4	RHO	5.03	6.14	2.09	1.04	0.5	2.02	4.18
RHO-18	NS-1	10.8	1	1.8	0.3	0.5	500	383	6	--	0	RHO-4	RHO	6.09	10.31	3.21	3.19	3.98	1.00	0.80
RHO-19	a-Al_2O_3	10	1	3	0.3	1	600	383	3	NaF	0.5	RHO-2	RHO	3.25	6.1	1.66	3.73	4.09	0.45	0.41
RHO-20	a-Al_2O_3	10.8	1	1.8	0.3	5	500	383	6	NaF	0.3	RHO-4	RHO	0.41	0.66	0.3	0.13	0.16	2.31	1.88

3.3.2 Single-gas permeance

Single-gas permeances of He, H_2, CO_2, N_2, CH_4 and SF_6, measured at 308 K and 0.1 MPa feed pressure for the membrane of RHO-17, are shown as a function of kinetic diameter in Figure 3-3. Since the kinetic diameter of CH_4 and SF_6 are larger than the RHO pore size so that the permeance of them through the membrane of RHO-18 mainly by the defective non-zeolite pores contribution. The SF_6 permeance is 1.12×10^{-8} mol m^{-2} s^{-1}, which indicted much amount of defects exist in the zeolite

layer.

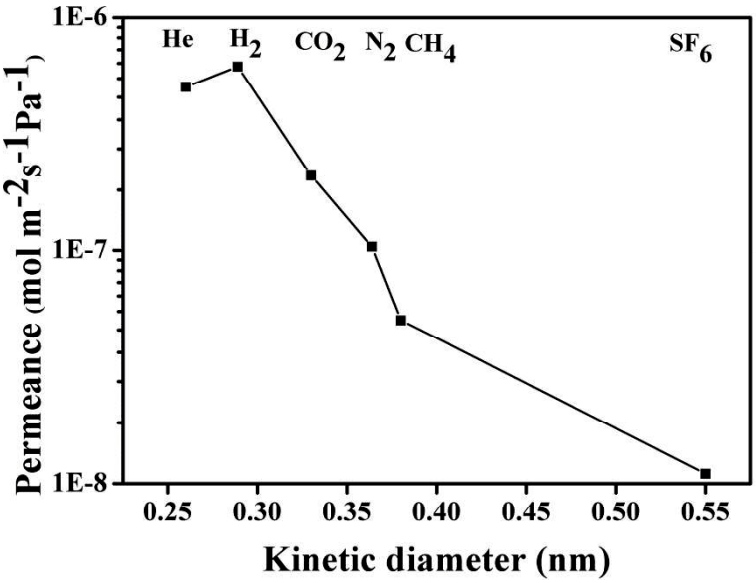

Figure 3-5. Single gas permeance of the membrane of RHO-17 as a function of kinetic diameter at 308 K and 0.1 MPa feed pressure.

The pressure dependence of the single-gas permeances for He, H_2, CO_2, N_2, CH_4 and SF_6 from 0.1 MPa to 0.6 MPa through the membrane of RHO-17 is shown in Figure 3-5. As seen in **Figure 3-6**, the ideal separation factors of CO_2 from CH_4 determined as the ratio of the single component permeances is 4.18 at the pressure of 0.1 MPa, which exceed the corresponding Knudsen coefficients (0.60). The CO_2 permeance decreased slightly with increasing pressure, whereas the CH_4 permeance increased slightly. The CO_2/CH_4 ideal selectivity decreased from 4.18 to 0.97 as the pressure increased from 0.1 MPa to 0.6 MPa. The CH_4 permeance increased slightly as the pressure increased, which indicated the relative high concentration of the large non-zeolite pores was existed in the membrane of RHO-17.

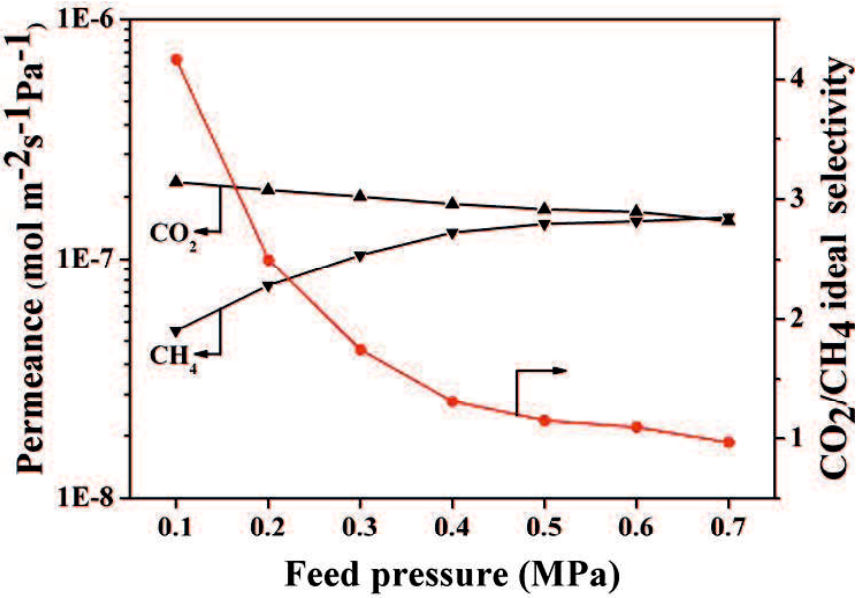

Figure 3-6. CO_2 and CH_4 permeances and CO_2/CH_4 ideal selectivity for the membrane of RHO-17 as a function of pressure at 308 K.

3.3.3 Effect of different synthesis temperature

Figure 3-7 shows XRD patterns of as-synthesized membranes synthesized at 373, 383, 393 and 423 K. The results of XRD patterns indicate that zeolite RHO phase are formed at synthesis temperatures from 373 to 393 K. Pure and high crystallinity RHO zeolitic layer was formed at the synthesis temperature of 383 K for 4 days. As synthesis temperature increased to 393 K, the intensity of XRD peaks significantly decreased. So, it can be said that synthesis temperature of 393 K is higher than the temperature needed to form RHO phase for 4 days of synthesis. Pure CHA phase were obtain from the same gel composition at a higher temperature of 423 K. High temperature may lead to phase transformation since RHO is a metastable phase.

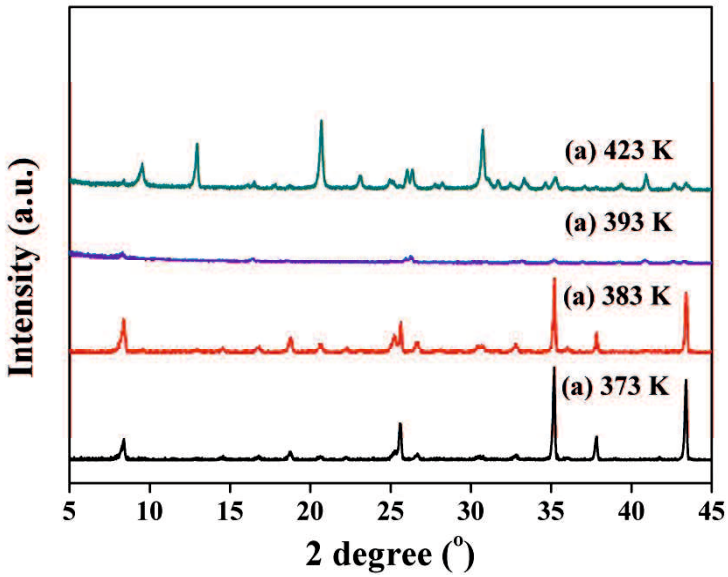

Figure 3-7. XRD patterns of as-synthesized membranes prepared as a function of different synthesis temperature (a) 373 K-RHO-1, (b) 383 K-RHO-2 (c) 393 K-RHO-3 and (d) 423 K-RHO-4.

3.3.4 Effect of coating different crystal seeds

It is much easy to form continuous zeolitic film by using seeded method, since it decouples nucleation from growth by the coated seeds on the surface of supports. The morphology and crystal size have great effect on the synthesis of zeolitic layer in the surface of porous tube. The mullite tube with 12 mm outer diameter, 1.5 mm thickness, 1.3 μm average pore size and 10 cm length. Table 3-2 shows the single-gas performance of as-synthesized RHO membranes prepared by using different crystal seeds. The membrane of RHO-2 displayed relative higher CO_2/CH_4 ideal selectivity and lower CO_2 permeance through single gas test, which was prepared by using RHOmbus RHO-4 crystal as seeds. From the results of XRD and the SEM characterization, RHO-2 and RHO-4 show high crystallinity and has RHOmbus morphology with size of 0.6 μm and 0.8 μm, respectively, whereas the RHO-1 and RHO-3 show relative low crystallinity and spheroidal morphology with size of 1.0 μm and 1.2 μm, respectively. It seems that RHOmbus seeds lead to form high crystallinity RHO crystals and much dense zeolitic layer in the suface of mullite tube, and the mullite tube with 1.3 μm average pore size may much match to the RHOmbus seeds

with size of 0.8 μm.

Table 3-2 Single gas performance of as-synthesized RHO membranes prepared by using different crystal seeds at 308 K and 0.1 MPa feed pressure.

No.	Seeds	Synthesis conditions		Phase(XRD)	Single gas Permeance (10^{-7}mol m^{-2} s^{-1} Pa^{-1})					Ideal selectivity	
		T (K)	Time(d)		He	H_2	CO_2	N_2	CH_4	CO_2/N_2	CO_2/CH_4
RHO-5	RHO-1	383	4	RHO		27.74	10.64	15.53	14.92	0.69	0.71
RHO-6	RHO-2	383	3	RHO	11.87	23.14	12.31	17.9	20.05	0.69	0.61
RHO-7	RHO-3	383	3	RHO	Leaked						
RHO-2	RHO-4	383	6	RHO	5.03	6.88	12.39	4.01	5.08	5.57	0.79

Note: Synthesis recipe: $1.0Al_2O_3$:$1.8Na_2O$:$0.3Cs_2O$:$10SiO_2$:0.5 18C6:500 H_2O:0.5NaF.

3.3.5 Effect of fluoride salts

It is well known that the addition of fluoride into the starting gel favored the crystallization of high-silica zeolites as a mineralizing agent and/or a structure-directing agent. It is interesting that different fluoride source may have difference effects on synthesis of zeolitic materials. The NaF remaining in the MOR-type zeolite crystals considerably reduces the thermal stability while the NH_4F remaining in the beta (BEA) zeolite crystals relatively improves the thermal stability. The addition of NH_4F in synthesis of beta zeolite needs much longer synthesis time, but on the contrary, the crystallization rate of zeolite T was greatly improved by added NaF. In order to gain defect-free or decrease defect druing preparation of RHO membrane, we attempted to synthesis of RHO membrane by using different fluoride salts, such as NaF, NH_4F, HF and KF.

Table 3-3 Single gas performance of RHO membranes prepared by using different fluoride salts and different F^-/Al_2O_3 ratios at 308 K and 0.1 MPa feed pressure.

No.	F-source	F-	Synthesis conditions		Phase (XRD)	Single-gas permeance (10^{-7}mol m_{-2} s^{-1} Pa^{-1})					Ideal selectivity	
			T(K)	Time(d)		He	H_2	CO_2	N_2	CH_4	CO_2/N_2	CO_2/CH_4
RHO-8	-	0	383	3	RHO	-	25.05	1.87	3.17	4.69	0.59	0.4
RHO-5	NaF	0.5	383	4	RHO	-	27.74	10.64	15.53	14.92	0.69	0.71
RHO-9	NaF	1.0	383	4	RHO	-	28.94	10.2	14.91	15.82	0.68	0.64
RHO-10	NaF	2.0	383	4	RHO	-	28.83	8.96	13.44	15.59	0.67	0.57
RHO-11	NH_4F	0.5	383	4	RHO	-	18.1	6.03	9.29	12.11	0.65	0.50
RHO-12	HF	0.5	383	4	RHO	-	20.88	5.21	9.72	11.98	0.54	0.43
RHO-13	KF	0.5	383	4	RHO	-	12.7	1.82	4.14	4.8	0.44	0.38

Note: Synthesis recipe: $1.0Al_2O_3:1.8Na_2O:0.3Cs_2O:10SiO_2:0.5$ 18C6:500 H_2O

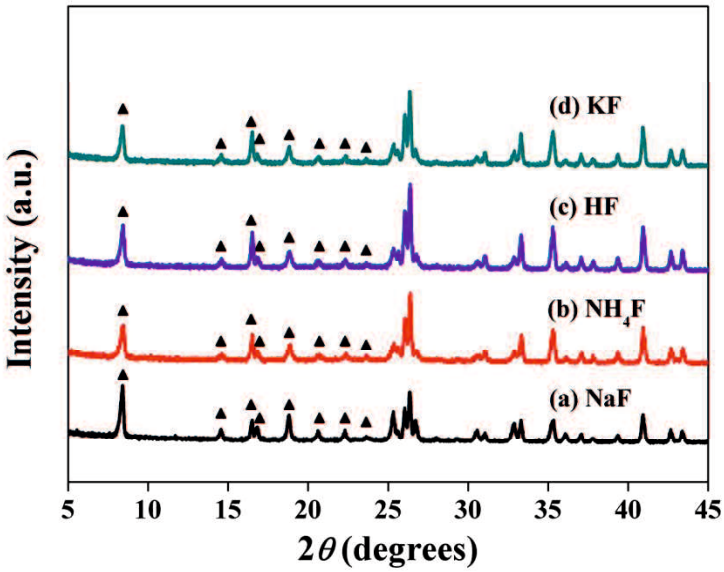

Figure 3-8. XRD patterns of RHO membranes prepared by using different fluoride salts as (a) NaF-RHO-5 (b) NH_4F-RHO-11 (c) HF-RHO-12 and (d) KF-RHO-13.

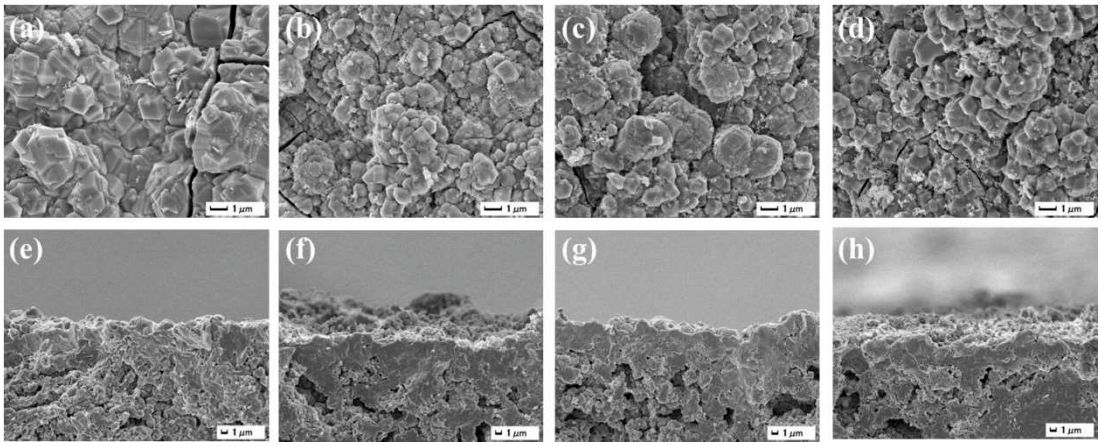

Figure 3-9. SEM images of RHO membranes prepared by using different fluoride salts as (a) NaF-RHO-5 (b) NH_4F-RHO-11 (c) HF-RHO-12 and (d) KF-RHO-13.

Table 3-3 shows the single gas performance of RHO membranes prepared by using different fluoride salts and different F^- /Al_2O_3 ratios. As showed in Figure 3-8, typical peaks of RHO structure are observed from the XRD patterns of as-synthesized membranes. Compare the intensity of the XRD peaks of the RHO membrane prepared by using different fluoride salts, the membrane of RHO-5, which were prepared by using NaF as fluoride salt displayed relative higher degree of crystallinity. As seen in Table 3-3, the membrane of RHO-5, which were prepared by using NaF as fluoride salt also displayed a relative higher CO_2/CH_4 ideal selectivity. Figure 3-10. Showed the XRD patterns of RHO membranes prepared as a function of different NaF/Al_2O_3 ratios. The intensity of the XRD peaks of the RHO membranes synthesis with different NaF/Al_2O_3 ratios is similar.

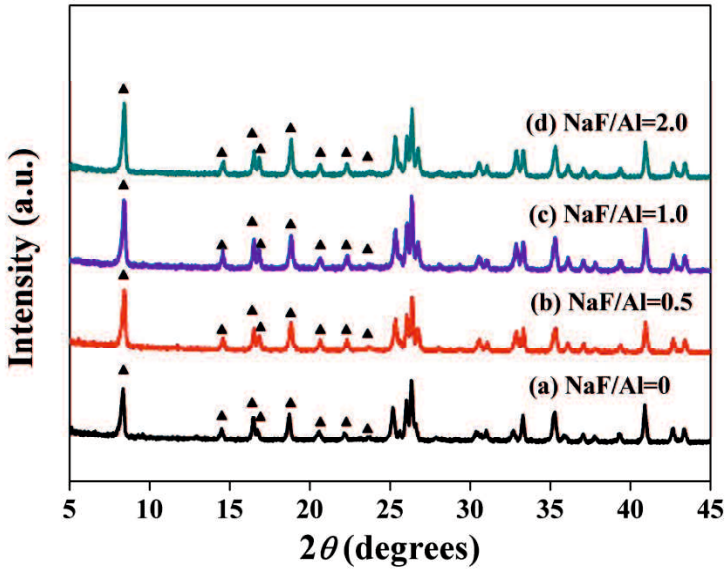

Figure 3-10. XRD patterns of RHO membranes prepared as a function of different NaF/Al ratios of (a) 0-RHO-8 (b) 0.5 –RHO-5 (c) 1.0 –RHO-9 and (d) 2.0-RHO-10.

NaF have effect on the morphologies of RHO crystals and lead to well intergrowth of RHO zeolite crystals (as shown in Figure 3-11b and f). However, there were nearly no change for the thickness of the as-synthesized RHO zeolitic layer by increased the NaF concentrations in initial gel (as seen in Figure 3-11f, g and h). Fluoride may favor the crystallization of RHO zeolite as a mineralizing agent.

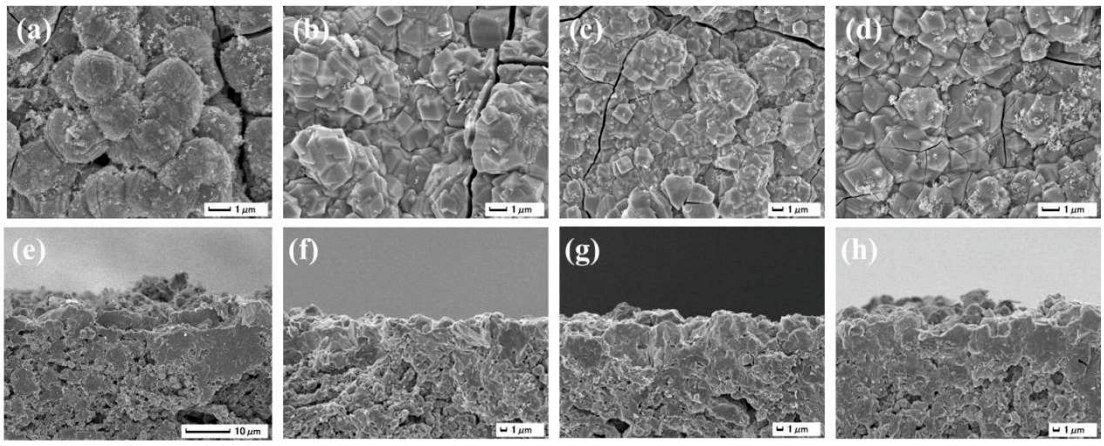

Figure 3-11. SEM images of RHO membranes prepared as a function of different NaF/Al_2O_3 ratios of (a, e) 0-RHO-8, (b, f) 0.5-RHO-5, (c, g) 1.0-RHO-9 and (d, h) 2.0-RHO-10.

3.3.6 Effect of different Na_2O/Al_2O_3

Among the synthesis variables, initial alkalinity has strong influence on film growth and crystallinity. Figure 3-12 illustrates the XRD patterns of RHO membranes prepared as a function of different Na_2O/Al_2O_3 ratios. By increased the Na_2O/Al_2O_3 ratios from 1.8 to 3 (as shown in Figure 3-13a and b), the synthesis time reduced significant but lead to a relative lower crystallinity. Higher alkalinity may lead to slower deposition and poorer crystallinity. Furthermore, zeolite dissolution is known to occur at high alkalinity. As the Na_2O/Al_2O_3 ratios further increased, the impurity CHA crystal observed (as seen in Figure 3-9c and d).

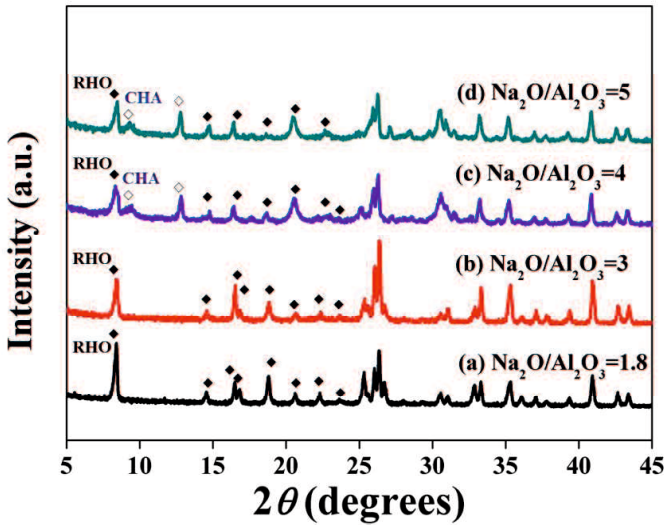

Figure 3-12. XRD patterns of RHO membranes prepared as a function of different Na_2O/Al_2O_3 ratios of (a) 1.8-RHO-2, (b) 3-RHO-14, (c) 4-RHO-15, and (d) 5-RHO-16.

3.3.7 Effect of different support tubes

For the preparation of supported zeolite membranes, the mismatch in the expansion coefficient between the zeolite membrane and the surface of supports have great effluence on the quality of zeolite membranes. Figure 3-14 illustrate the SEM images of RHO membranes prepared by using different support tubes. As seen in Figure 3-14e and f, RHO crystals could be well intergrowth on α-Al_2O_3 tube and NS-1 tube. RHO zeolite layer growth on the NS-1 porous tube showed well intergrowth but exist huge defect as large amount of big cracks, which lead to low CO_2/CH_4 ideal selectivity(as show in Table 3-4). As seen in Figure 3-14b and e, pure RHO membrane with high density and well intergrowth has been prepared on the out surface of α-Al_2O_3 porous tube support.

Table 3-4 Single gas performance of as-synthesized RHO membranes prepared by using different support tubes at 308 K and 0.1MPa feed pressure.

No.	support	Synthesis conditions		Phase(XRD)	Single gas Permeance (10^{-7}mol m_{-2} s^{-1} Pa^{-1})					Ideal selectivity	
		T (K)	Time(d)		He	H_2	CO_2	N_2	CH_4	CO_2/N_2	CO_2/CH_4
RHO-2	Mullite	383	6	RHO	6.88	12.39	4.01	5.08	5.57	0.79	0.72
RHO-17	α-Al_2O_3	383	6	RHO	5.03	6.14	2.09	1.04	0.5	2.02	4.18
RHO-18	NS-1	383	6	RHO	6.09	10.31	3.21	3.19	3.98	1.00	0.80

Note: Synthesis recipe: $1.0Al_2O_3$:$1.8Na_2O$:$0.3Cs_2O$:$10SiO_2$:0.5 18C6:500 H_2O:0.5NaF

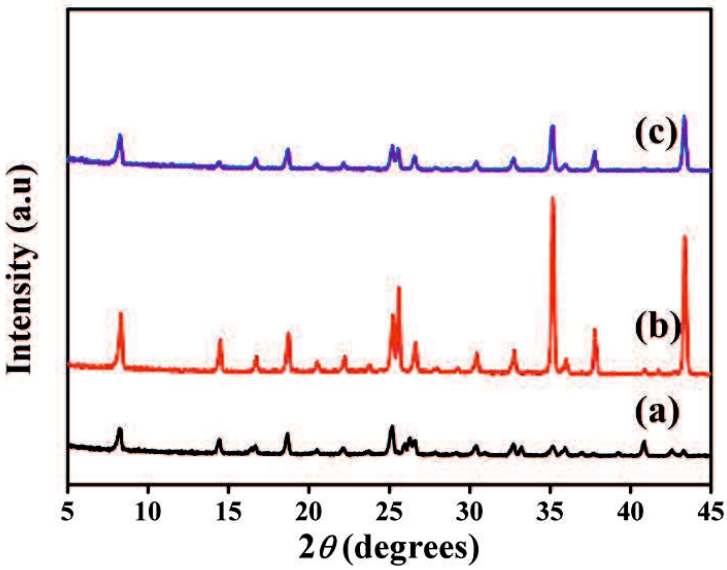

Figure 3-13. XRD patterns of as-synthesized RHO membranes prepared by using different support tubes (a) RHO-2 by using mullite support, (b) RHO-17 by using a-Al_2O_3 tube and (c) RHO-18 by using NS-1 tube.

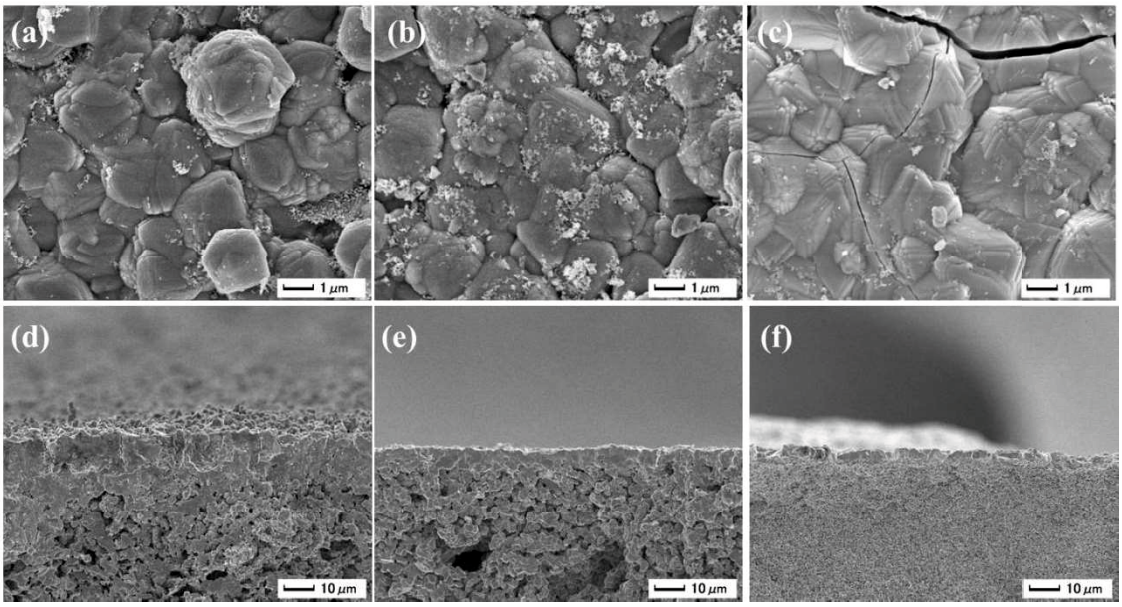

Figure 3-14. SEM images of RHO membranes prepared by using different support tubes. (a) and (d) surface and cross-section of RHO-2 by using mullite tube; (b) and (e) surface and cross-section of RHO-17 by using a-Al_2O_3 tube, (c) and (f) surface and cross-section of RHO-18 by using NS-1 tube.

3.3.8 Effect of different 18 Crown 6 content

Table 3-4 showed the single gas performance of as-synthesized RHO membranes prepared by different 18 crown 6 (OSDA) content at 308 K and 0.1 MPa feed pressure. The membrane prepared by using higher content of organic template lead to lower

CO_2 permeance but with relative higher CO_2/CH_4 ideal selectivity. Figure 3-15 showed the single gas permeance of the membrane of RHO-19 as a function of different kinetic diameter at 308 K and 0.1 MPa feed pressure. Before calcination, the He permeance was 3.0×10^{-10} mol m^{-2} s^{-1} and the CH_4 permeance was 6.9×10^{-11}mol m^{-2} s^{-1} at 308 K and 0.5 MPa feed pressure. It demonstrated that the membrane of RHO-19 with low amount of defects since any slight gas was difficult to pass through it even though be dehydrated under a vacuum at 473 K for overnight. Unfortunately, the membrane of RHO-19 may be broken during the calcination process since the CH_4 permeance was increased from 6.9×10^{-11}mol m^{-2} s^{-1} to 7.4×10^{-7}mol m^{-2} s^{-1}. The membrane of RHO-19 may be damaged through the calcination process.

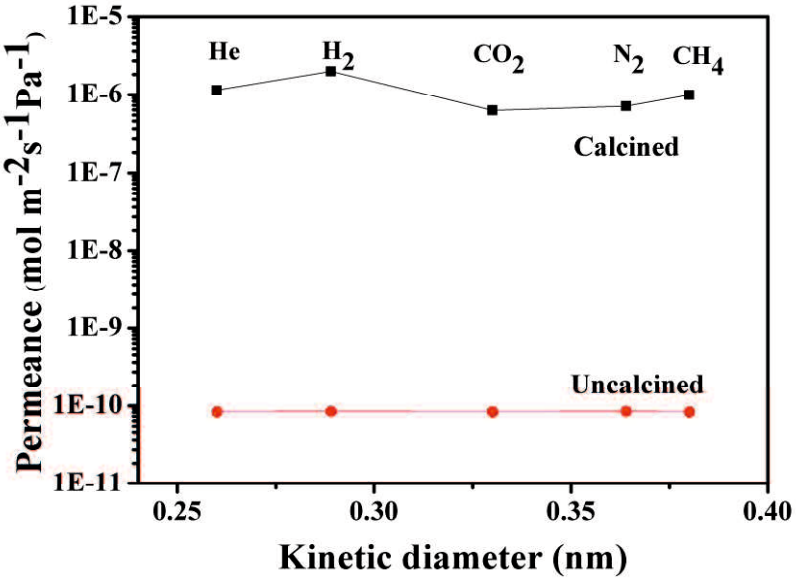

Figure 3-15. Single gas permeance of membrane RHO-19 as a function of kinetic diameter at 308 K and 0.1 MPa feed pressure.

Table 3-4 Single gas performance of as-synthesized RHO membranes prepared by different 18 crown 6 (OSDA) content at 308 K and 0.1 MPa feed pressure

No.	18Crown 6	Synthesis conditions		Phase (XRD)	Single-gas permeance (10^{-7}mol m_{-2} s^{-1} Pa^{-1})					Ideal selectivity	
		T(^{0}C)	Time(d)		He	H_2	CO_2	N_2	CH_4	CO_2/N_2	CO_2/CH_4
RHO-17	0.5	110	6	RHO	5.03	6.14	2.09	1.04	0.5	2.02	4.18
RHO-19	1.0	110	6	RHO	3.25	6.1	1.66	3.73	4.09	0.45	0.41
RHO-20	5.0	110	6	RHO	0.41	0.66	0.3	0.13	0.16	2.31	1.88

Note: Synthesis recipe: $1.0Al_2O_3$: $1.8Na_2O$: $0.3Cs_2O$: $10SiO_2$: (0.5-5) 18C6: 500 H_2O.

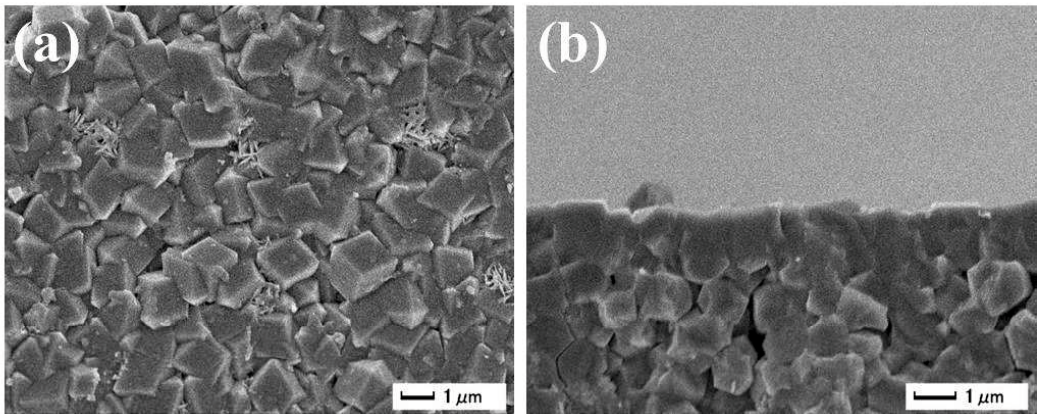

Figure 3-16. SEM images of the membrane of RHO-20 (a) surface and (b) cross section.

3.4 Conclusions

Pure RHO membrane with high density and well intergrowth have been prepared on the outer surface of α-Al_2O_3 porous tube support using 18 Crown 6 as organic structure directing agent. NaF have effect on the morphologies of RHO crystals and lead to well intergrowth of RHO zeolite crystals. Fluoride may favor the crystallization of RHO zeolite as a mineralizing agent. Higher content of organic template (18C6/Al_2O_3=5) may lead to form a dense intergrowth RHO zeolite crystal layer.

3.5 References

[1] M. Noack, P. Kölsch, A. Dittmar, Proof of the ISS-concept for LTA and FAU membranes and their characterization by extended gas permeation studies. Microporous and Mesoporous Materials, 102 (2007) 1-20.

[2] Y. Hasegawa, K. Kusakabe, S. Morooka, Effect of temperature on the gas permeation properties of NaY-type zeolite formed on the inner surface of a porous support tube. Chemical Engineering Science, 56 (2001) 4273-4281.

[3] K. Kusakabe, T. Kuroda, S. Morooka, Separation of carbon dioxide from nitrogen using ion-exchanged faujasite-type zeolite membranes formed on porous support

tubes, Journal of Membrane Science, 148 (1998) 13-23.

[4] Y. Cui, H. Kita, K. Okamoto, Preparation and gas separation performance of zeolite T membrane, Journal of Materials Chemistry, 14 (2004) 924-932.

[5] T. Tomita, K. Nakayama, H. Sakai, Gas separation characteristics of DDR type zeolite membrane, Microporous and Mesoporous Materials, 68 (2004) 71-75.

[6] Y. Zheng, N. Hu, H. Wang, Preparation of steam-stable high-silica CHA (SSZ-13) membranes for CO_2/CH_4 and C_2H_4/C_2H_6 separation, Journal of Membrane Science, 475 (2015) 303-310.

[7] T. Wu , M.C. Diaz, Y. Zheng, Influence of propane on CO_2/CH_4 and N_2/CH_4 separations in CHA zeolite membranes, Journal of Membrane Science, 473 (2015) 201-209.

[8] H.E. Robson, D.P Shoemaker, R.A. Ogilvie, Synthesis and crystal structure of zeolite Rho—a new zeolite related to Linde type A, 1973.

[9] L.B. McCusker, Crystal structures of the ammonium and hydrogen forms of zeolite rho, Zeolites, 4 (1984) 51-55.

[10] S.F. Mousavi, M. Jafari, Kazemimoghadam, Template free crystallization of zeolite Rho via Hydrothermal synthesis: Effects of synthesis time, synthesis temperature, water content and alkalinity, Ceramics International, 39 (2013) 7149-7158.

[11] T. Chatelain, J. Patarin, E. Fousson, Synthesis and characterization of high-silica zeolite RHO prepared in the presence of 18-crown-6 ether as organic template, Microporous Materials, 4 (1995) 231-238.

[12] M.M. Lozinska, E. Mangano, J.P.S. Mowat, Understanding Carbon Dioxide Adsorption on Univalent Cation Forms of the Flexible Zeolite Rho at Conditions Relevant to Carbon Capture from Flue Gases, Journal of the American Chemical Society, 134 (2012) 17628-17642.

[13] M. Palomino, A. Corma, J.L. Jordá, Zeolite Rho: a highly selective adsorbent for CO_2/CH_4 separation induced by a structural phase modification, Chemical Communications, 48 (2012) 215-217.

Chatper 4 Preparation of RHO Membrane by Organic Template-free Method

4.1 Introduction

Zeolite membranes have been investigated in various applications, including gas separations, such as CO_2/CH_4 and hydrogen recovery, and liquid separations such as dehydration. MFI type zeolite is the most studied type of zeolite membranes for gas separations, while various other types, such as A(LTA),[1] Y(FAU),[2, 3] T,[4] DDR[5] and CHA[6,7] membranes have also been reported for their unique CO_2-selective permeations.

RHO zeolite is an aluminosilicate zeolite firstly reported by H.E Robson *et al*.,[8] which is consisted by a connection of α-cages via double eight-rings (D8Rs).[9] Zeolite RHO has a small pores (0.36 nm ×0.36 nm), a relative low Si/Al ratio (2.5-5) and very high pore volume (0.26 $cm^3\ g^{-1}$, the pore volumes of 0.36 $cm^3\ g^{-1}$ if no pore space is taken up by extra-framework cations).[10-12]

A remarkably high CO_2/CH_4 adsorption selectivity of RHO zeolite, 75.2 at approx.. 100 KPa at ambient temperature, is reported,[13] which is originated from the smaller zeolitic pore size than the size of CH_4 molecule (0.38 nm), strong affinity to CO_2 and the high pore volume. The size of RHO zeolitic pore is larger than the size of water but smaller than the size of alcohols and other organics. Accordingly, RHO zeolite membrane is expected to show high separation properties in e.g. CO_2/CH_4 and water/organics mixture separations. However, RHO zeolite membranes have not been reported in our knowledge.

Pure zeolite RHO crystals could be much easily obtained using 18-Crown-6 as OSDA. However, OSDAs should be removed beforehand the applications of RHO zeolites. Formation of defects is often reported during the calcination process due to the difference in thermal expansion between the zeolite layer and the porous support. So we investigated OSDA-free synthesis conditions to prepare tubular supported

RHO zeolite membranes. Notably, the OSDA-free method averts calcination. Moreover, it also reduces the membrane preparation cost significantly. The properties of as prepared membranes were tested in single gas permeation and with pervaporation (PV) separations.

4.2 Experiment

4.2.1 Synthesis of RHO zeolite seeds

RHO crystals were prepared by an OSDA-free synthesis gel having a molar composition of 10.8 SiO_2:1 Al_2O_3:3 Na_2O:0.4 Cs_2O:110 H_2O.[10] At first, sodium hydroxide (Wako Pure Chemical Industries, Ltd) was added to deionized water and the mixture was stirred for about 10 min for complete dissolving. Then cesium hydroxide (Sigma–Aldrich, 50 wt% solution) was added to the solution under stirring, after that sodium aluminate (Wako Pure Chemical Industries, Ltd) was added. After stirring the solution for another 10 min, colloidal silica (LUDOX HS-40, 40 wt% suspension in water) was added to the solution, and the mixture gel was stirred for 24 hours at ambient temperature. Finally, the prepared gel was poured into PTFE autoclaves and heated for 4 days at 373 K. The products were washed with distilled water until the pH of the filtrate was neutral and then dried at 353 K overnight.

4.2.2 Preparation of RHO zeolite membranes

RHO Zeolite membranes were prepared on the outer surface of 10-cm-length porous α-Al_2O_3 tubes (o.d:12 mm, i.d:9 mm, average pore size: 1.3 μm, porosity: 43 %, Nikkato Corp.) by OSDA-free secondary growth method. The outer surface of porous α-Al_2O_3 supports were rub-coated with water slurry of RHO zeolite seeds. The synthesis solution had a molar composition of 10.8SiO_2:1Al_2O_3:3Na_2O:0.4Cs_2O:110 (220 or 440) H_2O:1HF. At first, sodium hydroxide was added to deionized water and the mixture was stirred for about 10 min to dissolve NaOH completely. Then cesium

hydroxide was added to the solution under stirring, after that sodium aluminate was added. Then the solution, containing aluminum source, was heated at 353 K for about 20 min to dissolve $NaAlO_2$ completely and form a clear solution, then cooled down to room temperature. In a separate beaker, hydrogen fluoride was mixed with colloidal silica and deionized water. Finally, the aluminum source was mixed with silica source. After 12 hours of aging at room temperature, 300 g of gel was placed into a stainless steel autoclave. Two pieces of seeded supports were vertically immersed into the gel. The hydrothermal synthesis was carried out at 383 K for 6 days. After synthesis, the autoclave was cooled down to room temperature and the as-synthesized membranes were washed using deionized water for several batches until the solution become neutral, and dried at 353 K overnight.

4.2.3 Characterization

Crystal structures of RHO membranes were identified by x-ray diffraction (XRD) using a SHIMADZU XRD-6100 diffractometer with CuKα radiation. The spectra were recorded over the range of Bragg angles $5° \leq 2\theta \leq 45°$ at a scanning rate of 0.02° per 10 seconds. The morphology of RHO zeolite membranes was observed using the field emission scanning electron microscopy (FE-SEM, JEOL JSM 6335F).

4.2.4 Single gas permeation measurements

Single-gas permeation was measured as function of pressure using a vacuum method for He, H_2, CO_2, N_2, CH_4 and SF_6, similar to the measurements by Cui et al. [4] The effective membrane area was about 19 cm^2. The membranes were mounted in a stainless steel module, and sealed at each end with three silicone O-rings and two stainless steel rings. The feed gas flowed through the gap between membrane outside surface and module inside surface. Prior to a series of experiments, the system with the membrane was degassed under a vacuum at 473 K for 20 h. The ideal selectivity is the ratio of single-gas permeances.

4.2.5 Pervaporation

PV performance test for a water/ethanol and water/*i*-propanol mixtures were carried out at 348 K using a PV experimental apparatus described elsewhere.[14] The effective membrane area was approximately 22 cm^2. The permeated gaseous mixture was collected by a cold trap in liquid nitrogen. Composition analysis of the feed and permeation were performed using a gas chromatograph (Shimadzu GC-14C) equipped with a TCD detector. The membrane separation performance was evaluated by the permeation flux [J/(kg m^{-2} h^{-1})] and the separation factor (α). The separation factor was determined as $\alpha_{A/B} = (Y_A/Y_B)/(X_A/X_B)$ where X_A, X_B, Y_A, and Y_B denote the mass fractions of components A and B in the feed and permeate sides, respectively. Specie A is preferentially permeated one.

4.3 Results and discussion

4.3.1 Characterization of RHO membranes

The morphology and structure of the RHO seeds and RHO zeolite membrane were characterized using SEM and XRD. Fig. 4-1 (b) shows the XRD patterns of as-synthesized seeds. All the peaks corresponds to the RHO zeolite (Fig. 4-1 (a)), suggesting the seed crystals were free from impurities. The as-synthesized RHO crystals displayed a dodecahedron shape with the size of 0.8 μm (as seen in Fig 4-2a), which is a typical morphology of RHO zeolite prepared from OSDA-free synthesis reported in literatures.[10,15]

RHO zeolites were not formed on the surface of α-Al_2O_3 support when the water concentration in the synthesis gel was changed from 110 to 220 and 440 as observed by XRD. Dissolution of RHO zeolites seemed to be faster than growth of RHO zeolites when dilute solutions were used. On the contrary, RHO zeolite membranes synthesized from $10.8SiO_2$:$1Al_2O_3$:$3Na_2O$:$0.4Cs_2O$:$110H_2O$:1HF, only exhibited the typical peaks of the RHO zeolite structure and α-Al_2O_3 as shown in Fig. 4-1 (c),

which indicated that pure RHO zeolite membrane was successfully prepared from OSDA-free synthesis with the synthesis recipe of $10.8SiO_2$:$1Al_2O_3$:$3Na_2O$:$0.4Cs_2O$:$110H_2O$:1HF. Fig. 4-2b and 4-2c shows the surface and the cross-sectional SEM images of RHO zeolite membrane. After hydrothermal synthesis, the surface of α-Al_2O_3 tube was completely covered with inter-grown crystals. A dense zeolite membrane with a thickness of 1-2 μm was formed on the support.

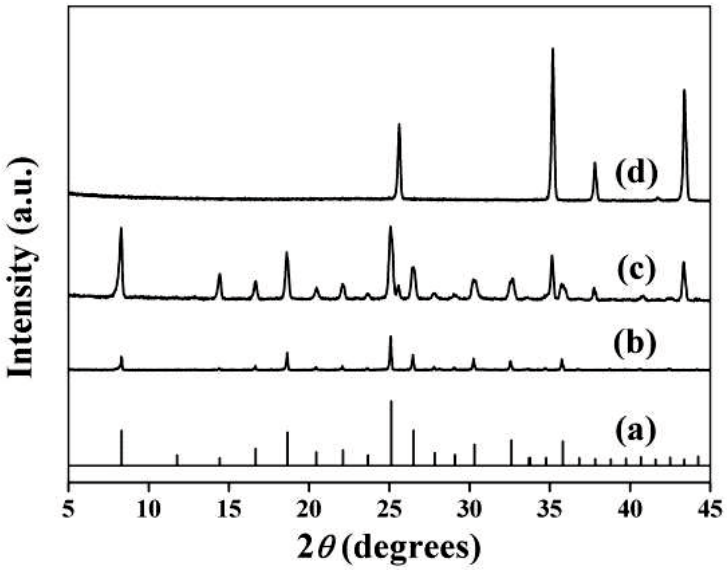

Figure 4-1. XRD patterns of (a) simulated RHO-type framework, (b) RHO seeds, (c) α-Al_2O_3 tubular RHO zeolite membrane and (d) α-Al_2O_3 support.

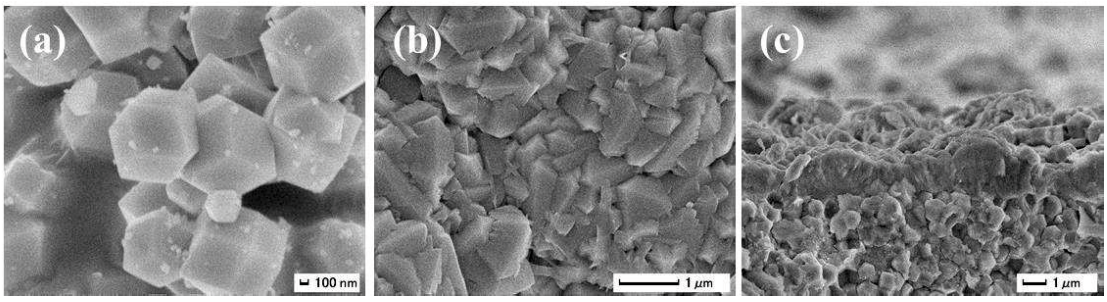

Figure 4-2. SEM images of RHO seeds (a), RHO zeolite membrane (b) surface and (c) cross section.

4.3.2 Single-gas performance

Single-gas permeances of He, H_2, CO_2, N_2, CH_4 and SF_6, measured at 308 K and

0.1 MPa feed pressure for the membrane of R1, are shown as a function of kinetic diameter in Fig. 4-3. Permeance showed a decrease when the kinetic diameter of the gas was close to the pore size of the RHO zeolite, showing the molecular sieving effect by the size of zeolitic pores. However, permeation of SF_6, having larger kinetic diameter than the RHO pore size, was also observed. The result showed the existence of two kinds of permeation pathways, zeolitic pores and non-zeolitic pores, in the RHO zeolite membrane.

The ratio of single gas permeances of CH_4 and SF_6 is about 3.5, which is similar to the value expected from the Knudsen mechanism, suggesting both gases mainly permeated through the non-zeolitic pores. The contribution of non-zeolitic premeation was subtracted from each single gas permeance value by assuming Knudsen mechanism and by using the SF_6 permeance as a standard. The subtraction was done by a following equation:

$$\Pi_{i,zeolitic} = \Pi_{i,total} - \Pi_{SF6}\sqrt{\frac{M_{SF6}}{M_i}}$$

, where $\Pi_{i,\ zeolitic}$ is assumed zeolitic permeance of component i, $\Pi_{i,\ total}$ and Π_{SF6} are the measured permeance of component i and SF_6, respectively, and M is a molar weigh.

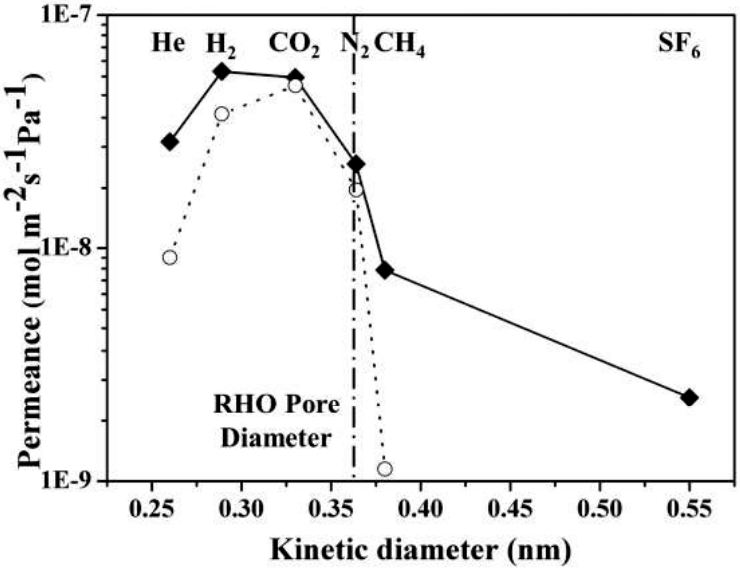

Figure 4-3. Single gas permeance of the membrane of R1 as a function of kinetic diameter at 0.1 MPa, 308 K. (closed symbols and solid line: experimental results, open symbols and dashed line: estimated zeolitic permeation by subtracting non-zeolitic permeation by assuming Knudsen mechanism).

A dashed line in the figure shows the permeance values after removing the non-zeolitic pore contribution. CO_2 permeance through RHO zeolitic pores is estimated to be ca. 5.0 $\times$ 10^{-8} mol m^{-2} s^{-1} Pa^{-1}, which is ca. 4-fold smaller compared to the reported values with CHA zeolite membranes having similar zeolitic pore size as RHO zeolite.[6] RHO zeolite is reported to show CO_2/N_2 adsorption selectivity over 48.9.[16] On the contrary, the ratio of permeance values of CO_2 and N_2, after subtracting the non-zeolitic permeation, is about 2.8. The much smaller CO_2/N_2 permeation selectivity suggests more than 10 times faster diffusivity of nitrogen than CO_2 in RHO zeolitic pathways. CO_2 diffusion may be limited by the strong affinity of CO_2 to RHO zeolite.

Influence of adsorbed water to the zeolitic pores may not be negligible. Reisner [17] reported that the Pb-RHO could not completely dehydrated under a gentle heating conditions as 473-573 K. In this study, Cs-RHO zeolite membranes were pre-heated at 473 K under vacuum beforehand the gas permeation tests. The pre-treatment temperature was decided by the heat stability of sealing materials. The pre-treatment conditions may not be enough to open complete the zeolitic pores, resulting relatively low gas permeance.

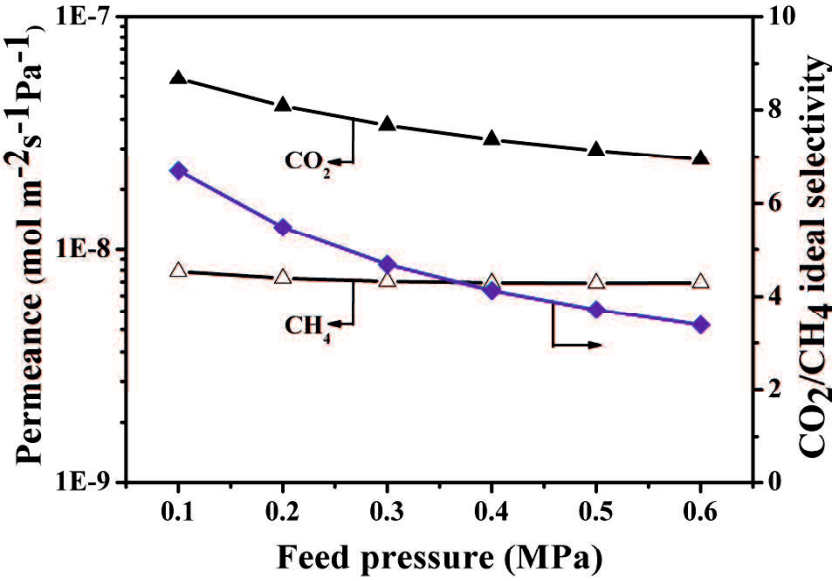

Figure 4-4. CO_2 and CH_4 permeances and CO_2/CH_4 ideal selectivities for the membrane of R1 as a function of pressure at 308 K.

Fig. 4-4 shows the pressure dependence of the single-gas permeances for CO_2 and

CH_4 from 0.1 MPa to 0.6 MPa. The CO_2 permeance decreased with increasing the feed pressure, suggesting a contribution of surface diffusion. On the contrary, the CH_4 permeance nearly kept constant, as it permeated mainly through the non-zeolitic pores with a Knudsen mechanism. The CO_2/CH_4 ideal selectivity decreased from 6.8 to 3.3 as the feed pressure increased from 0.1 MPa to 0.6 MPa.

4.3.3 Effect of different support tubes

Figure 4-5 illustrate the SEM images of RHO membranes prepared by using α-Al_2O_3 tube and mullite tube. As seen in Figure 4-5a and 4-5c, pure and thin RHO membrane with high density and well intergrowth could be prepared on the outer surface of α-Al_2O_3 porous tube support. It was difficult to form a well intergrowth zeolitic layer on the surface of mullite porous tube. The RHOmbus RHO crystals seems pile together through the cross section of zeolitic layer for the membrane R2, which prepared by using mullite tube as support. It is similar for the synthesis of RHO membrane by using the organic structure directing agent, α-Al_2O_3 porous tube seems much suitable for synthesis of high quality RHO membrane.

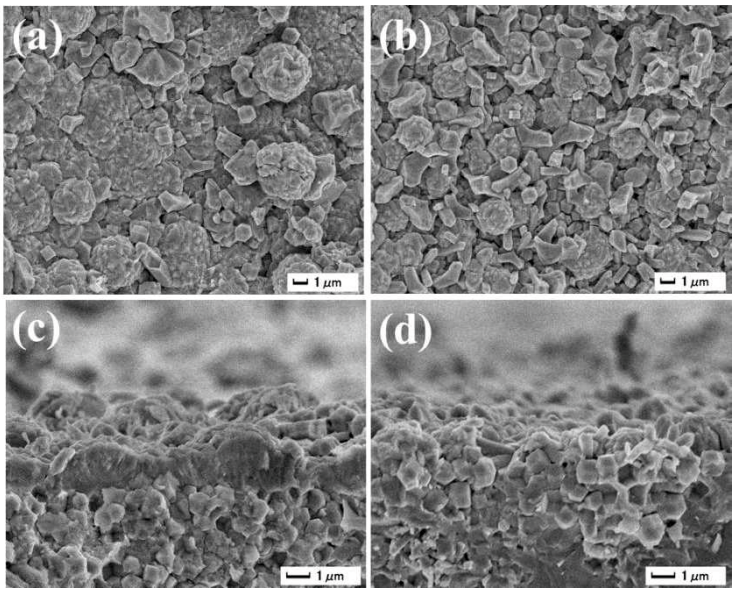

Figure 4-5. SEM images of RHO membranes prepared by using different support tubes (a) and (c) surface and cross section of R1 prepared by using α-Al_2O_3 tube; (b) and (d) surface and cross section of R2 prepared by using mullite tube.

4.3.4 Effect of water concentration

Table 4-1 shows the single-gas performance of RHO membranes prepared on the α-Al_2O_3 tubes with different H_2O/Al_2O_3 ratios. Since the initial gel was very dense with the H_2O/Al_2O_3 ratios of 110, we try to dilute the synthesis solution for the optimization. From Table 4-3, the more diluted synthesis solution was not suitable for preparation of the RHO membranes with high separation factors compared with the H_2O/Al_2O_3 ratio of 110. The sample prepared with H_2O/Al_2O_3 ratio of 200 was leaking after 7 days of hydrothermal treatment, suggesting that under the present synthesis conditions the solution was too diluted. It is clear that the high H_2O/Al_2O_3 ratio would not result in a continuous crystal layer because not only fewer nuclei were directly formed on the surface or attached onto the support surface from the solution, but also the limited nutrients were provided for their crystal growth. On the other hand, with a much more diluted H_2O/Al_2O_3 ratio of 440, no crystal was found on the support.

Table 4-1 Single gas performance of RHO membrane synthesis as a function of different water contents at 308 K and 0.1 MPa feed pressure.

No.	Synthesis conditions			Phase(XRD)	Single gas Permeance (10^{-7}mol m^{-2} s^{-1} Pa^{-1})					Ideal selectivity	
	H_2O	T (^{0}C)	Time(d)		He	H_2	CO_2	N_2	CH_4	CO_2/N_2	CO_2/CH_4
R1	110	110	6	RHO	0.29	0.57	0.54	0.23	0.08	2.35	6.75
R3	200	110	7	RHO	Leaked						
R4	440	110	7	α-Al_2O_3	Leaked						

Note: synthesis recipe: 10.8 SiO_2:1Al_2O_3:3 Na_2O:0.4 Cs_2O: (110-440) H_2O.

10-cm-porous α-Al_2O_3 tubular as support.

4.3.5 Pervaporation performance

Even if the zeolitic pores are partially plugged by water during the gas permeation,

the plugging of water will not affect the water permeation.[18] Therefore, the membrane performances were checked by PV. Table 1 shows PV performance of water/organics through RHO zeolite membranes. Results of three membranes are shown in the table. All the as-synthesized RHO zeolite membranes showed water-selective permeation from water/ethanol and water/isopropanol mixtures.

Table 4-2 Pervaporation performance of RHO zeolite membranes for 10/90 wt% Water/Organics.

No.	Water/Organics	Water content in permeation (wt%)	Total Flux(kg/m^2·h)	Separation factor
			1	1
R1	Water/ethanol	98.04	0.76 (0.72)*	473 (503)*
	Water/isopropanol	98.70	0.92	730
R2	Water/ethanol	97.93	0.72	450
	Water/isopropanol	98.17	0.89	501
R3	Water/ethanol	97.22	0.81	340
	Water/isopropanol	97.61	0.99	389

Note: * measured at the end of PV tests of different feed compositions
Synthesis recipe: 10.8SiO_2:1Al_2O_3:3Na_2O:0.4Cs_2O:110H_2O:1HF; Synthesis condition: 383 K, 6 d

Influence of the feed composition was examined further with the membrane of R1. After several pervaporation experiments, with total test time over 30 hours, the water/ethanol PV performance was retested. Both the total flux and separation factor showed almost the same values as fresh membranes as seen in Table 4-1, indicating that the robustness of a RHO zeolite membrane. Fig.5 shows the change in permeate flux and separation factor as a function of the ethanol feed concentration and isopropanol feed concentration. The total flux was about 0.83 kg m^{-2} h^{-1} at 85 wt% ethanol composition and it decreased to 0.62 kg m^{-2} h^{-1} at 95 wt% ethanol composition with an increase of the ethanol concentration in the feed. But the separation factor was increased from 280 to 1010 over the range from 85 to 95 wt%

composition. The total mass flux increased as the isopropanol feed concentration increases, which is similar as in the water/ethanol systems and a maximum separation factor of 1390 is observed at a feed concentration of 95 wt%. The decrease in total flux with increasing ethanol concentration is due to a large decrease in ethanol flux. The isopropanol flux decreases as the isopropanol concentration increases although the changes are very small. It decreases from about 0.015 to 0.012 kg m^{-2} h^{-1} when the isopropanol concentration increases from 85 to 95 wt%.

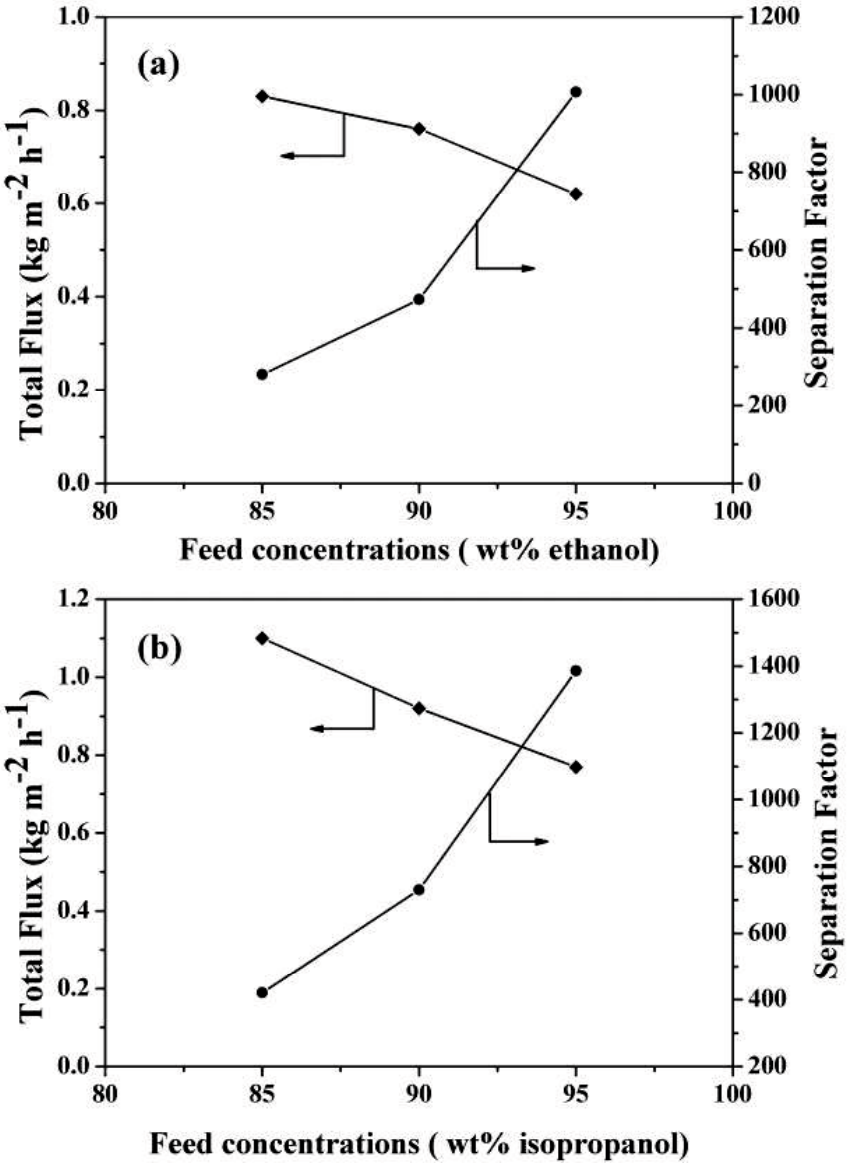

Figure 4-6. Effect of (a) ethanol and (b) isopropanol feed concentration on total flux and separation factor.

Fig. 4-6 shows permeances of water and alcohols as a function of feed concentration in molar ratio. Water permeance values obtained from PV tests with ethanol and isopropanol solutions were almost the same, suggesting water permeation was not hindered by the co-existing alcohols. The pore size of Rho zeolite is smaller than the size of alcohols and, thus, only allows water entering into. As large part of water permeated through zeolitic pores, and as alcohols cannot enter the zeolitic pores, the influence of co-existing alcohol on water permeance was negligible. Permeation of ethanol and isopropanol showed a contribution of non-zeolitic permeation as suggested with SF_6 permeation. Non-zeolitic pathways may have been generated during the drying step at 473K beforehand the gas permeation tests, but the PV results showed as-synthesized membranes have some defects already.

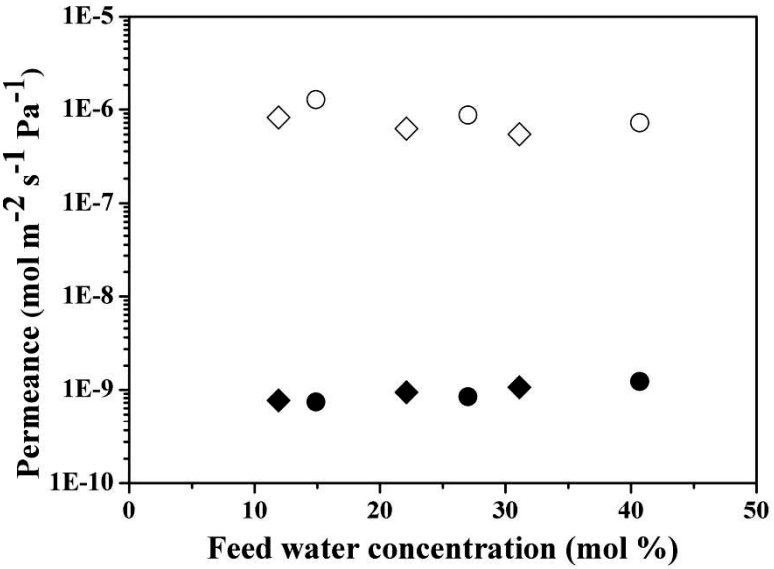

Figure 4-7. Effect of feed water concentration on the water and alcohol (ethanol/isopropanol) permeabilities for RHO zeolite membrane. (◇:water partial permeance in water/ethanol, ◆:ethanol partial permeance in water/ethanol,○:water partial permeance in water/isopropanol, ●:isopropanol parital permeance in water/isopropanol)

4.4 Conclusions

RHO zeolite membranes (0.36 nm pore diameter) were synthesized by using OSDA-free method on the outer surface of porous tubular α-Al_2O_3 supports.

CO_2 permeation through as-synthesized RHO zeolite membrane suggested a

contribution of surface diffusion. Accordingly, RHO zeolite membrane showed CO_2/N_2 and CO_2/CH_4 ideal selectivities higher than the Knudsen selectivities. On the other hand, the ideal CO_2 selectivities were smaller than the reported adsorption selectivities. Contribution of non-zeolitic permeation is one reason for the smaller selectivity. Diffusivity of CO_2 is suspected to be small in RHO zeolitic pores due to the strong affinity, resulting in inversed diffusion selectivity for CO_2 and lowering the CO_2-selectivity of RHO zeolite membranes.

RHO zeolite membranes showed dehydration performance in water/ethanol and water/isopropanol separations. The highest separation factor obtained for water/isopropanol was 1390 at an isopropanol feed concentration of 95 wt% with a total flux of 0.77 kg m^{-2} h^{-1}. The membrane showed similar separation properties after 30 hours of total testing time, suggesting robustness of the membrane.

4.5 References

[1] M. Noack, P. Kölsch, A. Dittmar, Proof of the ISS-concept for LTA and FAU membranes and their characterization by extended gas permeation studies. Microporous and Mesoporous Materials, 102 (2007) 1-20.

[2] Y. Hasegawa, K. Kusakabe, S. Morooka, Effect of temperature on the gas permeation properties of NaY-type zeolite formed on the inner surface of a porous support tube. Chemical Engineering Science, 56 (2001) 4273-4281.

[3] K. Kusakabe, T. Kuroda, S. Morooka, Separation of carbon dioxide from nitrogen using ion-exchanged faujasite-type zeolite membranes formed on porous support tubes, Journal of Membrane Science, 148 (1998) 13-23.

[4] Y. Cui, H. Kita, K. Okamoto, Preparation and gas separation performance of zeolite T membrane, Journal of Materials Chemistry, 14 (2004) 924-932.

[5] T. Tomita, K. Nakayama, H. Sakai, Gas separation characteristics of DDR type zeolite membrane, Microporous and Mesoporous Materials, 68 (2004) 71-75.

[6] Y. Zheng, N. Hu, H. Wang, Preparation of steam-stable high-silica CHA (SSZ-13)

membranes for CO_2/CH_4 and C_2H_4/C_2H_6 separation, Journal of Membrane Science, 475 (2015) 303-310.

[7] T. Wu , M.C. Diaz, Y. Zheng, Influence of propane on CO_2/CH_4 and N_2/CH_4 separations in CHA zeolite membranes, Journal of Membrane Science, 473 (2015) 201-209.

[8] H.E. Robson, D.P Shoemaker, R.A. Ogilvie, Synthesis and crystal structure of zeolite RHO—a new zeolite related to Linde type A, 1973.

[9] L.B. McCusker, Crystal structures of the ammonium and hydrogen forms of zeolite rho, Zeolites, 4 (1984) 51-55.

[10] S.F. Mousavi, M. Jafari, Kazemimoghadam, Template free crystallization of zeolite Rho via Hydrothermal synthesis: Effects of synthesis time, synthesis temperature, water content and alkalinity, Ceramics International, 39 (2013) 7149-7158.

[11] T. Chatelain, J. Patarin, E. Fousson, Synthesis and characterization of high-silica zeolite RHO prepared in the presence of 18-crown-6 ether as organic template, Microporous Materials, 4 (1995) 231-238.

[12] M.M. Lozinska, E. Mangano, J.P.S. Mowat, Understanding Carbon Dioxide Adsorption on Univalent Cation Forms of the Flexible Zeolite Rho at Conditions Relevant to Carbon Capture from Flue Gases, Journal of the American Chemical Society, 134 (2012) 17628-17642.

[13] M. Palomino, A. Corma, J.L. Jordá, Zeolite Rho: a highly selective adsorbent for CO_2/CH_4 separation induced by a structural phase modification, Chemical Communications, 48 (2012) 215-217.

[14] R. Zhou, Z. Hu, N. Hu, Preparation and microstructural analysis of high-performance mordenite membranes in fluoride media, Microporous and Mesoporous Materials, 156 (2012) 166-170.

[15] M. Park, S.H. Kim, N.H. Heo, Synthesis of zeolite rho: aging temperature effect, Journal of Porous Materials, 3 (1996) 151-155.

[16] S. Araki, Y. Kiyohara, S. Tanaka, Adsorption of carbon dioxide and nitrogen on

zeolite rho prepared by hydrothermal synthesis using 18-crown-6 ether, Journal of Colloid and Interface Science, 388 (2012) 185-190.

[17] B.A. Reisner, Y. Lee, J.C. Hanson, et al., Understanding negative thermal expansion and 'trap door'cation relocations in zeolite rho, Chemical Communications, 22 (2000) 2221-2222.

[18] S. Khajavi, F. Kapteijn, J.C. Jansen, Synthesis of thin defect-free hydroxy sodalite membranes: New candidate for activated water permeation, Journal of Membrane Science, 299 (2007) 63-72.

Chapter 5 Synthesis of Low-silica CHA Zeolite Chabazite in Fluoride Media without Organic Structural Directing Agents and Zeolites

5.1. Introduction

CHA-type molecular sieve framework owns a 3-dimensional interconnected pore system with 8-membered ring windows (3.8 Å×3.8 Å) and a relatively low framework density (15.1 T/1000 $Å^3$). Low-silica (chabazite), high-silica (SSZ-13) CHA zeolites and silicoaluminophosphate-34 (SAPO-34) that belongs to CHA-type molecular sieves have attracted many attentions for applications of the separation and catalysis, in the form of powder and membrane. SAPO-34 molecular sieve was an important catalyst for methanol-to-olefins process.[1] Chabazite and SSZ-13 zeolite were utilized to absorb CO_2 [2] and to catalysis NO_x to NH_3 [3]. Falconer and Noble group fabricated SSZ-13 zeolite [4] and SAPO-34 membranes [5,6] for light gas separation. SAPO-34 membrane exhibited a high CO_2 permeance [1×10^{-6} mol/(m^2 s Pa)] and high CO_2/CH_4 selectivity (70) even at 4.6 MPa at room temperature [6]. Hasegawa *et al.* reported that chabazite membrane showed excellent dehydration performance for water/alcohol mixtures [7].

CHA-type zeolites were usually synthesized using OH^- as mineralizing agent and adding either organic-structure-directing agents (OSDAs) or zeolite phases as seeds. On the other hand, OSDA-free synthesis shows advantages on cheap preparation without a necessity for calcination of the product. The calcination always leads to the formation of defects in/among crystals, especially for membranous zeolites. Chabazite crystals were also prepared by interzeolite conversion of zeolite HY [8] and MER-type zeolites [9], in which all silica and alumina sources came from crystalline zeolite phases. Very recently, we modified such interzeolite conversion method and utilized a small amount of heterogeneous seeds (*i.e.* nanosized zeolite T); however, this induced the formation of a large amount of amorphous aluminosilicate in the

product [10]. Hasegawa *et al.* [11,12] prepared the supported chabazite membranes by secondary growth using a strontium salt as additive. However, the MER-type phases always occurred in the crystal layers [12]. To our best knowledge, the OSDA-free and zeolites-free synthesis for pure CHA-type zeolite phase have not yet been reported.

Fluorides (F^-) as sole mineralizing agent or the combinative one were reported to accelerate the crystallization of high-silica and all-silica zeolites and decrease the crystal defects [13-20]. High-silica CHA zeolite [19,20] was also prepared using fluoride route in the presence of TMAdaOH. NMR and X-ray diffraction methods have been utilized to characterize the location and local structure of the F^- ion in the as-synthesized high-silica and all-silica zeolites [21,22]. Attfield *et al.* [23] summarized three types of F^- ion environments found in siliceous zeolites: (i) as part of an ion pair; (ii) in the center of a small cage far from any Si atoms; and (iii) coordinated to a Si atom to form a part of a pentacoordinated $SiO_{4/2}F^-$ units.

Few studies, however, reported the preparation and especially the role and location of F^- ion in view of low-silica zeolites. In our previous studies, we made zeolite T and mordenite crystals and membranes in fluoride media [24-26]. The crystallization rate for both powdery and membranous zeolites together with crystal morphologies depended on the addition amount of fluoride salts. In the current study, we reported a new fluoride route to *in-situ* prepare low-silica CHA zeolite (chabazite) in the absence of OSDAs and seeds. The role and location of fluoride ion were also clarified.

5.2. Experiment

5.2.1. Synthesis of chabazite using fluoride route

Ammonium fluoride, sodium fluoride and potassium fluoride were purchased from Sigma-Aldrich as fluoride source. Unless otherwise especially specified, ammonium fluoride was the standard fluoride additive. To prepare the reaction mixtures (hydrogels) having the batch molar compositions: $1SiO_2$: xAl_2O_3: $0.39K_2O$: yNH_4F:

$35H_2O$, where x varies from 0.05 to 0.33, and y varies from 0.1 to 0.5 (see Table 1), a certain amount of aluminum hydroxide (Wako Chemicals) was dissolved in alkaline solution containing 7.0 g of potassium hydroxide (Shanghai Qinxi Chemicals) and 67.6 g of demineralized water, under heating at 353 K. After cooling down, a certain amount of ammonium fluoride and Ludox TM-40 colloidal silica (Sigma-Aldrich, 40 wt. % SiO_2 water suspension) were added in the clear alkaline aluminate solution. The resulting mixture was stirred at room temperature for 6 h to form a milk-like hydrogel. The produced hydrogel was then divided among needed number of Teflon-lined stainless-steel autoclaves and hydrothermally treated at 433 K for various times (see Table 1). After hydrothermal treatment the product was separated by centrifuging, washed with demineralized water until pH of centrifuged solution was 7 and dried at 373 K overnight. Chabazite was also prepared by seeded synthesis by adding chabazite seeds with 0.5% of the weight of the entire reaction mixture under the same synthesis conditions with reduced synthesis time.

5.2.2. Ion-exchange of the as-synthesized chabazite

The as-synthesized chabazite was ion-exchanged to the calcium form. 2 g samples were dispersed in 200 ml 2 mol/l calcium chloride solution in a flask equipped with a condenser. The ion-exchange procedure was carried out under reflux and stirring for 24 h at 333 K. The ion-exchanged samples were separated by centrifugation. The ion-exchange procedure was repeated three times with the fresh solution. The final sample was washed four times with de-ionized water and dried at 373 K overnight. The ion-exchanged ratio was expressed by the two times mole ratio of Ca^{2+} divided the sum of two times mole ratio of Ca^{2+} and mole ratio of K^+ in the EDX results of the ion-exchanged sample.

5.2.3. Zeolite characterization

X-ray diffraction patterns of the solid powders were recorded on a Rigaku Ultima IV X-ray diffractometer using Cu-Kα radiation. The morphology of the crystals was observed by field-emission scanning electron microscopy (FE-SEM, Hitachi SU-8020). The element analysis of samples was measured by inductively-coupled plasma optical emission spectroscopy (ICP, Varian 725ES) and energy dispersive X-ray analysis (EDX, Bruker Quantax 200). The relative crystallinity of the solid products was calculated by comparing the sum of intensities of the desired sample with the standard sample (runs No. 5 in Table 1) for the typical peaks at $2\theta = 9.4$, 20.5 and 30.5°.

The ^{27}Al , ^{29}Si and ^{19}F magic-angle spinning nuclear magnetic resonance (MAS NMR) spectra of the zeolite powders were recorded at 104.2 , 79.5 and 376.8 MHz, respectively, using a zirconia rotor of 4 mm diameter, on a Bruker Advance III 400 WB spectrometer. The rotor was spun with dry air at 4 kHz for ^{29}Si MAS NMR, at 15 kHz for ^{27}Al MAS NMR and at 30 kHz for ^{19}F MAS NMR. The spectra were accumulated with 3 μs pulses, 2 s recycle delay and 1024 scans for ^{27}Al MAS NMR and with 4.5 μs pulses, 40 s recycle delay and 1024 scans for ^{29}Si MAS NMR. ^{19}F MAS NMR was recorded at 2.6 μs pulses, 30 s recycle delay and 2000 scans. $Al(NO_3)_3 \cdot 9H_2O$, $Si(CH_3)_4$ (TMS) and $CFCl_3$ were used as chemical shift reference for ^{27}Al, ^{29}Si and ^{19}F MAS NMR, respectively.

5.3. Results and discussion

5.3.1. The crystallization process of chabazite

Figure 5-1 shows the XRD patterns of the products prepared using fluoride route as a function of synthesis time. The crystallinity of bottom solids increased with synthesis time from 0 to 72 h (runs No. 1 to 5; see Table 5-1), and was independent of synthesis time from 72 to 120 h (runs No. 5 to 7; see Table 5-1). The typical peaks of

crystalline solids were quite close to the peaks of reported CHA framework [11,27], which indicated that our products were pure CHA phase. The crystallization processes of the CHA-type zeolite prepared by *in-situ* (runs No. 1 to 7; see Table 5-1) and chabazite-seeded (runs No. 8 to 17; see Table 5-1) synthesis were illustrated in Figure 5-2. The induction period for the *in-situ* synthesis was as long as 24 h, which was 3 times longer than that for chabazite-seeded synthesis. Meanwhile, the crystallization rate for the seeded synthesis was much higher than that for the *in-situ* synthesis. It suggests that the chabazite seeds supply effective nuclei for zeolite crystallization, by which both the nucleation rate and the nuclei number are greatly increased. The differences in crystallization curves of this chabazite by the *in-situ* and seeded methods were consistent to those for MFI crystals [28]. This conclusion was also supported by their SEM observations in Figure 5-3. Chabazite crystals (run No. 13; see Table 1) obtained by the seeded method for 24 h (Fig. 3f) had a walnut-like shape and the crystals (run No. 5; see Table 5-1) obtained by the *in-situ* method for 72 h (Figure 5-3b) had the similar shape. However, the crystal size of the former (~7 μm) is much smaller than that of the latter (~20 μm). The mass of as-synthesized crystals from seeded gel was just 20% higher than that from *in-situ* gel. The increased mass of the product almost corresponded to the added amount of chabazite seeds. Thus, the number of the crystals that were prepared by seeded method was much larger than that of the crystals prepared by *in-situ* method, which could be attributed to the nuclei effects of the chabazite seeds in gel. Crystal size increased slightly with the increase of synthesis time for both kinds of chabazite by *in-situ* and seeded synthesis. The walnut shape for the crystals tended to change to disk-like shape when synthesis time increased either from 24 to 72 h by seeded synthesis (Figure 5-3f-h), or from 72 to 120 h by *in-situ* synthesis (Figure 5-3b-d). In these two systems, the morphology changes occurred just after crystallization equilibrium as observed from Figure 5-2. At these courses after crystallization equilibrium, the rate of crystal growth is also equal to that of zeolite dissolution. However, the rate of dissolution is in general proportional to the surface area of the dissolving solid [29]. The disc-like crystals with

less surface area have more chances to survive than the walnut-like crystals when the hydrothermal treatment was prolonged.

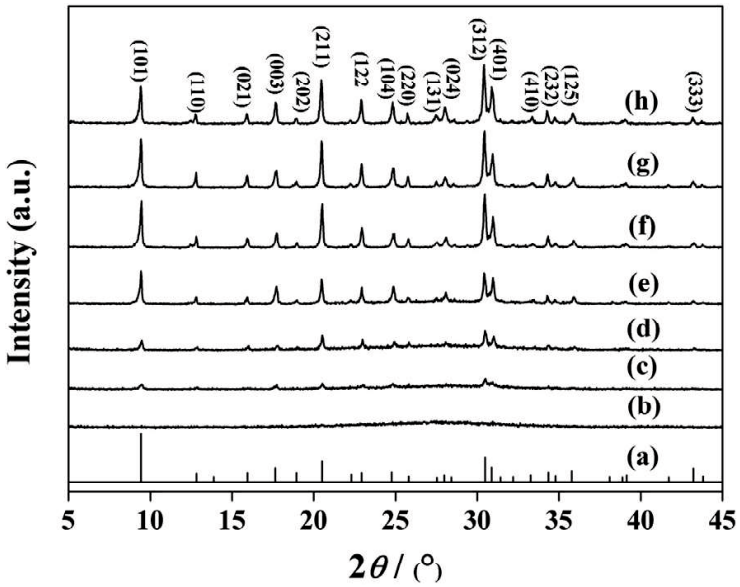

Figure 5-1. XRD patterns of (a) simulated CHA-type framework, and fluoride-derived crystals prepared by in situ synthesis at 433 K for (b) 24, (c) 30, (d) 36, (e) 48, (f) 72, (g) 96 and (h) 120 h (runs No. 1–7; see Table 1), respectively.

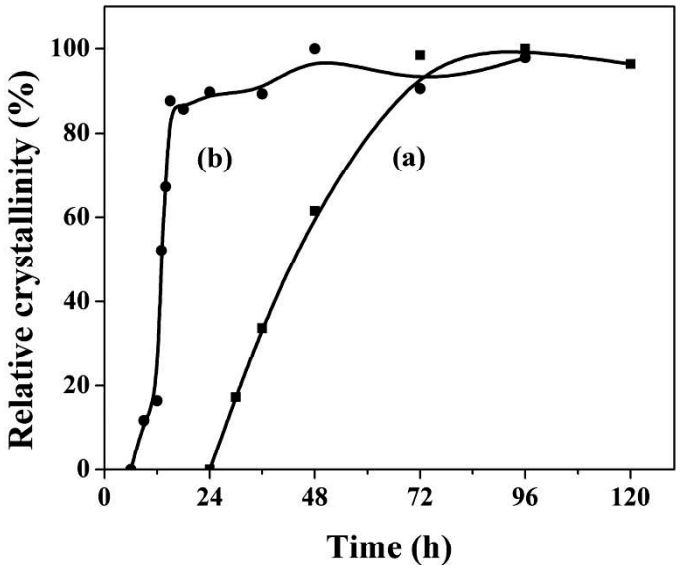

Figure 5-2. Crystallization curves of chabazite by (a) in situ synthesis (runs No. 1–7; see Table 1) and (b) chabazite-seeded synthesis (runs No. 8–17; see Table 1).

Table 5-1 The summary of synthesis conditions and the properties of as-synthesized solids.

No.	Synthesis condition					Product			
	F^- source	SiO_2/Al_2O_3 [a] ratio	F^-/SiO_2 [a] ratio	Temp. (K)	Time (h)	Si/Al ratio ICP	Si/Al ratio EDX	Size (μm)[b]	Phase[c]
1	NH_4F	5	0.3	433	24	-	-	-	Am
2	NH_4F	5	0.3	433	30	-	-	-	Am (CHA)[d]
3	NH_4F	5	0.3	433	36	2.4	2.2	20-30	CHA (Am)
4	NH_4F	5	0.3	433	48	2.4	2.2	20-30	CHA
5	NH_4F	5	0.3	433	72	2.5	2.3	20-30	CHA
6	NH_4F	5	0.3	433	96	2.4	2.2	20-30	CHA
7	NH_4F	5	0.3	433	120	2.4	2.1	20-30	CHA
8	NH_4F[e]	5	0.3	433	6	-	-	-	Am
9	NH_4F[e]	5	0.3	433	9	-	-	-	Am
10	NH_4F[e]	5	0.3	433	12	-	-	-	Am (CHA)
11	NH_4F[e]	5	0.3	433	14	2.4	2.2	5-10	CHA (Am)
12	NH_4F[e]	5	0.3	433	18	2.5	2.2	5-10	CHA (Am)
13	NH_4F[e]	5	0.3	433	24	2.5	2.3	5-10	CHA
14	NH_4F[e]	5	0.3	433	36	2.5	2.3	5-10	CHA
15	NH_4F[e]	5	0.3	433	48	2.4	2.3	5-10	CHA
16	NH_4F[e]	5	0.3	433	72	2.4	2.2	5-10	CHA
17	NH_4F[e]	5	0.3	433	96	2.4	2.2	5-10	CHA
18	NH_4F	3	0.3	433	72	2.2	2.1	1-4	LTL
19	NH_4F	10	0.3	433	72	2.7	2.5	15-20	CHA
20	NH_4F	20	0.3	433	96	-	-	-	Am
21	NH_4F[e]	3	0.3	433	120	-	-	-	Am
22	NH_4F[e]	10	0.3	433	48	2.7	2.5	5-10	CHA
23	NH_4F[e]	20	0.3	433	96	3.5	3.3	5-10	CHA
24	NH_4F[e]	30	0.3	433	48	-	-	-	Am
25	NH_4F	5	0.3	393	144	-	-	-	Am
26	NH_4F	5	0.3	413	120	2.5	2.3	10-15	CHA
27	NH_4F	5	0.3	453	60	2.4	2.1	15-20	CHA
28	NH_4F	5	0	433	96	2.0	1.8	20-30	MER
29	NH_4F	5	0.1	433	72	2.1	2.0		MER (CHA)
30	NH_4F	5	0.2	433	72	2.3	2.2		CHA (MER)
31	NH_4F	5	0.4	433	72	2.6	2.5	5-10	CHA (Am)
32	NH_4F	5	0.5	433	72	-	-	-	Am
33	NaF	5	0.3	433	72	2.2	2.1	20-30	OFF
34	KF	5	0.3	433	72	2.8	2.3	0.5-2	CHA (MER)

Note: [a] Chemical composition in the initial gel; [b] Determined by SEM; [c] Determined by XRD and SEM; [d] the phase included in brackets is the minor phase; [e] with the addition of 0.5 wt.% chabazite (runs No. 5) in synthesis gel.

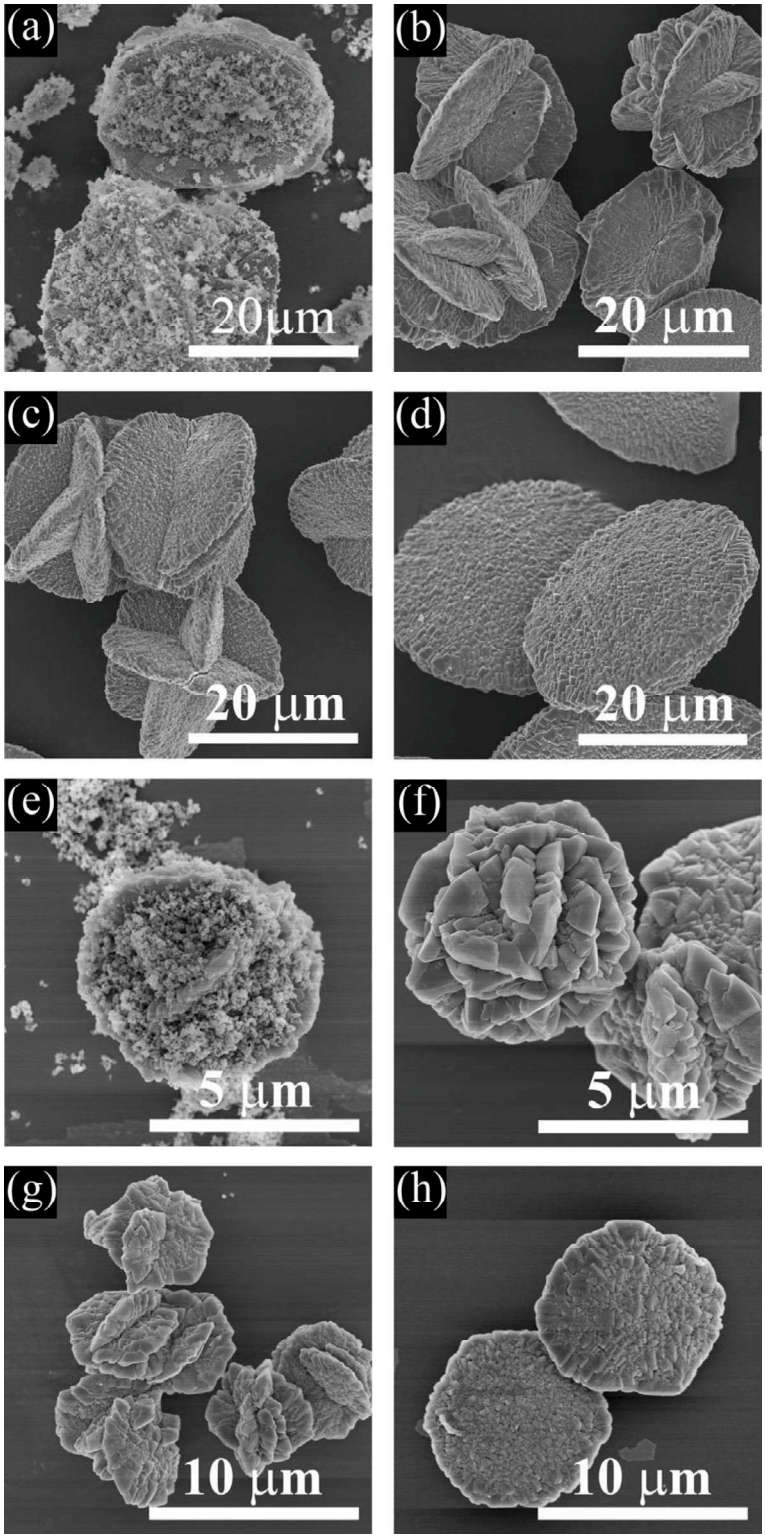

Figure 5-3. SEM images of fluoride-derived chabazite obtained by in situ synthesis at 433 K for (a) 36, (b) 72, (c) 96 and (d) 120 h and obtained by chabazite-seeded synthesis for (e) 14, (f) 24, (g) 48 and (h) 72 h, respectively.

5.3.2. NMR characterizations

The fluoride-derived chabazite (run No. 5; see Table 1) were tested by ^{27}Al, ^{29}Si

and ^{19}F MAS NMR to investigate the location of fluoride ion. Only one peak at approximate 59 ppm was found in ^{27}Al MAS NMR spectrum in Figure 5-4a, corresponding to tetrahedrally-coordinated aluminum in framework. There was no extraframework aluminum since no peak was observed at 0 ppm. The ^{29}Si MAS NMR spectra in Fig. 4b had four peaks at -109, -104, -98 and -93 ppm. These peaks were assigned to Si(0Al), Si(1Al), Si(2Al) and Si(3Al) species, respectively [14,30]. The ^{19}F MAS NMR spectra (Fig. 4c) show one significant peak at around -123 ppm together with three spinning sideband peaks at -43, -176 and -203 ppm.

Similar to our previous works [24-26], the main peak of our fluoride-derived chabazite at -123 ppm was due to the presence of F^- counterion in zeolite channel as the counterion of K^+ and H^+ cation. The weak peaks at -43, -176 and -203 ppm were probably assigned to spinning sidebands [16]. They can be due to either ^{19}F chemical shift anisotropy or homo- or heteronuclear dipole interactions [16].

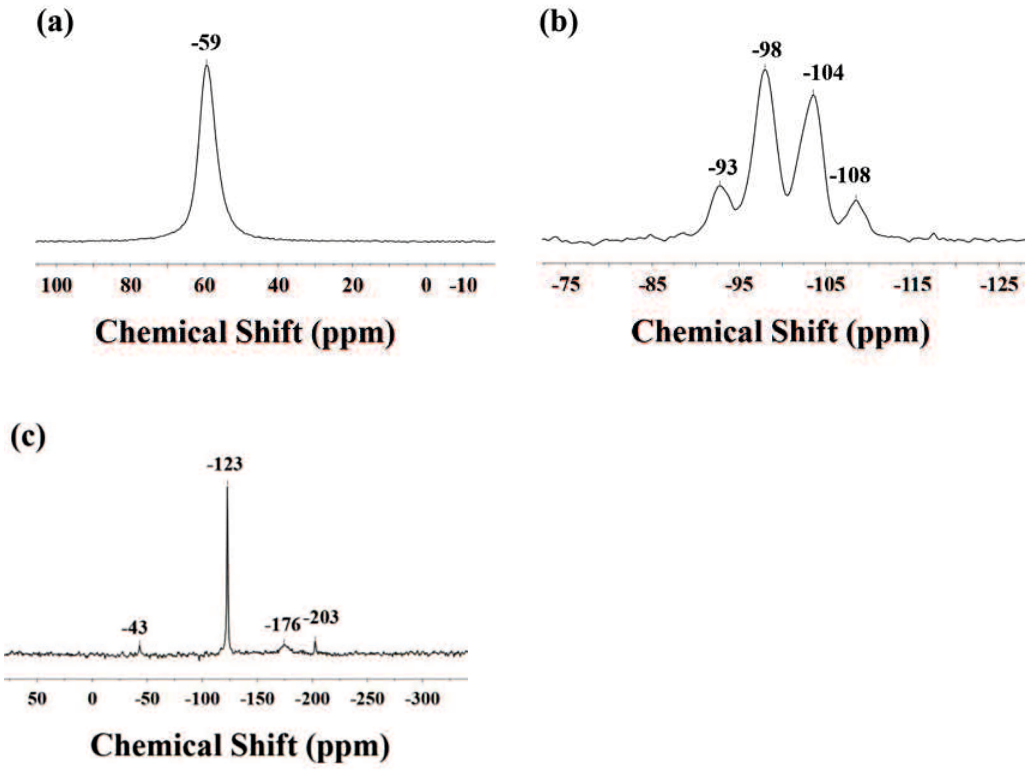

Figure 5-4. Solid NMR spectra of fluoride-derived chabazite (run No. 5; see Table 1) (a) 27Al MAS NMR (b) 29Si MAS NMR and (c) 19F MAS NMR. Spinning sidebands are marked with asterisk.

5.3.3. Nitrogen adsorption

Figure 5-5 shows the nitrogen adsorption-desorption isotherms of as-synthesized and Ca^{2+}-ion-exchanged samples. Note that the as-synthesized fluoride-derived sample (run No. 5; see Table 5-1) shows only a very low nitrogen adsorption amount as shown in Fig. 5a. The adsorption amount of nitrogen in Fig. 5b for the crystals after Ca^{2+} ion exchange increased by one order of magnitude. This adsorption-desorption curve was classified as typical Type I curves according to the IUPAC classification, which indicated their micropore properties. The low nitrogen loading for the as-synthesized CHA-type zeolite crystals was probably attributed to the fact that the existence of K^+ in the 8-ring small channel strongly hindered adsorption of nitrogen. It was consistent to the previously reported K^+ and Na^+ types of chabazite [10]. The chabazite (run No. 13; see Table 5-1) prepared by seeded synthesis and after Ca^{2+} ion exchange had the same Type I adsorption-desorption curve and the highest adsorption amount of nitrogen. External surface area for the chabazite (run No. 13; see Table 5-1) prepared by seeded synthesis after Ca^{2+} ion exchange was almost twice larger than that for the chabazite (run No. 5; see Table 5-1) by *in-situ* synthesis (as shown in Table 5-2). It was mainly attributed to the smaller crystal size for the crystals by seeded synthesis. The seeded sample also had the larger BET surface area than the *in-situ* sample. And the difference in BET surface area was close to the difference in external surface area between the two samples, indicating the inner surface areas for the both samples are quite close. This conclusion was consistent to the crystallinity results in Figure 5-2, where both samples had the similar relative crystallinity.

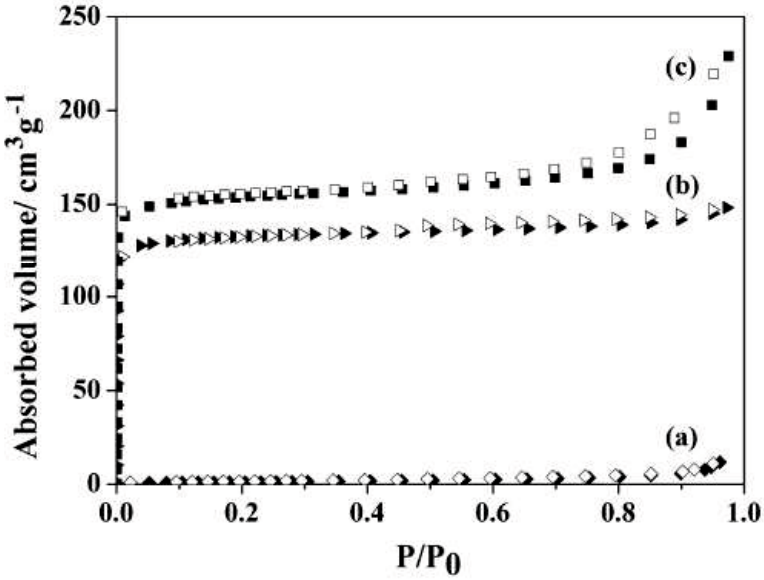

Figure 5-5. Nitrogen adsorption–desorption isotherms for (a) fluoride-derived chabazite (run No. 5; see Table 5-1), (b) fluoride-derived chabazite (run No. 5; see Table 5-1) after ion exchange and (c) chabazite by seeded synthesis (run No. 13; see Table 5-1) after ion exchange.

Table 5-2 Adsorption properties of as-synthesized and ion-exchanged CHA-type zeolite crystals.

Sample	Cation	Exchanged ratio (%)[a]	BET Surface area (m^2/g)[b]	External surface area (m^2/g)[c]	Pore volume (cm^3/g)	
					Total[d]	Micropore[c]
F-derived	K^+	0	45	20	0.0387	0.0230
F-derived, Ca^{2+}-exchanged	K^+, Ca^{2+}	55.6	537	24	0.2292	0.2182
F-derived, Seeded, Ca^{2+}-exchanged	K^+, Ca^{2+}	57.8	569	69	0.4095	0.2972

[a] Test by EDX.

[b] BET method

[c] t-Pot method

[d] Volume adsorbed at P/P_0=0.99

5.3.4. Effect of gel SiO_2/Al_2O_3 ratios

Zeolites were prepared by gel SiO_2/Al_2O_3 ratios from 3 to 30 by *in-situ* and seeded

synthesis as shown in Table 5-1. For the *in-situ* synthesis, pure chabazite was only obtained by gel SiO_2/Al_2O_3 ratios of 5 and 10 (runs No. 4-7, 19, 26 and 27; see Table 5-1). Figure 5-6 shows the XRD patterns of as-synthesized crystals prepared by different gel SiO_2/Al_2O_3 ratios in seeded reaction mixture. Seed-in-gel synthesis broadened the crystallization intervals in gel SiO_2/Al_2O_3 ratio (runs No. 13-17, 22 and 23; see Table 5-1). The framework Si/Al ratio of the as-synthesized crystals increased from 2.5 to 3.5 with the increase of gel SiO_2/Al_2O_3 ratio from 5 to 20. The gel SiO_2/Al_2O_3 ratio of 30 resulted into the main amorphous phase (run No. 24; see Table 5-1). The results also showed that prolonged hydrothermal treatment does not affect type of zeolite phase, chemical composition and crystal size of chabazite (runs No. 13-17; see Table 5-1) when the other synthesis conditions are kept constant. It was found that pure chabazite would be obtained in the runs No. 13 (SiO_2/Al_2O_3=5, t=24 h), No. 22 (SiO_2/Al_2O_3=10, t=48 h) and No. 23 (SiO_2/Al_2O_3=20, t=96 h) (see Table 5-1). The rate of crystallization decreased with the increase of gel SiO_2/Al_2O_3 ratio. Hasegawa *et al.* [12] reported that the gel SiO_2/Al_2O_3 ratio affected the formation of chabazite layers on porous substrates. When SiO_2/Al_2O_3 ratio was higher than 35, the crystallization rate of chabazite layers became lower and the polycrystalline layer could not be formed on the support surface [12]. Our results were also consistent of the results of NaY crystallization [31,32]. The Si/Al ratio of NaY crystals increased but the rate of crystallization decreased with the increase of gel SiO_2/Al_2O_3 ratio. In the case of our seeded synthesis, the lower and upper SiO_2/Al_2O_3 limits for obtaining pure chabazite can be defined as: lower limit as $3< SiO_2/Al_2O_3 <5$ and upper limit as $20< SiO_2/Al_2O_3 <30$. For the case of gel SiO_2/Al_2O_3 ratio of 3, the *in-situ* synthesis yielded LTL phase (run No. 18; see Table 5-1), but the seed-in-gel synthesis gained amorphous phase (run No. 21; see Table 5-1). This result implies that the addition of chabazite seeds influences the formation of zeolite precursor and the zeolite nucleation, and suppressed the formation of LTL phase. The gel SiO_2/Al_2O_3 ratio of 3 was beyond the crystallization intervals of chabazite and thus yielded the main amorphous phase in presence of chabazite seeds.

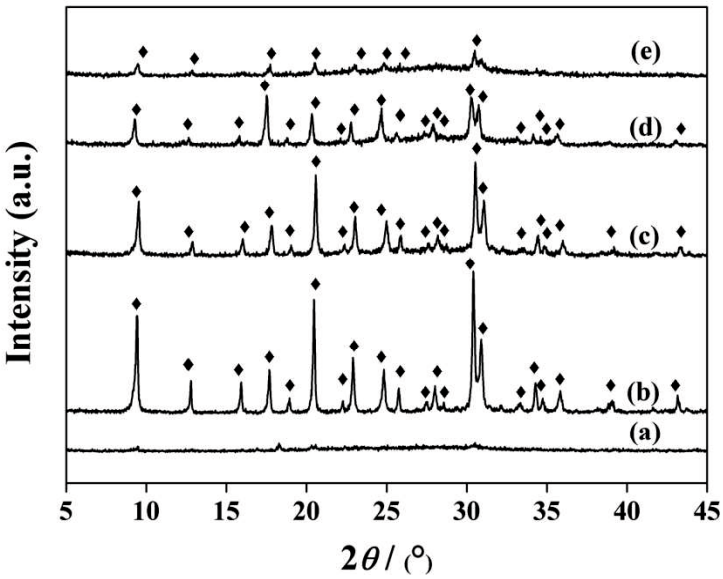

Figure 5-6. XRD patterns of the solids prepared by seeded synthesis at 433 K with gel SiO_2/Al_2O_3 ratios of (a) 3, (b) 5, (c) 10, (d) 20, (e) 30 , respectively. (♦) represents the peaks of CHA phase.

5.3.5. Effect of synthesis temperature

Chabazite was prepared at a temperature range from 393 to 453 K (runs No. 25, 26, 5 and 27; see Table 5-1) using the standard gel. The amorphous phase was obtained at the synthesis temperatures of 373 and 393 K even for 120 h of synthesis time. Pure CHA phase could be obtained at synthesis temperatures higher than 413 K. The synthesis time decreased much with the increase of synthesis temperature for the samples (runs No. 26, 5, and 27; see Table 5-1). Framework Si/Al ratio of crystals were independent of synthesis temperature and time. From the SEM observations in Figure 5-7, the crystals obtained at 413 K had the walnut-like shape with a better symmetry (Figure 5-7a) compared with those crystals (Figure 5-7b and c) prepared at higher temperatures of 433 and 453 K. The morphologies of the crystals changed from walnut-like to disc-like when the synthesis temperature increased to 433 and 453 K, as shown in Figure 5-7b and c. The crystallization rate increased with the increase of synthesis temperature, which could be the reason for the decreased synthesis time and increased particle sizes. On the other hand, the change of crystal morphology with temperature is probably caused by the change of crystal growth rate with temperature [33].

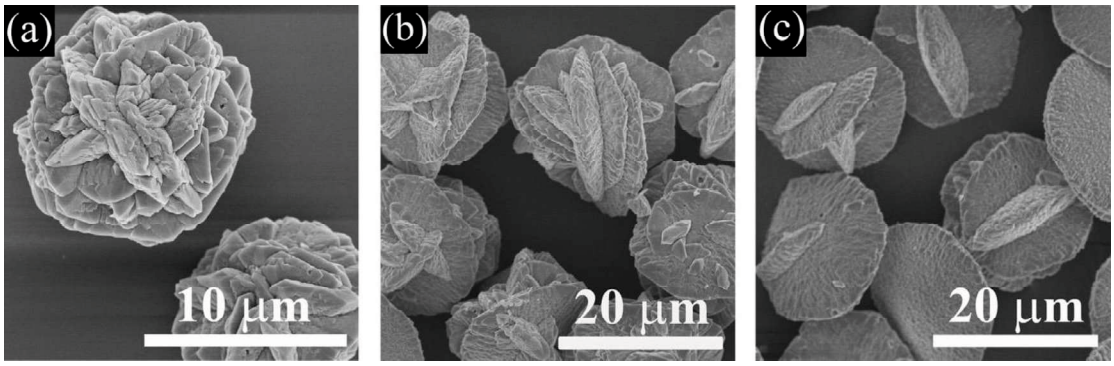

Figure 5-7. SEM images of fluoride-derived chabazite by in situ synthesis for 72 h at temperatures of (a) 413, (b), 433 and (c) 453 K (runs No. 26, 5 and 27), respectively.

5.3.6. Effect of fluoride source

In order to obtain a better understanding of the role of F^- anion on the crystallization of CHA-type zeolite, the effects of fluoride concentration and fluoride source were investigated for the synthesis of chabazite. Figure 5-8 shows the phase choice for zeolites as a function of gel NH_4F/SiO_2 ratio (runs 28-30, 5, 31 and 32; see Table 5-1). The pure MER zeolite phase was crystallized from the fluoride-free gel (run No. 28; see Table 5-1). The addition of small amount of NH_4F (NH_4F/SiO_2 ratio of 0.1) in the initial gel changed the crystallization process, and caused a new CHA phase to form in the products (run No. 29; see Table 5-1). The content of chabazite in products increased with fluoride concentration in gel. A pure CHA-type zeolite phase with high crystallinity was obtained when gel NH_4F/SiO_2 ratio increased to 0.3 and 0.4. Note that the relative crystallinity of products increased from 50 to 80 % when synthesis time increased from 72 to 120 h when NH_4F/SiO_2 ratio was 0.4. However, the NH_4F/SiO_2 ratio of 0.5 in gel caused amorphous phases even if the synthesis time increased to 120 h .

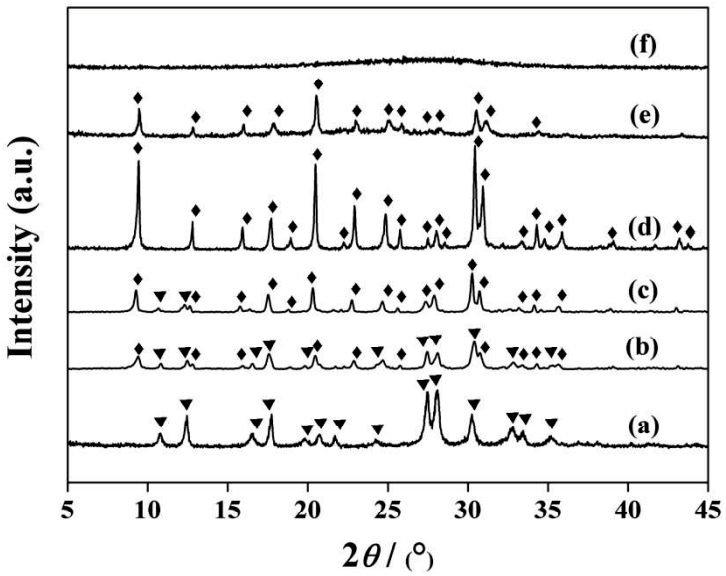

Figure 5-8. XRD patterns of the solids prepared by in situ synthesis at 433 K for 72 h with gel NH_4F/SiO_2 ratios of (a) 0, (b) 0.1, (c) 0.2, (d) 0.3, (e) 0.4 and (f) 0.5, respectively. (▲) Indicates the peaks of MER phase and (♦) represents the peaks of CHA phase.

Figure 5-9 shows XRD patterns of the as-synthesized products obtained with NH_4F, NaF and KF as fluoride source (runs No.5, 33 and 34; see Table 5-1), respectively. The obtained zeolite phases considerably depended on the type of fluoride salts. The addition of NaF yielded pure OFF phase. The main phase MER together with CHA phase was gained when KF was used. Pure CHA phase was only obtained by NH_4F. The differences between alkalinities of F-modified gels before and after synthesis were quite high but it was difficult to follow the relation between alkalinities when different fluoride source were used, as shown in Table S1. Thus, the phase choice was probably attributed to both the type of cations of fluoride salts and the gel alkalinity that was changed by the type of fluoride salts.

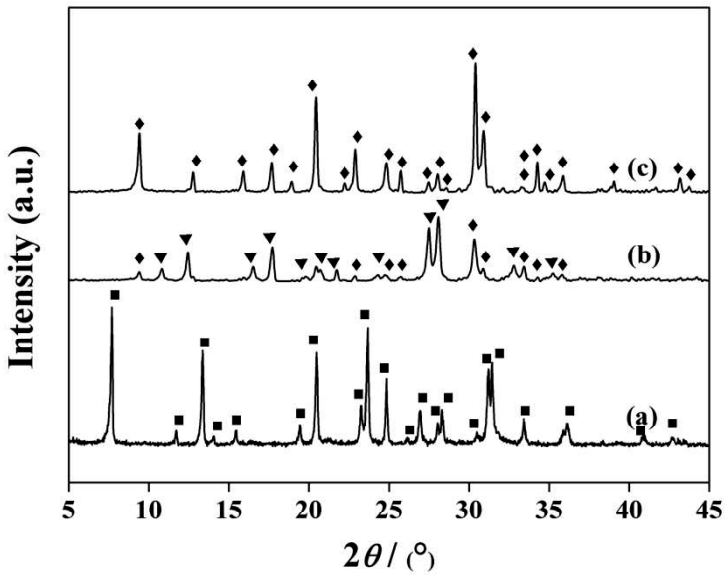

Figure 5-9. XRD patterns of the fluoride-derived solids by in situ synthesis at 433 K for 72 h using (a) NaF, (b) KF and (c) NH_4F (runs No. 33, 5 and 34; see Table 5-1) as fluoride source, respectively. (■) Indicates the characteristic peaks of OFF phase; (▲) does the peaks of MER phase and (♦) represents the peaks of CHA phase.

In our synthesis system, chabazite crystallization was highly dependent on the fluoride source and fluoride concentration. We consider that those influences come from both fluoride ion and balanced cations. Fluoride ion is regarded as one of the mineralizing agents in our gel to improve the gel dissolution. The fluoride ion is easily bonded with Si as SiF_6^{2-} and it could be released since the SiF_6^{2-} undergoes hydrolysis [17] in the basic gel. The content of CHA phase in the MER/CHA mixture increased from 0 to 100% when gel NH_4F/SiO_2 ratio increased from 0 to 0.3 as shown in Fig. 8. We believe that fluoride ion probably exists in the aluminosilicate hydrates, and enter the 'center' of nuclei as counterion when the hydrates are being condensed. Finally, fluoride ion exists in the channels of the crystals when the nucleation and crystal growth further undergo [17]. ^{19}F MAS NMR spectra in Fig. 4c verified the existence of fluoride ion in the channel. Because fluoride ion and aluminum tetrahedron are both negatively charged, the existence of fluoride ion in the nuclei probably restrains the entrance of AlO_2^- to a certain extent since our gels are the alumina-rich gel. Thus, the as-synthesized crystals had an increased framework Si/Al ratio from 2.0 to 2.6 with the increase of gel NH_4F/SiO_2 ratio from 0 to 0.4 (runs No. 28-31 and 5; see Table 5-1). In our case, MER phase that was obtained from

fluoride-free gel had the lowest Si/Al ratio (2.0) (run No. 28; see Table 5-1). The addition of fluoride ion may change the composition of the nuclei and therefore result in the CHA phase that had a higher Si/Al ratio. An appropriate concentration of fluorine (NH_4F/SiO_2=0.3 and 0.4) dominates the nucleation of CHA phase and cause the pure chabazite product. Because of the repulsive interaction between F^- and AlO_2^-, the stability of the aluminosilicate group at the initial nucleation stage is somewhat affected by the concentration of fluoride ions. The increase of fluoride ions in gel could take a certain negative effect on chabazite crystallization rate. And the nuclei of chabazite might be hardly formed when the concentration of fluoride ion reached a certain value (*i.e.* NH_4F/SiO_2=0.5). As a result, the crystallization rate of chabazite decreased at NH_4F/SiO_2=0.4 (run No. 31; see Table 1) and amorphous phase as main product was formed at NH_4F/SiO_2=0.5 (run No. 32; see Table 5-1).

The balanced cation of fluoride salts also had great effect on zeolite crystallization. Some literatures reported that the MER and OFF phase were the common impurity of CHA phase [34-37]. The dual sodium and potassium cations favored the formation of OFF phase [34,35]. In our previous work, we prepared the OFF phase from fluoride-derived and fluoride-free gels in the dual sodium and potassium system [25,34]. Similarly, our current dual-cation system caused a pure OFF phase. When KF replaced NH_4F, the mixed phases of MER and CHA were obtained. The possible reason could be the differences in gel alkalinity and the concentration of potassium cation in gel.

5.4 Conclusions

Low-silica CHA zeolite chabazite was prepared in fluoride media in the absence of organic structure directing agents. ^{19}F MAS NMR evidence showed the fluoride ion was located in the framework channels of chabazite as the balanced ion with H^+ and K^+ cations. A certain amount of NH_4F benefited the formation of pure CHA phase

from the competitive growth of MER and CHA phases; but the further addition of fluoride source decreased the crystallization rate.

5.5 References

[1] T. Inui, M. Kang, Appl. Catal. A 164 (1997) 211.

[2] M.R. Hudson, W.L. Queen, J.A. Mason, D.W. Fickel, R.F. Lobo, C.M. Brown, J. Am. Chem. Soc., 134 (2012) 1970.

[3] L.M. Ren, L.F. Zhu, C.Q. Yang, Y.M. Chen, Q. Sun, H.Y. Zhang, C.J. Li, F. Nawaz, X.Q. Meng, F.S. Xiao, Chem. Commun., 47 (2011) 9789.

[4] H. Kalipcilar, T.C. Bowen, R.D. Noble, J.L. Falconer, Chem. Mater., 14 (2002) 3458.

[5] M.A. Carreon, S. Li, J.L. Falconer, R.D. Noble, J. Am. Chem. Soc., 130 (2008) 5412.

[6] R.F. Zhou, E.W. Ping, H.H. Funke, J.L. Falconer, R.D. Noble, J. Membr. Sci., 444 (2013) 384.

[7] Y. Hasegawa, C. Abe, M. Nishioka, K. Sato, T. Nagase, T. Hanaoka, J. Membr. Sci., 364 (2010) 318.

[8] M. Bourgogne, J.L. Guth, R. Wey, US Patent 4503024 (1985).

[9] I. Goto, M. Itakura, S. Shibata, K. Honda, Y. Ide, M. Sadakane, T. Sano, Micropor. Mesopor. Mater., 158 (2012) 117.

[10] R.F. Zhou, Y.Q. Li, B. Liu, N. Hu, X.S. Chen, H. Kita, Micropor. Mesopor. Mater., 179 (2013) 128.

[11] Y. Hasegawa, H. Hotta, K. Sato, T. Nagase, F. Mizukami, J. Membr. Sci., 347 (2010) 193.

[12] Y. Hasegawa, C. Abe, M. Nishioka, K. Sato, T. Nagase, T. Hanaoka, J. Membr. Sci., 363 (2010) 256.

[13] O. Larlus, V.P. Valtchev, Chem. Mater., 17(2005) 881.

[14] M.A. Camblor, P.A. Barrett, M.-J. Diaz-Cabañas, L.A. Villaescusa, M. Puche, T. Boix, E. Pérez, H. Koller, Micropor. Mesopor. Mater., 48 (2001) 11.

[15] C.A. Fyfe, D.H. Brouwer, A.R. Lewis, J.M. Chézeau, J. Am. Chem. Soc., 123 (2001) 6882.

[16] H. Koller, A. Wölker, L.A. Villaescusa, M.J. Díaz-cabañas, S. Valencia, M.A. Camblor, J. Am. Chem. Soc., 121 (1999) 3368.

[17] H.M. Kao, Y.C. Chen, J. Phys. Chem. B, 107 (2003) 3367.

[18] B.W. Lu, T. Tsuda, H. Sasaki, Y. Oumi, K. Itabashi, T. Teranishi, T. Sano, Chem. Mater., 16 (2004) 286.

[19] E.A. Eilertsen, B. Arstad, S. Svelle, K. Lillerud, Micropor. Mesopor. Mater., 153 (2012) 94.

[20] M. Miyamoto, Y. Fujioka, K. Yogo, J. Mater. Chem., 22 (2012) 20186.

[21] L.A. Villaescusa, P.S. Wheatley, I. Bull, P. Lightfoot, R. E. Morris, J. Am. Chem. Soc., 123 (2001) 8797.

[22] A. Pulido, A. Corma, G. Sastre, J. Phys. Chem. B., 110 (2006) 23951.

[23] M.P. Attfield, C. Richard, A. Catlow, A.A. Sokol, Chem. Mater., 13 (2001) 4708.

[24] R.F. Zhou, F. Zhang, N. Hu, X.S. Chen, H. Kita, Chem. Lett., 40 (2011) 1383.

[25] F. Zhang, Y.H. Zheng, N. Hu, M.H. Zhu, R.F. Zhou, X.S. Chen, H. Kita, J. Membr. Sci., 456 (2014) 107.

[26] R.F. Zhou, Z.L Hu, N. Hu, L.Q. Duan, X.S. Chen, H. Kita, Micropor. Mesopor. Mater., 156 (2012) 166.

[27] K. Sato, K. Sugimoto, N. Shimotsuma, T. Kikuchi, T. Kyotani, T. Kurata, J. Membr. Sci., 82 (2012) 409.

[28] R. Grau-Crespo, E. Acuay, R.R. Ruiz-Salvador, Chem. Commun., 21 (2002) 2544.

[29] C.S. Cundy, P.A. Cox, Micropor. Mesopor. Mater., 82 (2005) 1.

[30] G. Ikuhiro, I. Masaya, S. Syohei, H. Koutaro, I. Yusuke, S. Masahiro, T. Sano, Micropor. Mesopor. Mater., 158 (2012) 117.

[31] H. Kacirek, Hans Lechert, J. Phys. Chem., 80 (1976) 1291.

[32] H. Kacirek, Hans Lechert, J. Phys. Chem., 79 (1975) 1589.

[33] B. Subotic, J. Broni, Theoretical and practical aspects of zeolite crystal growth, in S.M. Auerbach, K.A. Carrado, P.K. Dutta (Eds.), Handbook of zeolite science and technology, Marcel Dekker Inc. New York - Basel, 2003, pp. 129-203.

[34] R.F. Zhou, S.L. Zhong, X. Lin, N.P. Xu, Micropor. Mesopor. Mater., 124 (2009) 117.

[35] A. Cichocki, J. Chem. Soc. Faraday Trans., 81 (1985) 1297.

[36] S. Ueda, M. Nishimura, M. Koizumi, Stud. Surf. Sci. Catal., 24 (1985) 105.

[37] X.Q. Wang, R.R. Xu, Stud. Surf. Sci. Catal., 24 (1985) 111.

Chapter 6 Gas Separation Properties of the Room-Temperature Ionic Liquid Modified CHA Zeolite Membrane

6.1 Introduction

High volume discharge of CO_2 into the atmosphere due to consumption of large amounts of fossil fuels has become one of the most serious global environmental problems.[1-5] Separation and recovery of CO_2 from natural gas and flue gas are, therefore, of great interest. Zeolite membranes grew on porous substrates become good candidates for CO_2 separation from natural gas due to its unique molecular sieve, selective absorption and high thermal pressure stabilities. Microporous silica,[6, 7] carbon molecular sieve,[8-10] metal organic frameworks (MOF),[11-13] and zeolite membranes[14-16] have been reported for gas (vapor) mixture separation. Because of the small pore size as well as excellent thermal and chemical stabilities in harsh environments, CHA zeolite membranes (including SSZ-13(high-silica CHA) and SAPO-34 membranes) have been widely studied for their potential applications in separation of some important industrial gases and organic isomers.

Boundary defects often appear in zeolite membranes during hydrothermal growth and/or calcination process. If the non-zeolitic pores that are larger than the zeolite pores, resulting in low separation selectivity due to Knudsen diffusion and viscous flow.[17] Therefore, some modification methods have been proposed to enhance membrane separation. Hong *et al.*[18] silylated the B-ZSM-5 and SAPO-34 membranes by the catalytic cracking of methyldiethoxysilane to increase their selectivity for H_2 separation. The H_2/CO_2 separation selectivity at 473 K increased from 1.4 to 37 but the H_2 permeance decreased more than 1 order of magnitude in the B-ZSM-5 membranes. Chen *et al.*[19] functional defects by grafting polymer groups on MOR membranes to improve acid-resistance. Yu *et al.*[20] modified SAPO-34 membrane using a molecular layer deposition for H_2 separation. The H_2/N_2 selectivity increased from 11 to 550 at 473 K. Kanezashi *et al.*[21] modified DDR membranes by

chemical vapor deposition tetraethylorthosilicate vapor on the surface of membrane to eliminate the inter-crystalline micropores. But the H_2/CO_2 selectivity did not change after modification.

Room-temperature ionic liquids (RTILs) have also been proposed as an alternative or next-generation CO_2-selective separation media.[22-24] CO_2 could be desorbed without loss of solvent since the RTIL solvent is nonvolatile. The solubility and the selectivity of CO_2 in RTILs are independence of the cation and/or anion. [25, 26]

In the present work, the concept of modifying CHA zeolite with room-temperature ionic liquid to increase the CO_2 adsorption was applied to CHA membranes to increase the CO_2 selectivity for the first time. This novel post-modification process require moderate operation conditions make the operation easy and are suitable to be scaled up. Predominant anion species (X) include hexafluorophosphate (PF_6), tetrafluoroborate (BF_4) and bis(trifluoromethane)-sulfonimide (Tf_2N) were chosen for discussion. This paper defines RTILs as only those salts whose melting points are below ambient temperature. Thus, [C_1mim] cations with halide anions do not fit the criteria to be included in this discussion. The separation properties for single gas and binary CO_2/CH_4 mixtures were studied.

6.2 Experiment

6.2.1 Synthesis of the modification precursors

All chemicals were used as received from Sinopharm Chemical Reagent Co., Ltd. 1-Methylimidazole (8.37 g, 0.102 mol) and 3-Chloropropyltrimethyoxysilane (19.87 g, 0.1 mol) were mixed (250 mL) in a flask. The reaction was heated at reflux (373 K) for 12 h. The imidazolium 3-Chloropropyltrimethyoxysilane was dissolved in a hydrous ethanol (250 mL) and $NaBF_4$ (12.08g, 0.110 mol) was added and then an anion-exchange reaction occurred. The reaction was heated at reflux (373 K) for 24 h. The mixture phase was filtered and the solvent was removed by rotary evaporation.

The product was dried under vacuum at 333 K overnight to give [C_1mim][BF_4] as a colorless liquid. The another two modification precursor ([C_1min][Tf_2N] and [C_1min][PF_6]) were synthesis through the similar process.

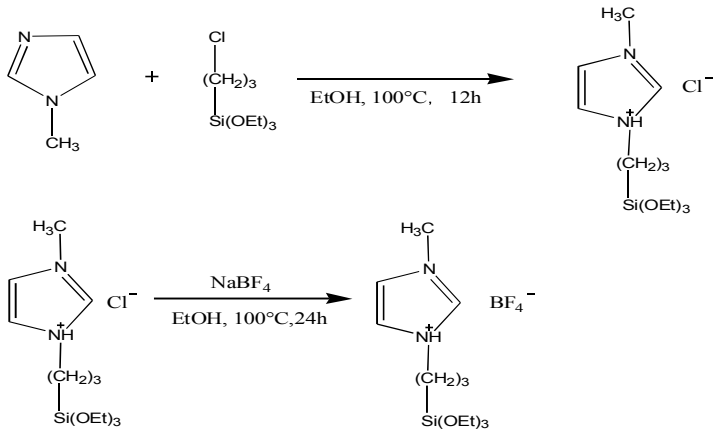

Figure 6-1. The schematic diagram of the synthesis of modification precursors ([C_1mim][BF_4]).

6.2.2 RTILs modify the CHA membrane

CHA membranes were prepared by a secondary hydrothermal synthesis method on the outer surface of a-Al_2O_3 tubes (Nikkato, o.d:12 mm, i.d:9 mm, average pore size: 1.3 μm, porosity: 43 %.) with a molar composition of SiO_2:Al_2O_3:K_2O:NH_4F:H_2O = 1:0.2:0.39:0.3:65. After 6 h aging, 270 g gel was placed in an autoclave and two seeded supports were vertically immersed into the gel. The hydrothermal synthesis was carried out at 423 K for a given time. After synthesis, the autoclave was cooled down to room temperature and the as-synthesized membranes were washed using running taping water for 15 min, and soaked into DI water for several batches until the solution become neutral, and dried at 353 K overnight. The as-synthesized CHA membranes were washed in 5 wt. % hydrochloric acid solution at 303 K for 1 h to increase the density of hydroxyl group on the surface of membrane. The fresh membranes after drying were immersed in a 5 wt. % [C_1mim][BF_4] precursor ethanol solution. The silanization was carried out at 333 K for 12 h with stirring under oil bath. Both ends of the tubes were sealed with solid teflon inserts to eliminate the silanization reaction on the inner surface of the support. The silanized RTIL modified

membrane was washed using ethanol three times and then dry in vacuum at 373 K for overnight. The modification process was illuminated in Figure 6-2.

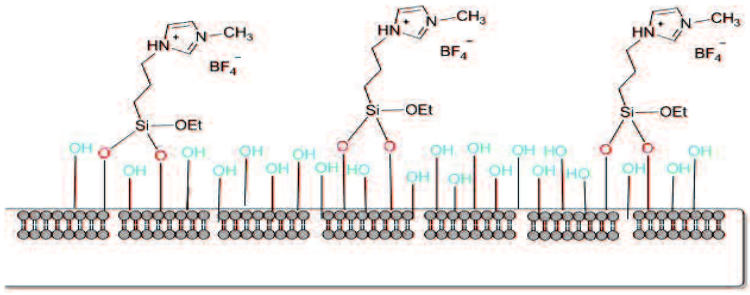

Figure 6-2. The schematic diagram of the modification of CHA membrane with RTILs

6.2.3 Characterization and separation measurements

The crystal phases of the crystals and membranes were identified by X-ray diffraction (XRD, Ultima IV) using Cu Kα radiation with 2 θ from 5° to 45° at a step size of 0.05°. Fourier-transform infrared spectroscopy (FT-IR) analysis was carried out on a spectrophotometer (Thermo, Nicolet 6700) in the range of 600-4000 cm^{-1}.

Single-gas permeation was measured as a function of pressure and temperature using a dead-end (retentate stream blocked) system without sweep gas for H_2, CO_2, N_2, CH_4, C_2H_6 and *i*-C_4H_{10}. The ideal selectivity is the ratio of the single-gas permeances.

Separations were measured using the Wiche-Kallenbach method with hydrogen as a sweep gas with a permeate pressure of 0.1 MPa (atmospheric pressure), or a pressure-drop was maintained across the membrane and no sweep gas was used. The module temperature was controlled between 303 and 363 K and the feed pressure could be varied from 0.2 to 1.0 MPa. Mass flow controllers were used to mix pure gases in equimolar ratio, and the compositions of the feed, retentate and permeate streams were measured by a GC (J-science Lab. Co. Ltd., GC7100T) with a thermal conductivity detector. The flow rates for CO_2 and CH_4 and the H_2 sweep gas were 150, 150 and 400 standard ml/min (SMLPM), respectively. Selectivity is the ratio of

permeances.

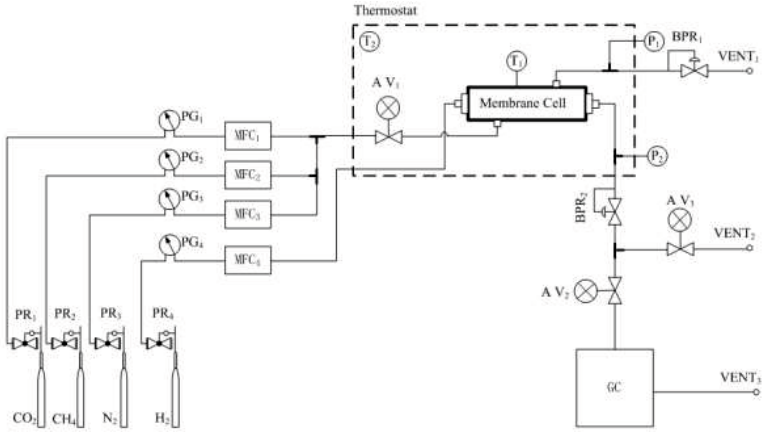

Figure 6-3. The schematic diagram of CO_2/CH_4 mixture gas separation device.

6.3 Results and discussion

6.3. 1 Infrared characterization

The real capacity of room temperature ionic liquids and silane coupling agent grafted on the surface of the porous support membrane is limited. In this work, in order to demonstrate that ionic liquid is able to grafting effective on the surface of CHA membrane layer, we combined with silane coupling agent and imidazolium-based ionic liquids and then grafted on the surface of CHA zeolite crystal particles, which the modification procedures for the CHA crystals and membranes are the same. Figure 6-4 shows the FT-IR spectroscopy of fresh CHA zeolite crystal powder particles and imidazolium-based ionic liquid modified CHA zeolite. As seen in Figure 6-4, the characteristic peaks of imidazole ring appeared at 1302 cm^{-1} and 832 cm^{-1} correspond to C-C/ C=N strectching vibration and bending vibration, respectively, which confirmed that RTILs grafted on the surface of CHA zeolite crystals.

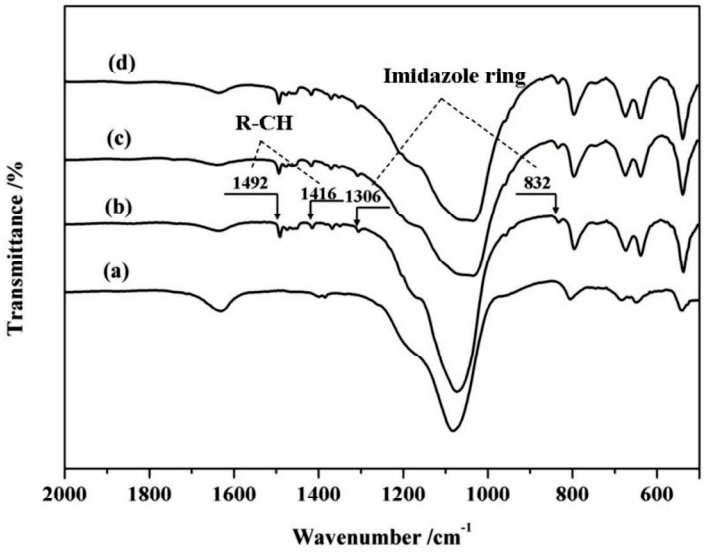

Figure 6-4. IR Spectra of (a) as-synthesized CHA zeolite; (b) $[C_1min][BF_4]^-$ modified CHA zeolite; (c) $[C_1min]$ $[Tf_2N]^-$ modified CHA zeolite and (d) $[C_1min]$ $[PF_6]^-$ modified CHA zeolite. $[C_1min]$ represents 1-methylimidazole

6.3. 2 Single-gas permeances

Single-gas permeances of H_2, CO_2, N_2, CH_4, C_3H_8 and i-C_4H_{10}, measured at room temperature and 0.2 MPa feed pressure for the fresh and modified CHA membrane ILM-4, are shown as a function of kinetic diameter in Figure 6-5. Both the fresh and modified membrane showed the same permeance order: CO_2>H_2>N_2>CH_4>>C_3H_8>>i-C_4H_{10}. After the membrane was modified, the permeances of all light gas decreased but the permeances of C_3H_8 and i-C_4H_{10} significant decreased by approximately 1 orders of magnitude. Since the kinetic diameter of C_3H_8 and i-C_4H_{10} are larger than the CHA pore size so that the permeance of them through CHA membrane mainly by the defective non-zeolite pores contribution. Thus, modification may lead to reduce non-zeolite defects on the surface of CHA membrane. Even though the kinetic diameter of CO_2 is larger than that of H_2, the CO_2 permeance through CHA membrane IML-4 was higher than H_2 permeance and decreased slightly after modied. The ideal selectivities of the light gases at a feed pressure of 0.2 MPa through the fresh and modified membranes ILM-4 are shown in Table 6-1. Their high selectivities for C_3H_8 and i-C_4H_{10} after modified indicate

relatively good quality membranes.

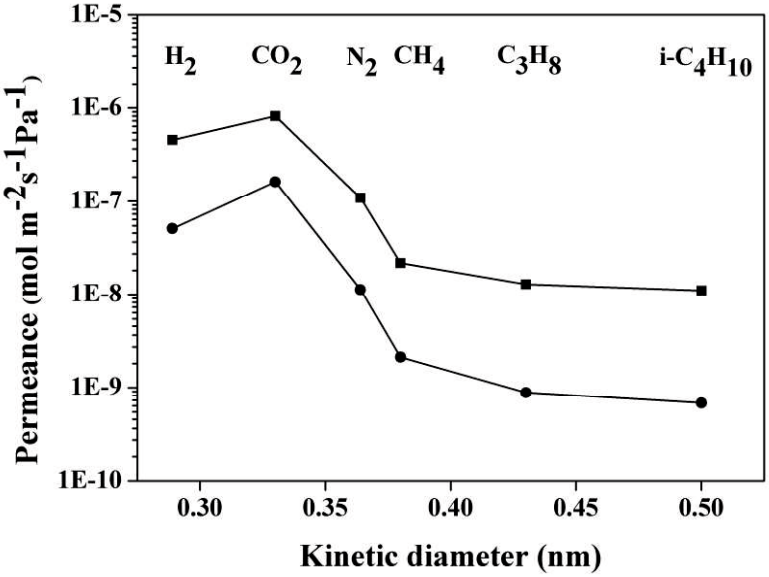

Figure 6-5. Single-gas permeances for the fresh and the [C_1min][BF_4] modified CHA membrane of IML-4 as a function of kinetic diameter at room temperature and a feed pressure drop of 0.2 MPa without sweep gas.

Table 6-1. Ideal selectivity of the fresh and the [C_1min][BF_4] modified CHA membrane IML-4.

Membrane	Ideal selectivity				
	CO_2/H_2	CO_2/N_2	CO_2/CH_4	CO_2/C_3H_8	CO_2/i-C_4H_{10}
Fresh	2	8	41	69	74
Modified	3	14	76	183	237

The pressure dependence of the single-gas permeances for H_2, CO_2, N_2, CH_4 and C_3H_8 from 0.2 to 1.0 MPa through modified membrane ILM-4 is shown in Figure 6-6. When the feed and permeate pressures were both increased so as to maintain a constant pressure drop of 0.2 MPa, the CO_2 permeance at room temperature decreased slightly with increasing pressure, whereas the CH_4 permeance increased slightly. The CO_2/CH_4 ideal selectivity decreased from 76 to 55 as the feed pressure increased from 0.2 MPa to 1.0 MPa. The permeance of relative smaller kinetic diameter of H_2

increased with increasing pressure, whereas the permeance of relative larger kinetic diameter of C_3H_8 was almost constant. These results indicated the concentration of the large non-zeolitic pores was low on the modified CHA membrane ILM-4.

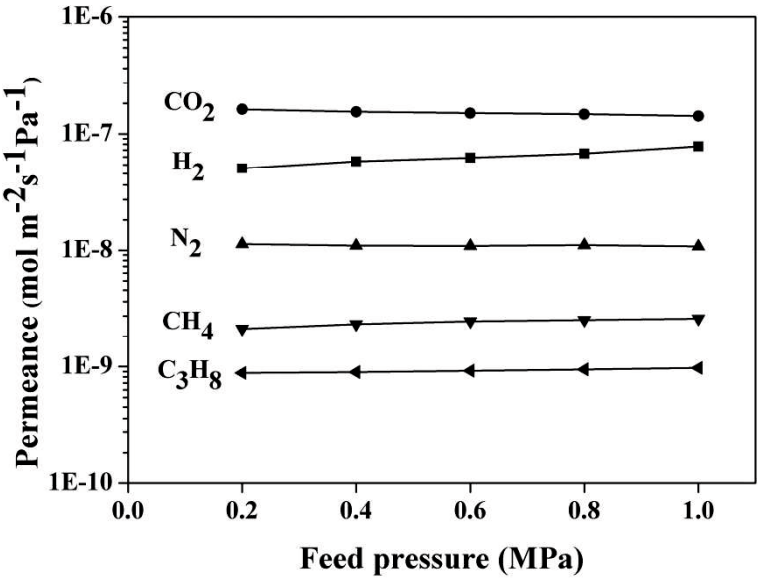

Figure 6-6. Single-gas permeances of CO_2, H_2, N_2, CH_4 and C_3H_8 through modified membrane IML-4 as a function of feed pressure at room temperature.

6.3.3 Effect of the precursors

Table 6-2 shows the separation performances of the modified CHA membranes as a function of the precursors. Silylation of the CHA membranes had slightly decreased the CO_2 permeance but increased the CO_2/CH_4 selectivities. The γ-chloropropyl triethoxysilane (CPTES) should fit into CHA pores with difficulty since the CHA pore diameter is 0.38 nm, which is approximately the size of the smallest diameter of CPTES, and thus, CPTES would not be expected to modify the CHA pore size. However, CPTES could adsorb and react in larger non-zeolitic pores and reduce their size. During silylation, CPTES apparently react at acid sites in defects in the CHA membranes, and lead to reduce the defect size. Since CH_4 is so close to the CHA pore size, a large fraction of the CH_4 likely permeates through non-zeolitic pores, reducing their size decreased the CH_4 permeance significantly. Thus, the CO_2/CH_4 selectivities increased after silylation.

Table 6-2. Separation performances of the modified CHA membranes as a function of the precursors.

No.	Modified materials	CO_2 permeance $\times 10^{-7}$ (mol m^{-2} s^{-1} Pa^{-1})		CO_2/CH_4 Selectivity	
		fresh	modified	fresh	modified
ILM-1	γ -Chloropropyl Triethoxysilane	1.3	0.9	10	26
ILM-2		2.1	1.1	9	28
ILM-3		1.9	1.0	12	25
Average		1.8	1.0	10	26
ILM-4	γ -Chloropropyl Triethoxysilane + $[C_1min][BF_4]$	1.8	1.0	11	89
ILM-5		2.5	1.3	9	79
ILM-6		1.8	0.7	13	90
Average		1.8	1.0	11	87

When using imidazolium-based ionic liquids $[C_1min]$ $[BF_4]$ combined with a silane coupling agent (CPTES) on the surface of CHA zeolite layer with post-processing after modification, the CO_2/CH_4 mixed gas separation selectivity, on average, significantly increased by a factor of 7 (from the initial value of 11 to 87) at room temperature and 0.2 MPa feed pressure, and the permeance showed a less than 50% decrease compared with the initial value. These results indicated that the imidazolium-based ionic liquids $[C_1min]$ $[BF_4]$ were effectively grafted on the surface of the CHA membrane and helps to significantly improve the CO_2/CH_4 mixed gas separation selectivity, but also almost no further sacrifice the CO_2 permeance. This novel post-modification using RTIL precursors was adopted to effectively patch membrane defects and improved CO_2/CH_4 selectivity and also has good reproducibility.

6.3.4 Effect of the ionic liquid with different anions.

Table 6-3. shows the separation performance of the ionic liquid ($[C_1min][X]$) modified membranes as a function of different anions. Relevant experiments and simulation results show that CO_2 is more easily dissolved in alkyl imidazolium-based

ionic liquids ([$C_n$min] [X]). Different kinds of anion of the alkyl imidazolium-based ionic liquids may lead to difference CO_2 adsorption ability. The modification precursors of [C_1min] [BF_4] lead to has the greatest effect on improving CO_2/CH_4 selectivity, followed by [C_1min] [Tf_2N] and [C_1min] [PF_6]. Modification with RTILs increased the CO_2/CH_4 separation selectivity at room temperature, as shown in Table 6-3. The CO_2 permeance in a CO_2/CH_4 mixture decreased about 76 %, 58 % and 44 % due to modification with [C_1min] [Tf_2N], [C_1min] [PF_6] and [C_1min] [BF_4], respectively. Although [C_1min] [Tf_2N] may has relative high CO_2 adsorption ability, but it was more likely to sacrifice CO_2 permeance of CHA membrane. These results indicated that adsorption properties of RTILs over CO_2 are important for CO_2/CH_4 separation

Table 6-3. Separation performance of the ionic liquid ([C_1min][X]) modified membranes as a function of different anions.

No.	[C_1min][X]	CO_2 permeance $\times 10^{-7}$ (mol m^{-2} s^{-1} Pa^{-1})		CO_2/CH_4 Selectivity	
		fresh	modified	fresh	modified
ILM-7	$[PF_6]^-$	2.5	0.6	9	27
ILM-8	$[Tf_2N]^-$	1.2	0.5	11	59
ILM-4	$[BF_4]^-$	1.8	1.0	11	89

6.3.5 CO_2/CH_4 separation

Figure 6-7 shows the 50/50 CO_2/CH_4 separation performance for the fresh and the [C_1min][BF_4] modified membrane ILM-4 as a function of feed pressure at room temperature. This membrane was tested without sweep gas. The CO_2/CH_4 selectivity of modified membrane ILM-4 exhibited a maximum of 81 at feed pressure of 0.2 MPa and dropped off to 46 at 1.0 MPa, the CO_2 permeance was 0.96×10^{-7} mol m^{-2} s^{-1} Pa^{-1}. The CO_2 mixture permeances were about 67% of the single gas permeances, whereas the CH_4 mixture permeances were only about 13 % of the single gas

permeances at the range of feed pressure. It may be more strongly adsorbed CO_2 inhibited CH_4 adsorption, so competitive adsorption increased the CO_2/CH_4 selectivity. Therefore the mixture selectivity was higher than the ideal selectivity. These results indicated that although the post-modification using $[C_1min][BF_4]$ precursors was adopted to patch membrane defects and improved CO_2/CH_4 selectivity. But the modified CHA membrane ILM-4 may still has a small number of large pore defects since the CH_4 permeance increased slightly with increasing feed pressure.

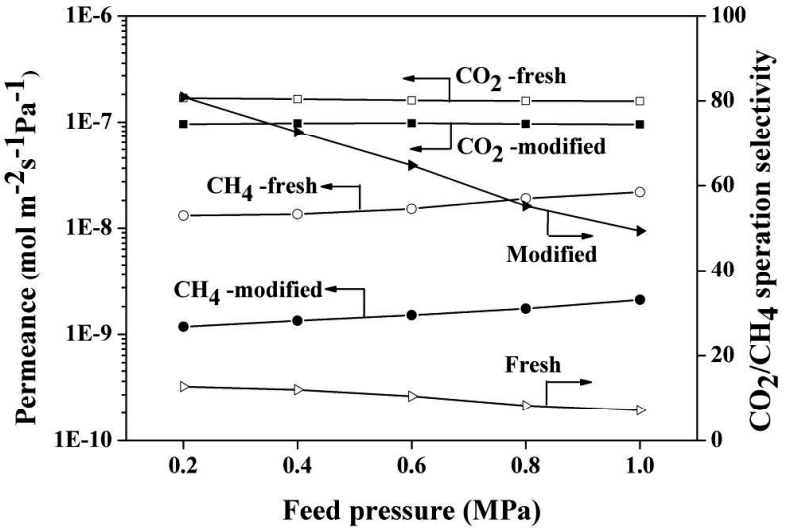

Figure 6-7. The 50/50 CO_2/CH_4 separation performance for the fresh and the $[C_1min][BF_4]$ modified membrane ILM-4 as a function of feed pressure at room temperature.

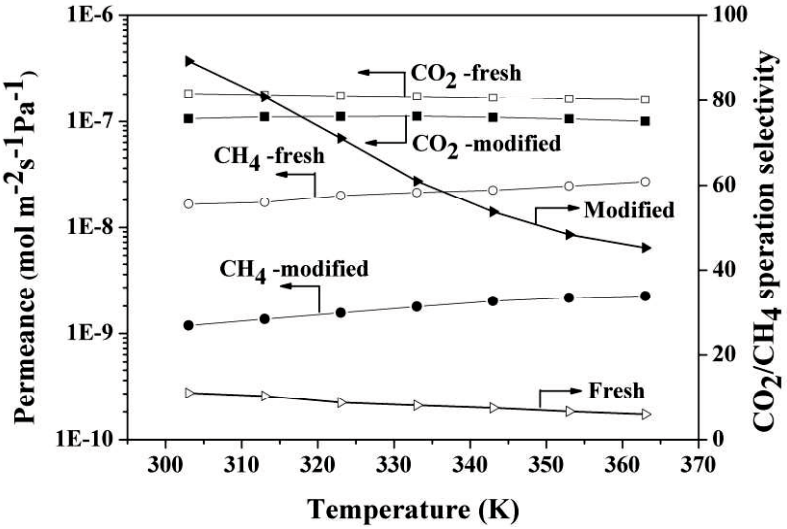

Figue 6-8. The 50/50 CO_2/CH_4 separation performance for the fresh and the $[C_1min][BF_4]$ modified membrane as a function of temperature at 0.2 MPa feed pressure with sweep gas.

Figure 6-8 shows the 50/50 CO_2/CH_4 separation performance for the fresh and the $[C_1min][BF_4]$ modified membrane as a function of temperature at feed pressure of 0.2 MPa. The CO_2/CH_4 selectivity of membrane ILM-4 exhibited a maximum improvement from 11 to 89 at the temperature of 303 k, the CO_2 permeance decreased from 1.8×10-7 mol m^{-2} s-1 Pa^{-1} to 1.0×10^{-7} mol m^{-2} s^{-1} Pa^{-1}. It indicated that our post-modification method dramatically decreases the contributions of non-zeolitic defects and improved the gas separation selectivity. As the temperature increased, the CO_2 permeance slightly decreased and the CH_4 permeance slightly increased, so the CO_2/CH_4 separation selectivity decreased with increasing temperature.

6.4 conclusions

A novel post-modification using imidazolium-based room temperature ionic liquids (RTILs) precursors were adopted to effectively patch the defects of CHA membrane and improved CO_2/CH_4 selectivity. CO_2/CH_4 selectivity depended on the anion type of RTILs, which indicates that the adsorption properties of RTILs over CO_2 are important for CO_2/CH_4 separation. $[C_1min][BF_4]$-modified membranes had an improved CO_2/CH_4 separation selectivity increased by a factor of 7 (average CO_2/CH_4 selectivity of 87) for an equimolar CO_2/CH_4 mixture at room temperature and 0.2 MPa feed pressure, and the permeance showed a less than 50% decrease compared with the initial value (decreased from 1.8×10^{-7} mol m^{-2} s^{-1} Pa^{-1} to 1.0×10^{-7} mol m^{-2} s^{-1} Pa^{-1}).

6.5 References

[1] M. Pera-Titus, Porous inorganic membranes for CO_2 capture: present and prospects, Chemical Reviews, 114 (2013) 1413-1492.

[2] R.K. Pachauri, M. Allen, V. Barros, J. Broome, W. Cramer, R. Christ, J. Church, L.

Clarke, Q. Dahe, P. Dasgupta, Climate Change 2014: Synthesis Report. Contribution of Working Groups I, II and III to the Fifth Assessment Report of the Intergovernmental Panel on Climate Change, (2014).

[3] N.V. Rees, R.G. Compton, Electrochemical CO_2 sequestration in ionic liquids; a perspective, Energy Environ. Sci., 4 (2011) 403-408.

[4] C. Gough, State of the art in carbon dioxide capture and storage in the UK: an experts' review, International Journal of Greenhouse Gas Control, 2 (2008) 155-168.

[5] H. Balat, C. Öz, Technical and economic aspects of carbon capture and storage–a review, Energy, Exploration & Exploitation, 25 (2007) 357-392.

[6] Y. Gu, P. Hacarlioglu, S.T. Oyama, Hydrothermally stable silica–alumina composite membranes for hydrogen separation, Journal of Membrane Science, 310 (2008) 28-37.

[7] M. Kanezashi, T. Shioda, T. Gunji, T. Tsuru, Gas permeation properties of silica membranes with uniform pore sizes derived from polyhedral oligomeric silsesquioxane, AIChE Journal, 58 (2012) 1733-1743.

[8] D.Q. Vu, W.J. Koros, S.J. Miller, High Pressure CO_2/CH_4 Separation Using Carbon Molecular Sieve Hollow Fiber Membranes, Industrial & Engineering Chemistry Research, 41 (2002) 367-380.

[9] B.J. Hinds, N. Chopra, T. Rantell, R. Andrews, V. Gavalas, L.G. Bachas, Aligned multiwalled carbon nanotube membranes, Science, 303 (2004) 62-65.

[10] Y.H. Sim, H. Wang, F.Y. Li, M.L. Chua, T.-S. Chung, M. Toriida, S. Tamai, High performance carbon molecular sieve membranes derived from hyperbranched polyimide precursors for improved gas separation applications, Carbon, 53 (2013) 101-111.

[11] J.R. Li, R.J. Kuppler, H.C. Zhou, Selective gas adsorption and separation in metal-organic frameworks, Chemical Society Reviews, 38 (2009) 1477-1504.

[12] Y. Pan, Z. Lai, Sharp separation of C_2/C_3 hydrocarbon mixtures by zeolitic imidazolate framework-8 (ZIF-8) membranes synthesized in aqueous solutions, Chemical Communications, 47 (2011) 10275-10277.

[13] A. Huang, N. Wang, C. Kong, J. Caro, Organosilica-functionalized zeolitic imidazolate framework ZIF-90 membrane with high gas-separation performance, Angewandte Chemie, 51 (2012) 10551-10555.

[14] M. Tsapatsis, Materials science. Toward high-throughput zeolite membranes, Science, 334 (2011) 767-768.

[15] T.C. Pham, H.S. Kim, K.B. Yoon, Growth of uniformly oriented silica MFI and BEA zeolite films on substrates, Science, 334 (2011) 1533-1538.

[16] M. Yu, R.D. Noble, J.L. Falconer, Zeolite membranes: microstructure characterization and permeation mechanisms, Accounts of Chemical Research, 44 (2011) 1196-1206.

[17] G. Bonilla, M. Tsapatsis, D.G. Vlachos, Fluorescence confocal optical microscopy imaging of the grain boundary structure of zeolite MFI membranes made by secondary (seeded) growth, Journal of Membrane Science, 182 (2001) 103-109.

[18] M. Hong, J.L. Falconer, R.D. Noble. Modification of zeolite membranes for H_2 separation by catalytic cracking of methyldiethoxysilane, Industrial & Engineering Chemistry Research, 44 (2005) 4035-4041.

[19] Z. Chen, D. Yin,Y. Li, Functional defect-patching of a zeolite membrane for the dehydration of acetic acid by pervaporation, Journal of Membrane Science, 369 (2011) 506-513.

[20] M. Kanezashi, J. O'Brien‐Abraham, Y.S. Lin, Gas permeation through DDR‐type zeolite membranes at high temperatures, AIChE Journal, 54 (2008) 1478-1486.

[21] M. Yu, H.H. Funke, R.D. Noble, H_2 separation using defect-free, inorganic composite membranes, Journal of the American Chemical Society, 133 (2011) 1748-1750.

[22] J.L. Anthony, S.N. Aki, E.J. Maginn, J.F. Brennecke, Feasibility of using ionic liquids for carbon dioxide capture, International Journal of Environmental Technology and Management, 4 (2004) 105-115.

[23] R.E. Baltus, R.M. Counce, B.H. Culbertson, H. Luo, D.W. DePaoli, S. Dai, D.C. Duckworth, Examination of the potential of ionic liquids for gas separations,

Separation Science and Technology, 40 (2005) 525-541.

[24] X. Zhang, Z. Liu, W. Wang, Screening of ionic liquids to capture CO_2 by COSMO‐RS and experiments, AIChE Journal, 54 (2008) 2717-2728.

[25] T.K. Carlisle, J.E. Bara, C.J. Gabriel, R.D. Noble, D.L. Gin, Interpretation of CO2 solubility and selectivity in nitrile-functionalized room-temperature ionic liquids using a group contribution approach, Industrial & Engineering Chemistry Research, 47 (2008) 7005-7012.

[26] C. Cadena, J.L. Anthony, J.K. Shah, T.I. Morrow, J.F. Brennecke, E.J. Maginn, Why is CO_2 so soluble in imidazolium-based ionic liquids?, Journal of the American Chemical Society, 126 (2004) 5300-5308.

Chapter 7 Summary

In this thesis, we devoted our attention to investigate the preparation and application of catalytic titanium silicalite-1(TS-1) membrane, RHO zeolite membrane and CHA membrane, studying the PV-aided catalytic performance of titanium silicalite-1 (TS-1) membrane, optimization the preparation process of TS-1 membrane, studying the single gas performance of tubular supported RHO membrane, Synthesis of low-silica CHA zeolite chabazite in fluoride media without organic structural directing agents and zeolites, modification of CHA membrane by using imidazolium-based room temperature ion liquids (RTILs).

In chapter 2, the TS-1 membrane with high catalytic activity was prepared on porous mullite tubular support by *in-situ* hydrothermal synthesis with the synthesis recipe of SiO_2: 0.031Titanium n-butoxide: 0.35Tetrapropylammonium hydroxide: 28 H_2O. Optimized preparation process displayed well reproducibility. Supplementary addition of H_2O_2 to the synthesis solution after removals of bubbles in preparation process had great effect on the catalytic performance of as-synthesized TS-1 membrane. Furthermore, the pretreatment of support may have effect on the morphology of surface zeolitic layer of TS-1 membrane.

In chapter 3, pure RHO membrane with high density and well intergrowth have been prepared on the surface of porous α-Al_2O_3 tube support using 18 Crown 6 as OSDA. Fluoride salts such as NaF have great effect on the morphologies of RHO crystals and lead to well intergrowth of RHO zeolite crystals. Fluoride may favor the crystallization of RHO zeolite as a mineralizing agent. Higher content of organic template (18C6/Al_2O_3=5) may lead to form a dense intergrowth RHO zeolite crystal layer.

In chapter 4, an organic template-free route for synthesizing RHO membranes by the secondary growth method is provided. RHO zeolite membrane showed CO_2/N_2 and CO_2/CH_4 ideal selectivities higher than the Knudsen selectivities. On the other hand, the ideal CO_2/N_2 selectivities were smaller than the reported adsorption

selectivities. Contribution of non-zeolitic permeation is one reason for the smaller selectivity. Diffusivity of CO_2 is suspected to be small in RHO zeolitic pores due to the strong affinity lowering the CO_2-selectivity of RHO membranes. RHO membranes showed dehydration performance in water/ethanol and water/isopropanol separations. The highest separation factor obtained for water/isopropanol was 1390 at an isopropanol feed concentration of 95 wt% with a total flux of 0.77 kg m^{-2} h^{-1}. The membrane showed similar separation properties after 30 hours of total testing time, suggesting robustness of the membrane.

In chapter 5, CHA membranes were prepared in the absence of OSDAs. The crystallization kinetics of the fluoride-derived CHA and the effects of gel SiO_2/Al_2O_3 ratio, gel F^-/SiO_2 ratio, fluoride source and synthesis temperature on the morphology and composition of crystals were investigated. A certain amount of the specific fluoride source (NH_4F) dominated the crystallization of CHA phase in the competitive growth of MER/CHA phases. The fluoride-derived CHA by in-situ synthesis had a particle size of 15-20 μm. Seeded-in-gel synthesis increased the crystallization rate and resulted in the smaller crystals with higher BET surface area and micropore volume. The location of fluorine anion in zeolite framework and the role of fluoride salts on CHA crystallization were also demonstrated.

In chapter 6, the novel precursors were used for membrane surface modification for CHA membranes. Imidazolium-based room temperature ion liquids (RTIL) were effectively grafted on membrane surface by silylation reaction in order to reduce the numbers and sizes of the defects, and thus CO_2/CH_4 selectivies of the membranes were greatly improved. The influences of the type of the cation of RTILs, the type of the balanced anions and treatment conditions on membrane performance were studied. CO_2/CH_4 selectivity of modified membranes was mostly depended on the type of the balanced anion of RTILs, which indicates that the adsorption properties of RTILs over CO_2 are important for CO_2/CH_4 separation by membranes.

Acknowledgements

For the first of all, I would like to express my special appreciation and thanks to my advisor Professor Dr. Hidetoshi Kita, you have been a tremendous mentor for me. He has provided guidance at key moments in my work while also allowing me to work independently the majority of the time. I have learned a great deal from his unique perspective on research, conscientious scientific attitude, his sharp insight on almost any issue, and his personal integrity and expectations of excellence.

I'm in debt to Associate Professor Izumi Kumakiri, Associate Professor Kazuhiro Tanaka and Research Assistant Tomoko Koga for their kind help advice and valuable suggestions, and much thankfulness is expressed.

I'd like to thanks to Professor Xiangshu Chen, my master's supervisor, special appreciate for him to recommend me to study the Ph.D. program in Yamaguchi. I also want to thank my master's co-supervisor, Professor Rongfei Zhou, who led me toward the road of scientific research.

I am also very grateful to all those at the green chemical process laboratory, especially Dr. Lingfang Qiu, Dr. Ting Wu, Mr. Yuta Yamashita, Mr. Tomoya Masuda, Mr. Kyosuke Tamura and any others who were always so helpful and provided me with their assistance throughout my dissertation and daily life in these two years. Mr. Yuta Yamashita is gratefully acknowledged due to your tremendous helpful on my research and in my daily life, not only as a tutor or a good friend, more like a brother.

A special thanks to my family. Words cannot express how grateful I am to my parents, who provide a carefree environment for me and for all of the sacrifices that they have made on my behalf. And finally to Yang Dian, who has been my side and encouraged me through this PhD and will keep on my way together toward a bright future. I would also like to thank all of my friends who supported me in this period, and incented me to strive towards my goal.

柳 波 (LIU BO)